QUANTIFICATION AND ANALYSIS OF UNCERTAINTIES IN RESERVOIR MODELING USING MULTIPLE-POINT GEOSTATISTICS

A THESIS SUBMITTED TO
THE GRADUATE SCHOOL OF NATURAL AND APPLIED SCIENCES
OF
THE MIDDLE EAST TECHNICAL UNIVERSITY

BY

MOHAMED MOHIELDIN FADLELMULA FADLELSEED

IN PARTIAL FULFILLMENT OF THE REQUIREMENTS
FOR
THE DEGREE OF DOCTOR OF PHILOSOPHY
IN
PETROLEUM AND NATURAL GAS ENGINEERING

DECEMBER 2012

Approval of the thesis:

QUANTIFICATION AND ANALYSIS OF UNCERTAINTIES IN RESERVOIR MODELING USING MULTIPLE-POINT GEOSTATISTICS

submitted by **MOHAMED MOHIELDIN FADLELMULA FADLELSEED** in partial fulfillment of the requirements for the degree of **Doctor of Philosophy in Petroleum and Natural Gas Engineering Department, Middle East Technical University** by,

Prof. Dr. Canan Özgen _____
Dean, Graduate School of **Natural and Applied Sciences**

Prof. Dr. Mahmut Parlaktuna _____
Head of Department, **Petroleum and Natural Gas Engineering**

Prof. Dr. Serhat Akin _____
Supervisor, **Petroleum and Natural Gas Engineering Dept., METU**

Prof. Dr. H. Şebnem Düzgün _____
Co-Supervisor, **Mining Engineering Dept., METU**

Examining Committee Members:

Prof. Dr. Mahmut Parlaktuna _____
Petroleum and Natural Gas Engineering Dept., METU

Prof. Dr. Serhat Akin _____
Petroleum and Natural Gas Engineering Dept., METU

Prof. Dr. Şakir Şimşek _____
Geological Engineering Dept., Hacettepe University

Prof. Dr. Nurkan Karahanoğlu _____
Geological Engineering Dept., METU

Assoc. Prof. Dr. Hakkı Gücüyener _____
General Manager, KarKim Drilling Fluids

Date: 20.12.2012

I hereby declare that all information in this document has been obtained and presented in accordance with academic rules and ethical conduct. I also declare that, as required by these rules and conduct, I have fully cited and referenced all material and results that are not original to this work.

Name, Last name: Mohamed Mohieldin Fadlelmula Fadlelseed

Signature :

ABSTRACT

QUANTIFICATION AND ANALYSIS OF UNCERTAINTIES IN RESERVOIR MODELING USING MULTIPLE-POINT GEOSTATISTICS

Fadlelmula Fadlelseed, Mohamed Mohieldin

Ph.D., Department of Petroleum and Natural Gas Engineering

Supervisor : Prof. Dr. Serhat Akin

Co-Supervisor: Prof. Dr. H. Şebnem Düzgün

December 2012, 171 pages

This study analyzed and quantified uncertainties of reservoirs modeled using multiple-point geostatistics (MPG). The uncertainty types analyzed herein are training image (TI) and hard data (porosity) uncertainties.

Aiming at studying the impact of TI uncertainty, this study provides a tool to parameterize TIs having channel structure by a mathematical (Sine) function so that a TI is a function of four parameters. These parameters are channels' number, waves' number in each channel, amplitude level of waves, and Z-direction slices' number. These parameters are used to generate 2D and 3D TIs to remodel a reservoir utilizing a proposed MPG methodology.

Analysis of cumulative oil production values showed that TI having 5 Z-direction slices and 3 channels with 2 medium or low amplitude level waves or more produced representative and reliable reservoir models. Thus, these values are set as thresholds of the TI's parameters. Additionally, increasing the number of channels and waves of a TI decreased the uncertainty of the simulated reservoir. However, increasing the number of Z slices beyond 5 and the amplitude level had no effect on the uncertainty.

Analysis of the original and recoverable oil in place (OOIP and ROIP) values showed that the effect of channel number and amplitude level are random. However, the number of waves is directly proportional to OOIP and ROIP values. Moreover, utilization of the thresholds defined decreased the uncertainty range of OOIP and ROIP prediction.

Finally, the investigation of hard data uncertainty revealed that porosity data uncertainty has great impact on the simulated reservoir.

Keywords: Multiple-Point Geostatistics, Training Image Uncertainty, Hard Data Uncertainty, Uncertainty Quantification

ÖZ

ÇOK NOKTALI JEOİSTATİSTİK KULLANARAK REZERVUAR MODELLERİNDE BELİRSİZLİĞİN ANALİZİ VE ÖLÇÜLMESİ

Fadlelmula Fadlelseed, Mohamed Mohieldin
Doktora, Petrol ve Doğal Gaz Mühendisliği Bölümü
Tez Yöneticisi : Prof. Dr. Serhat Akin
Ortak Tez Yôneticisi: Prof. Dr. H. Şebnem Düzgün

Aralık 2012, 171 sayfa

Bu çalışmada, çok noktalı jeostatistik teknikler kullanılarak modellenen rezervuarların belirsizlikleri analiz edilmiş ve ölçülmüştür. Analiz edilen belirsizlik tipleri başlıca eğitim görüntüsü ve sabit veri (gözeneklilik) belirsizlikleridir.

Bu çalışma, eğitim görüntüsünün belirsizliğinin etkisini çalışmak üzere, matematiksel (Sinüs) fonksiyonu kullanarak kanal yapısındaki eğitim görüntüsünü parameterlendiren bir araç sunmaktadır. Böylece, eğitim görüntüsünün yapısı dört parametre ile kontrol edilmektedir. Bu parametreler kanal sayısı, kanaldaki dalga sayısı, dalganın yükseklik seviyesi ve görüntünün Z eksenindeki dilimlerinin sayısıdır. Bu parametreler kullanılarak 2 ve 3 boyutlu eğitim görüntüleri oluşturulmuştur.

Çalışmada çok noktalı bir jeostatistik metodu önerilmiş ve oluşturulan eğitim görüntüleri kullanılarak önceden modellenen bir rezervuar tekrar modellenmiştir.

Kümülatif petrol üretim değerlerinin analizi sonucunda, en az 5 Z ekseni dilimli ve 2 orta ya da düşük yükseklik seviyesindeki dalgaya sahip 3 kanallı eğitim görüntüsünün temsili ve güvenilir rezervuar modeli ürettiği görülmüştür. Bulunan bu değerler, eğitim görüntülerinin parametrelerininde eşik değeri olarak kullanılmıştır. Ayrıca, eğitim görüntülerinin kanal sayısını artırmak ya da dalga sayısını artırmak rezervuar modelinin belirsizliğini düşürmüştür. Ancak, Z ekseni dilimlerini 5 üzerine çıkarmak ve yükseklik seviyesini artırmak rezervuar belirsizliği üzerinde herhangi bir etki yaratmamıştır.

Yerinde Orjinal ve Yerinde Üretilebilir Petrol (YOP ve YÜP) analizleri sonucunda kanal sayısı ve yükseklik seviyesinin rastgale olduğu tespit edilmiştir. Ancak, dalga sayısı YOP ve YÜP değerleri ile doğrudan ilişkili bulunmuştur. Ayrıca, tanımlanan eşik değerlerinin kullanımı tahmin edilen YOP ve YÜP değerlerinin belirsizlik aralığını azaltmıştır.

Son olarak, sabit veri belirsizliği analizi sonucunda gözeneklerdeki belirsizliğin modellenen rezervuar üzerinde büyük etkiye sahip olduğu görülmüştür.

Anahtar Kelimeler: Çok Noktalı Jeostatistik, Eğitim Görüntüsünün Belirsizliği, Sabit Veri Belirsizliği, Belirsizlik Ölçülmesi

To my family

ACKNOWLEDGMENTS

I would like to express my sincere thanks to my supervisor Prof. Dr. Serhat Akin for his support, encouragement, advice and guidance throughout the study. Without his invaluable insights, this study would not have been accomplished. I really believe that I was lucky to work under his supervision.

I would like to thank my co-supervisor Prof. Dr. H. Şebnem Düzgün for her encouragement, advice and guidance.

I also extend my appreciation to the supervising committee members, Prof. Dr. Mahmut Parlaktuna and Prof. Dr. Nurkan Karahanoğlu for their guidance and insights. I would also like to express my gratitude to Prof. Dr. Şakir Şimşek and Assoc. Prof. Dr. Hakkı Gücüyener from the defense committee.

I would like to thank Asst. Prof. Dr. Çağlar Sinayuç for his time and advices. I also wish to thank my friend Tuğçe Bayram Ertürk for her invaluable friendship and for helping me with the CMG software. My special thanks are to Dr. Sevtaç Bülbül who is a friend and a teacher, at the same time, for her help, support, and encouragement. My thanks also go to everybody in the department of Petroleum and Natural Gas Engineering specially my dear friends; Dr. Reza Ettehadi Osgouei, Berkay Gürbüz, Aslı Gündoğar, Gizem Gül, Dalkhaa Chantsalma, Cihan Ertürk, Emre Özgür, and Göker Ertunç for their respect, friendship and encouragement.

I wish to express my special thanks to my friend Baran Tunç for his help with the coding part of this dissertation. It would have been really hard to complete that part without him.

I greatly acknowledge the Scientific and Technological Research Council of Turkey (TUBITAK) for providing a doctoral research fellowship.

I also would like to express my sincere gratitude to my friends Tolga and Eda Özgüneylioğlu for their invaluable friendship, encouragement, and endless help. They were always there whenever my family and I needed them.

Finally, I would like to express my deepest gratitude to my family for believing in me, even when I doubted myself. I would like to thank my parents for everything they gave me all through my life and I am really proud to be their son. My thanks also go to my sisters and brothers for their endless encouragement. I specially would like to thank my beautiful wife for her endless love, support and encouragement. Really without her by my side it would not be possible for me to complete this study. Last but not least I would like to thank my little daughter Esra for the fruit dishes she offered me while I was working.

TABLE OF CONTENTS

ABSTRACT iv

ÖZ vi

ACKNOWLEDGMENTS ix

TABLE OF CONTENTS xi

LIST OF TABLES xv

LIST OF FIGURES xvii

CHAPTERS

1. INTRODUCTION 1
   1.1 Dissertation Outline 3
2. LITERATURE REVIEW 4
   2.1 Introduction 4
   2.2 Multiple-Point Geostatistics 6
      2.2.1 Training Images 7
      2.2.2 The SNESIM Algorithm 9
   2.3 Previous Research Studies on MPG Simulation 13
   2.4 Uncertainty in the Hard Data 20
      2.4.1 Analysis of Hard Data Uncertainties 21
3. STATEMENT OF PROBLEM 24
4. METHODOLOGY 25
   4.1 The Proposed MPG Modeling Methodology 26
   4.2 3D Dataset 28
   4.3 Original Reservoir 31
      4.3.1 Simulation with SNESIM Algorithm 31
      4.3.2 Simulation with SGSIM Algorithm 35

4.3.3 Exporting Simulated Porosity Data 38
4.3.4 Upscaling the Porosity Data 38
4.3.5 Permeability Calculation 39
4.3.6 Building the Synthetic Original Reservoir 40
4.3.6.1 Model Construction Steps 40
4.3.6.2 Running the Model in CMG (IMEX Tool) 44
4.4 Sensitivity Analysis of the SNESIM Algorithm and the Methodology Proposed 47
4.4.1 Simulation of the Original Reservoir 47
4.4.2 Analysis of the Results 47
4.5 Sensitivity Analysis of the Variogram Model 48
4.6 Analysis of Training Image Uncertainty Impact on Reservoir Model 49
4.6.1 Parameterization of Original Training Image Structure and Modeling of 2D Training Images 49
4.6.1.1 One-Wave Channel Cases 51
4.6.1.2 Two and Three-Wave Channel Cases 52
4.6.2 Modeling of 3D Training Images 57
4.6.3 Construction of reservoirs using the generated Training Images 58
4.6.4 Analysis of Training Image Parameters Effects on Reservoir Model ... 58
4.6.4.1 Impact of Training Image Parameters on Cumulative Oil Production 58
4.6.4.2 Impact of Training Image Parameters on OOIP and ROIP 59
4.7 Analysis of Porosity Uncertainty Impact on Reservoir Model 59
4.7.1 Modeling of Porosity Uncertainty 59
4.7.2 Analysis of Porosity Uncertainty Impact 61
5. RESULTS AND DISCUSSIONS 63
5.1 Sensitivity Investigation of the SNESIM Algorithm and the Methodology Proposed 63
5.2 Sensitivity Investigation of the Variogram Model 66
5.3 Impact of Training Image Parameters on Reservoir Model 71

5.3.1 Effect of Training Image Parameters on Cumulative Oil Production.... 71
5.3.1.1 Effect of Z slice number..... 71
5.3.1.2 Effect of other parameters (channel number, wave number, and amplitude level)..... 76
5.3.1.3 Effect of parameters' variation 84
5.3.2 Effect of Training Image Parameters on OOIP and ROIP..... 89
5.4 Porosity Uncertainty Impact on Reservoir Model 98
5.4.1 Porosity Uncertainty Modeling 98
5.4.2 Analysis of Porosity Uncertainty Impact..... 101
5.4.2.1 Analyzing the Impact of Different Porosity Uncertainty values .. 103
5.4.2.2 Analysis of Porosity Uncertainty Impact Utilizing Different Upscaling Method 106
6. CONCLUSIONS..... 108
7. RECOMMENDATIONS 111
REFERENCES 113
APPENDICES
A. PARAMETERS DESCRIPTION OF THE USED ALGORITHMS 121
1. Parameters Description of SNESIM Algorithm 121
2. Parameters Description of SGSIM Algorithm..... 127
B. VARIOGRAM COMPUTATION..... 130
1. Hard Data (Facies) Variogram..... 130
1.1 Lag Number Selection 131
2. Simulated Realizations Variogram 132
2.1 Computation of the Omni-directional Variogram in 3D..... 133
C. PARAMETER FILES OF THE SIMULATION ALGORITHMS 134
1. SNESIM Algorithm Parameter File..... 134
2. SGSIM Algorithm Parameter File 137
D. DEVELOPED CODES 139
1. Python Code for Porosity Exporting..... 139

2. Visual Basic Code for Arithmetic Upscaling of Porosity Data 141
3. Visual Basic Code to Convert Training Images into Binary Files Having GSLIB Format 145
4. Visual Basic Code to Perform MCS for the Clustered Porosity Hard Data 151
5. Visual Basic Code to Extract the MCS Realizations From Excel into Text Files of the GSLIB Format 152
6. Visual Basic Code for Arithmetic And Median Upscaling of Porosity Data 154
E. CMG DATA OF THE ORIGINAL RESERVOIR 159
1. PVT and Relative Permeability Data 159
2. CMG Data File 161
CURRICULUM VITA 169

LIST OF TABLES

TABLES

Table 4. 1. Variogram model fitted to the experimental variogram of the hard data. Ranges are shown in feet 32

Table 4. 2. Values of the parameters used by SNESIM algorithm to model the original reservoir 33

Table 4. 3. Values of the parameters used by SGSIM algorithm to convert the original reservoir facies into porosity numbers 35

Table 4. 4. Variogram model fitted to the experimental variogram of the simulated realization shown in Figure 4.6. Ranges are in feet 35

Table 4. 5. The relation between the phase value and the number of waves in a channel 55

Table 4. 6. Modification of parameters and the corresponding number of the 2D training images generated 55

Table 4. 7. Modification of parameters and the corresponding number of training images generated 57

Table 4. 8. Descriptive statistics of the porosity hard data 62

Table 5. 1. The parameters of the Spherical variogram model fitted to the experimental variogram of the original reservoir. Ranges are shown in feet 67

Table 5. 2. The parameters of the Gaussian variogram model fitted to the experimental variogram of the original reservoir. 67

Table 5. 3. The parameters of the Exponential variogram model with lower ranges fitted to the experimental variogram of the original reservoir. 68

Table 5. 4. The parameters of the Exponential variogram model with larger ranges fitted to the experimental variogram of the original reservoir. 68

Table 5. 5. Comparison of the reservoirs generated using different variogram models with the original reservoir 71

Table 5. 6. Categories' proportions of the training images used to investigate the effect of Z slice number 75

Table 5. 7. Comparison of the reservoir models given in Figure 5.12 78

Table 5. 8. The sand and shale proportions of the original training image and the training image with the highest channel proportion among the developed training images 84

Table 5. 9. The training images that meet the thresholds of the parameters defined..... 97

Table 5.10. Probabilities of finding an error within or beyond the limits of the calculated distribution using 50 MCS 103

Table 5. 11. Descriptive statistics of the porosity data generated using different coefficient of variation (c.o.v) (i.e. uncertainty) values..... 104

Table 5. 12. The highest and lowest limits for the OOIP and ROIP of the reservoir models generated using different coefficient of variation (c.o.v) (i.e. uncertainty) values, and their corresponding percentage errors 105

LIST OF FIGURES

FIGURES

Figure 2. 1. Three different geological heterogeneities result in three similar variograms (Caers and Zhang, 2004) 5

Figure 2. 2. A 2D training image of size 250 x 250 representing a channel structure (Caers and Zhang, 2004) 7

Figure 2. 3. Examples of a non-stationary training image, A, and a stationary training image, B (Arpat, 2005) 8

Figure 2. 4. Illustration of how a data template is used to scan a TI for the frequencies of occurrence of observed outcomes for the central nodal value (Caers, 2002) 10

Figure 2. 5. Explanation of how unsampled nodes are simulated conditional to available data (Caers, 2002) 11

Figure 2. 6. A multiple-point simulation workflow (Liu, 2003; Liu et al., 2005) 12

Figure 2. 7. Simplified multiple-point simulation workflow illustration 12

Figure 2. 7. Sources of uncertainties (Duzgun, 2004) 21

Figure 4. 1. A flowchart of the proposed MPG modeling methodology 27

Figure 4. 2. Seismic (i.e. facies probability) data (p(sand|seis); (A), and p(mud|seis)); (B) 28

Figure 4. 3. Original training image used for modeling the original reservoir. The size of the training image is 200 × 200 × 5, each slice in the z - direction is shown here from top to bottom (Castro, 2007)..... 29

Figure 4. 4.The 46 wells of Stanford VI dataset showing the porosity property..... 30

Figure 4. 5. Histograms of the porosity and permeability data of Stanford VI data set..... 30

Figure 4. 6. Variogram model of the hard data..... 32

Figure 4. 7. Original reservoir's facies realization generated by SNESIM algorithm. The size of the model and the realization is 150 × 200 × 80 34

Figure 4. 8. The facies histograms of the hard data and the simulated reservoir realization illustrated in Figure 4.6..... 34

Figure 4. 9. Variogram model of the simulated realization shown in Figure 4.6 36

Figure 4. 10. Original reservoir's porosity realization generated by SGSIM algorithm..... 37

Figure 4. 11. The porosity histograms of the hard data and the simulated reservoir realization illustrated in Figure 4.9..... 37

Figure 4. 12. The method followed in exporting and upscaling the simulated porosity data 39

Figure 4. 13. The logarithmic relations between porosity and permeability hard data 40

Figure 4. 14. Relative permeability curves used in modeling the original reservoir..... 41

Figure 4. 15. 3D view of the reservoir constructed in CMG Builder tool showing the positions of the three wells used. The depth is given in feet 42

Figure 4. 16. Perforation of the eight K layer in wells 1 and 2. The depth is given in feet 43

Figure 4. 17. Production rate verses time plot of the original reservoir 45

Figure 4. 18. Cumulative oil production verses time plot of the original reservoir.... 45

Figure 4. 19. Summary of the methodology followed in the generation of the original reservoir model 46

Figure 4. 20. Summary of the proposed methodology for training image generating 50

Figure 4. 21. One-wave channel cases having high, medium, and low amplitudes and a fixed phase value..... 51

Figure 4. 22. Training images of size 200 x 200 x 1 pixels for the one-wave cases having high (A1 = 75 pixels), medium (A2 = 57 pixels), and low (A3 = 30 pixels) amplitudes and an equal phase (φ1 = φ2 = φ3 = 100 pixels). 52

Figure 4. 23. Two-wave channel cases having high, medium, and low amplitudes and a fixed phase values 53

Figure 4. 24. Three-wave channel cases having high, medium, and low amplitudes and a fixed phase values 53

Figure 4. 25. Training images of size 200 x 200 x 1 pixels for the two-wave cases having high (A1 = 75 pixels), medium (A2 = 57 pixels), and low (A3 = 30 pixels) amplitudes and an equal phase (φ1 = φ2 = φ3 = 50 pixels) 54

Figure 4. 26. Training images of size 200 x 200 x 1 pixels for the three-wave cases having high (A1 = 75 pixels), medium (A2 = 57 pixels), and low (A3 = 30 pixels) amplitudes and an equal phase (φ1 = φ2 = φ3 = 33.33 pixels) 54

Figure 4. 27. Training images of the one-wave channel cases. The channel having high; (A), medium; (B), and low amplitudes; (C) are shown. Up to three, five, and eight channels could be fitted to the fixed size of the training image for the high, medium, and low amplitude cases, respectively 56

Figure 4. 28. Two groups of the porosity hard data 61

Figure 5. 1. The OOIP values of the 50 generated reservoir models and their percentage errors with respect to the OOIP of the original reservoir model 64

Figure 5. 2. The ROIP values of the 50 generated reservoir models and their percentage errors with respect to the ROIP of the original reservoir model 64

Figure 5. 3. Goodness of fit details 65

Figure 5. 4. The Spherical variogram model fitted to the experimental variogram of the original reservoir 68

Figure 5. 5. The Gaussian variogram model fitted to the experimental Variogram of the original reservoir 69

Figure 5. 6. The Exponential variogram model with lower ranges fitted to the experimental variogram of the original reservoir 69

Figure 5. 7. The Exponential variogram model with larger ranges fitted to the experimental variogram of the original reservoir 70

Figure 5. 8. Medium Amplitude_ One Wave_ Three Channels Cases; (A). Exaggerated plot of the highlighted part of A; (B)..... 72

Figure 5. 9. Medium Amplitude_ Two Waves_ Two Channels Cases..... 73

Figure 5. 10. Low Amplitude_ Three Waves_ Seven Channels Cases..... 73

Figure 5. 11. Cumulative oil production versus time plots of the reservoirs generated using the four training images of Table 5.6 76

Figure 5. 12. Cumulative oil production for reservoirs generated using training images with different numbers of channels. The abbreviation (m_1_1_7Z) stands for medium amplitude_ one wave_ one channel_ 7 Z slices training image 78

Figure 5. 13. Cumulative oil production for reservoirs generated using training images having different numbers of channels, two waves, medium amplitude, and eight Z slices 79

Figure 5. 14. Cumulative oil production for reservoirs generated using training images having different numbers of channels, medium amplitude, three waves, and six Z slices 79

Figure 5. 15. Cumulative oil production for reservoirs generated using training images having different numbers of channels, medium amplitude, three waves, and six Z slices 80

Figure 5. 16. Cumulative oil production for reservoirs generated using training images having different numbers of channels, low amplitude, one waves, and five Z slices..... 81

Figure 5. 17. Cumulative oil production for reservoirs generated using training images having different numbers of channels, low amplitude, one waves, and seven Z slices..... 81

Figure 5. 18. Cumulative oil production for reservoirs generated using training images having different numbers of channels, low amplitude, two waves, and eight Z slices 82

Figure 5. 19. Cumulative oil production for reservoirs generated using training images having different numbers of channels, low amplitude, three waves, six Z slices 82

Figure 5. 20. The high amplitude cases fitted to the limited size training image 83

Figure 5. 21. (Effect of channel's number): medium amplitude_ one channel_ eight Z slices cases; (A), medium amplitude_ two channels_ eight Z slices cases; (B), medium amplitude_ three channels_ eight Z slices cases; (C) 85

Figure 5. 22. (Effect of wave's number): low amplitude_ one wave_ seven Z slices cases; (A), low amplitude_ two waves_ seven Z slices cases; (B), low amplitude_ three waves_ seven Z slices cases; (C)..... 86

Figure 5. 23. (Effect of Z slices' number): medium amplitude_ two waves_ five Z slices cases; (A), medium amplitude_ two waves_ six Z slices cases; (B), medium amplitude_ two waves_ seven Z slices cases; (C)..... 87

Figure 5. 24. (Effect of amplitude): three wave_ five channels_ five Z slices cases; (A), three wave_ five channels_ six Z slices cases; (B), three wave_ five channels_ eight Z slices cases; (C)..... 88

Figure 5. 25. OOIP and ROIP values for the reservoirs modeled using training images having different numbers of Z slices and one channel containing one wave having medium amplitude (m) level 89

Figure 5. 26. OOIP and ROIP values for the reservoirs modeled using training images having different numbers of Z slices and four channels each contains three waves having medium amplitude (m) level 90

Figure 5. 27. OOIP and ROIP values for the reservoirs modeled using training images having different numbers of Z slices and four channels each contains two waves having low amplitude (L) level 90

Figure 5. 28. OOIP and ROIP values for the reservoirs modeled using 6 Z slice-training images having different numbers of channels; each of these channels contains two medium amplitude waves 91

Figure 5. 29. OOIP and ROIP values for the reservoirs modeled using 8 Z slice-training images having different numbers of channels; each of these channels contains two low amplitude waves 92

Figure 5. 30. OOIP and ROIP values for the reservoirs modeled using 6 Z slice-training images having different numbers of channels; each of these channels contains three low amplitude waves 92

Figure 5. 31. OOIP and ROIP values for the reservoirs modeled using 7 Z slice-training images having a single channel with different numbers of medium amplitude waves 93

Figure 5. 32. OOIP and ROIP values for the reservoirs modeled using 8 Z slice-training images having eight channels; each of these channels contains different numbers of low amplitude waves 93

Figure 5. 33. OOIP and ROIP values for the reservoirs modeled using 5 Z slice-training images having three one-wave channels with different amplitude levels 94

Figure 5. 34. OOIP and ROIP values for the reservoirs modeled using 6 Z slice-training images having three two-wave channels with different amplitude levels 94

Figure 5. 35. The OOIP values of the reservoirs generated by using the developed 368 training images and their percentage errors with respect to the OOIP of the original reservoir 95

Figure 5. 36. The ROIP values of the reservoirs generated by using the developed 368 training images and their percentage errors with respect to the ROIP of the original reservoir 96

Figure 5. 37. Percentage error associated with the prediction of OOIP using the developed training images after excluding the cases that fail to meet the defined thresholds 96

Figure 5. 38. Percentage error associated with the prediction of ROIP using the developed training images after excluding the cases thatail to meet the defined thresholds 97

Figure 5. 39. Porosity histogram of the first MCS realization 99

Figure 5. 40. Porosity histogram of the thirty-first MCS realization 99

Figure 5. 41. Variogram of the first MCS realization 100

Figure 5. 42. Variogram of the eleventh MCS realization 100

Figure 5. 43. The OOIP values of the 50 reservoir models generated using the 50 porosity MCS and their percentage errors with respect to the OOIP of the original reservoir model 102

Figure 5. 44. The ROIP values of the 50 reservoir models generated using the 50 porosity MCS and their percentage errors with respect to the ROIP of the original reservoir model 102

Figure 5. 45. The OOIP and ROIP values corresponding to reservoir models generated using different coefficient of variation (c.o.v) (i.e. uncertainty) values 104

Figure 5. 46. The percentage errors in OOIP and ROIP values corresponding to reservoir models generated using different coefficient of variation (c.o.v) (i.e. uncertainty) values with respect to the original reservoir model 105

Figure 5. 47. The OOIP and ROIP values corresponding to reservoir models generated with 50 MCS using both the median and average upscaling methods. The black arrows show the maximum and minimum differences between the results of the upscaling methods 107

CHAPTER 1

INTRODUCTION

The scarcity of geological subsurface information is one of the most significant sources of uncertainty in a reservoir modeling process. As a result, stochastic simulation techniques are developed to reduce such kind of uncertainty. These techniques generate multiple equiprobable reservoir models while maintaining the geological structure. The traditional geostatistical modeling techniques use the variogram model to represent the spatial heterogeneity or continuity and the kriging for spatial interpolation. Thus, these traditional techniques are limited to the reproduction of two-point statistics. However, modeling complex geological structures such as channels, which are curvilinear formation meandering in 3D space, requires multiple-point correlation. Thus, the traditional two-point based geostatistical modeling techniques, such as the sequential indicator simulation (Deutsch and Journel, 1998), fail to capture complex geological structures (Journel, 1992; Caers and Journel, 1998; Strebelle, 2000; Strebelle and Journel, 2001; Caers and Zhang, 2004). On the contrary, the multiple-point geostatistics (MPG) simulation technique proposed by Guardiano and Srivastava (1993) is proven to be a powerful technique in modeling such complex structures (Journel, 2005). However, the technique of Guardiano and Srivastava (1993) was central processing unit (CPU) demanding, in other words, it was processor demanding. Thus, MPG was not widely used until the implementation of the search tree by Strebelle (2000). In addition, Strebelle (2000) developed the single normal equation simulation (SNESIM) algorithm, a non-iterative sequential simulation algorithm that obtains multiple-point statistics from conceptual geological models called “training images” and anchors them to the subsurface well-log, seismic and production data (Feyen and Caers, 2006).

In the last two decades, a lot of work was conducted to improve MPG simulation techniques. As a result, different MPG algorithms were developed. Some of these Algorithms are SNESIM (Strebelle, 2000; Strebelle, 2002), SIMPAT (Arpat, 2005; Arpat and Caers, 2007), FILTERSIM (Zhang, 2006), IMPALA (Straubhaar et al, 2011), and CCSIM (Tahmasebi et al, 2012). Among these algorithms SNESIM, which models only categorical variables, is used in this study.

A training image (TI) is defined as the representation of expected subsurface heterogeneities believed to exist in the area being modeled and not necessarily carry any locally accurate information (Strebelle, 2000; Strebelle and Journel, 2001; Arpat and Caers, 2007). However, a training image should reflect a spatial continuity style similar to the actual phenomenon (Arpat and Caers, 2007). Training images should be stationary, i.e. the spatial patterns are reasonably homogeneous all over the training image (Strebelle and Zhang, 2005; Maharaja, 2008). However, some implementations of MPG provided tools to use non-stationary training images (Caers and Zhang, 2004; Arpat, 2005; Liu 2006; Strebelle, 2006; Wu, 2007; de Vries et al., 2009). training images are obtained from nearby field analogues, outcrop photographs as well as interpretation of actual data such as cores, well logs, and seismic (Strebelle and Remy, 2005; Boucher, 2009; Barrera et al, 2005; Okabe and Blunt, 2005). In addition, training images are hand-drawn by geologists, then numerically digitized (Strebelle and Remy, 2005) or created using unconditional object-based modeling techniques (Strebelle and Remy, 2005; Arpat and Caers, 2007).

Selection of the right training image that represents the target spatial phenomenon is crucial for an effective use of MPG simulation technique (Strebelle, 2002; Boisvert et al., 2007). Although, a lot of work was conducted to improve MPG simulation techniques the use of the optimum training image remains a challenge. The uncertainty in the selection of the most representative training image for the data under consideration is addressed by Boisvert et al. (2007) and Arslan (2005). However, the construction of training images involves uncertainty too. Strebelle

(2000) has investigated some parameters that cause such type of uncertainty. He studied the sensitivity of MPG simulation to the size of the training image, width of the structure displayed by the training image, and the rotation of the training image. Nevertheless, the literature addressing the issue of training image construction and the uncertainty associated is very limited.

1.1 Dissertation Outline

This dissertation is divided into seven chapters. In Chapter 2, a brief literature review about the limitation of the traditional two-point based geostatistical modeling techniques is provided. Then, the Multiple-point geostatistics (MPG) simulation technique and its Algorithm, the Single Normal Equation Simulation (SNESIM) are introduced. After that, summary of the past work related to MPG simulation is presented. Following that, brief information about the uncertainty in hard data, its sources, and the way it is analyzed is presented.

The main objectives of this research are provided in Chapter 3. Next, a detailed description of the methodology followed in this dissertation is presented in Chapter 4. This chapter includes four main parts. The first part covers the method followed in the generation of an original hypothetical reservoir using a proposed MPG modeling methodology. The second part provides information about a sensitivity analysis of the proposed method. The third part explains the steps followed in the construction of training images and the modeling of their corresponding reservoirs. In the last part hard data uncertainty analyzing method is presented. The results of this work and their discussions are offered in Chapter 5. In Chapter 6 the main conclusions of the study are drawn. Finally, some recommendations for future work are provided in Chapter 7.

CHAPTER 2

LITERATURE REVIEW

2.1 Introduction

In the past, reservoirs were modeled by simplistic layer cake models. These models were not producing accurate flow response predictions. Afterward, regression methods were developed to represent reservoir layers by interpolating the data recorded from wells (Strebelle, 2000). Among these the kriging method is the most popular one. It depends on a prior model of spatial correlation called the variogram model. However, in reservoir modeling the kriging method have smoothing problem which may results in overestimating the low petrophysical values and under-estimating the high ones (Arpat, 2005).

Aiming at correcting the smoothing effect of kriging, Journel (1974) introduced the stochastic simulation. This simulation allowed the reproduction of spatial variance predicted by the variogram model. Based on that a number of simulation algorithms including the sequential simulation were developed (Barrera, 2006). However, these variogram-based techniques fail to produce complex spatial patterns such as curvilinear structures and fractured systems because they are based on the correlation of only two points (Caers and Zhang, 2004). Figure 2.1 shows a good example of such failure since three different structures resulted in three similar variograms.

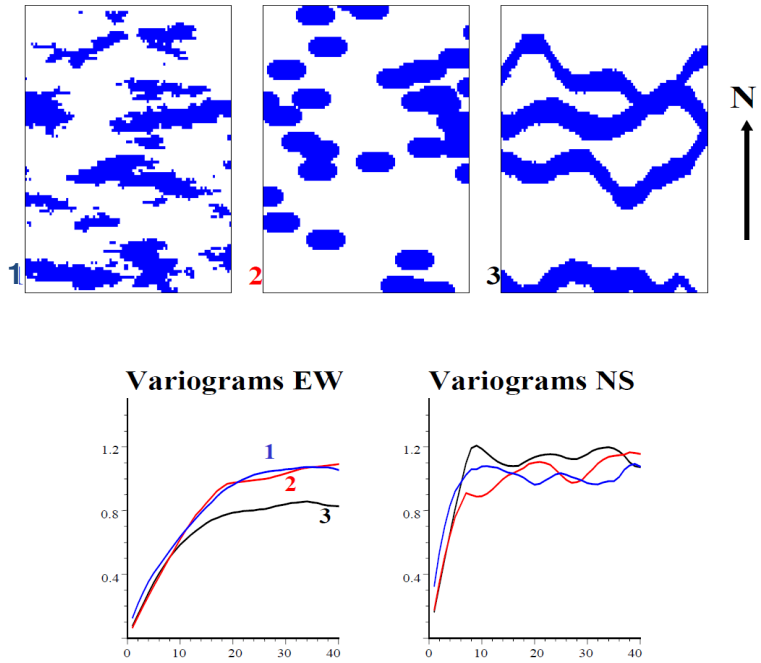

Figure 2. 1. Three different geological heterogeneities result in three similar variograms (Caers and Zhang, 2004)

From another point of view, there are two main techniques to model a spatial distribution, namely, pixel-based and object-based techniques. The former simulate each node of reservoir model one pixel at a time and all the unsampled nodes are visited sequentially along a random path. Then, based on both hard and soft data, the conditional probability distribution function of a given node is estimated. The simulated value at each node is recorded as a hard data for the simulation of the subsequent unknown nodes. These pixel-based techniques are very flexible and easy to condition to any conditional data since they simulate pixel by pixel. However, most of the pixel-based techniques fail to represent complex geological structures such as meandering channels because they are based on the traditional two-point variogram model (Liu, 2003). The most notable pixel based techniques known to produce complex geological structures are: simulated annealing (Farmer, 1988; Deutsch, 1992), post-processing iterative algorithm (Srivastava, 1992), stochastic

simulation using neural networks (Caers and Journel, 1998), and extended normal equations algorithm (Guardiano and Srivastava, 1993). However, these techniques have other shortcomings, such as the convergence problems and extreme random access memory (RAM) and CPU demand, which render them impractical (Strebelle, 2000).

On the other hand, the object-based techniques introduced by Stoyan et al. (1987), and Haldorsen and Damsleth (1990) perform a simulation by adding different geobodies one after another to the simulated field. Every added geobody is accepted, rejected, or modified based on some objective functions. The object-based techniques are proven to be good at the reproduction of crisp shapes which are used in reservoir characterization since they are based on parameters provided by prior vision of the questioned geobody (Liu, 2003). However, these techniques are time consuming and often CPU demanding especially when intensive well data have to be honored as they are iterative techniques (Eskandari, 2008; Liu, 2003; Strebelle, 2000). Moreover, the algorithms used for the object-based techniques have to be modified when dealing with different types of objects or reservoirs because every single object has its own specific parameterizations (Eskandari, 2008; Strebelle, 2000).

2.2 Multiple-Point Geostatistics

Due to the limitation of the traditional modeling techniques that are based on two-point statistics (i.e. variogram) several studies (Strebelle, 2000; Strebelle, 2002; Caers and Zhang, 2004; Karishnan and Journel, 2003; Barrera, 2005; Journel, 2005; Lima, 2005; Journel and Zhang, 2006) have suggested the newly developed Multiple-Point Geostatistics (MPG) simulation technique which is based on a training image (TI) concept. By combining the strengths of both pixel-based and object-based techniques, MPG method has become one of today's most important geostatistical modeling techniques. MPG was first introduced by Journel (1992) and was initially coded by Guardiano and Srivastava (1993). This method was proven to be extremely CPU

demanding because it requires complete scanning of the TI for every new data event used to inform a node being simulated. However, this changed with the development of the search tree technique proposed by Strebelle (2000).

2.2.1 Training Images

MPG method requires a training image (TI) such as the one shown in (Figure 2.2). A training image is defined as a numerical representation of the geological structure and patterns believed to exist in the area being modeled and not necessarily carry any locally accurate information (Strebelle, 2000; Strebelle and Journel, 2001; Arpat and Caers, 2007). However, a training image should reflect a spatial continuity style similar to the actual phenomenon (Arpat and Caers, 2007). In other words, a training image is used to deliver prior geological concepts about the geometry of the questioned heterogeneities.

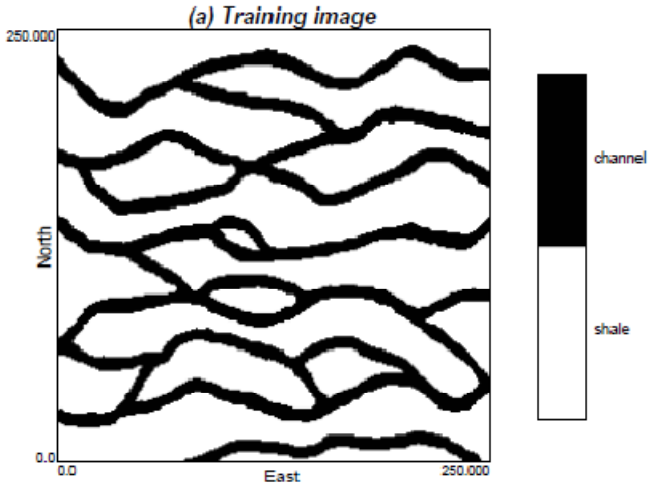

Figure 2. 2. A 2D training image of size 250 x 250 representing a channel structure (Caers and Zhang, 2004)

Training Images are obtained from nearby field analogues, outcrop photographs as well as interpretation of actual data such as cores, well logs, and seismic (Strebelle and Remy, 2005; Boucher, 2009; Barrera et al, 2005; Okabe and Blunt, 2005). Training images are hand-drawn by geologists, then numerically digitized (Strebelle and Remy, 2005) or created using unconditional object-based simulations such as the ones proposed by Deutsch and Wang (1996), Holden et al. (1998), Viseur (1999), and Maharaja (2008). Training images should be stationary, i.e. the spatial patterns are reasonably homogeneous all over the training image (Strebelle and Zhang, 2005; Maharaja, 2008). However, some implementations of MPG provided tools to use non-stationary training images as well (Caers and Zhang, 2004; Liu 2006; Strebelle, 2006; Wu, 2007; de Vries et al., 2009) (Figure 2.3).

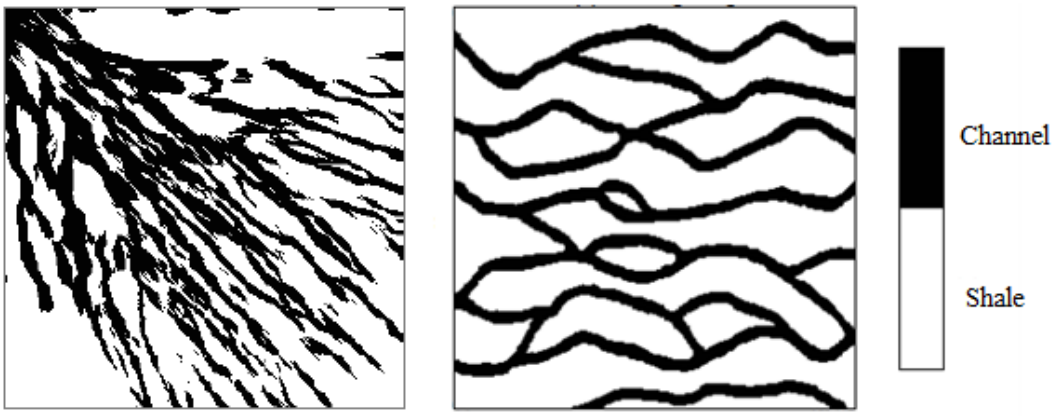

Figure 2. 3. Examples of a non-stationary training image, A, and a stationary training image, B (Arpat, 2005)

Like the variogram model the training image provides statistics relating unsampled value to conditioning data, but in jointly multiple locations. In other words, MPG technique accounts correlations between three or more locations at a time. Thus, MPG technique is capable of producing complex curvilinear geological structures accurately (Strebelle, 2002). The simulation carried out by the MPG technique is

taking the patterns from the training image and anchoring them to the actual data (Liu, 2003; Liu et al, 2005). This process when first proposed by Guardiano and Srivastava (1993) was slow and CPU demanding because it was calling for rescanning of training image for each new data event. However, the development of the Single Normal Equation Simulation algorithm (SNESIM) of (Strebelle, 2000), which scans the training image only once, significantly speeded up the MPG simulation process and decreased its CPU demand.

2.2.2 The SNESIM Algorithm

SNESIM was first developed by Strebelle (2000) to carry out pattern reproduction conditional to hard data. Later SNESIM has been modified to account for auxiliary constraints such as those presented by seismic data (Strebelle et al., 2002). SNESIM deals only with categorical variables. It scans a training image only once to retrieve the frequencies of occurrence of observed outcomes for the central nodal value utilizing a template of neighboring conditioning data. The probabilities found are then stored in a data structure called "search tree". This search tree allows fast storage and retrieval of probabilities corresponding to the actual data events encountered during a sequential simulation (Strebelle, 2002). Figure 2.4 illustrates an example of such search tree. In order to construct the search tree of Figure 2.4, a given data template is used to scan the training image in which the yellow and the white nodes represent the channel and the non-channel structures, respectively. For example, in level '0' the training image is scanned to calculate the probabilities of finding a channel or non-channel structures using only the central node 'u' of the data template. In other words, no conditional data (no CD) is used when scanning the training image at this stage. In this case, the probability of finding a channel structure (yellow node) in the training image is 11 while that of the non-channel structure (white node) is 14. Following that the training image is scanned using the central node 'u' and one conditional data (1 CD) of the data template. In this case, the training image is scanned for the probabilities of finding: 1) channel structure in u when the

conditional data is also channel, 2) non-channel structure in u when the conditional data is channel, 3) channel structure in u when the conditional data is non-channel, 4) non-channel structure in u when the conditional data is also non-channel. Next, the training image is scanned similarly with two, three, and four conditional data of the data templates.

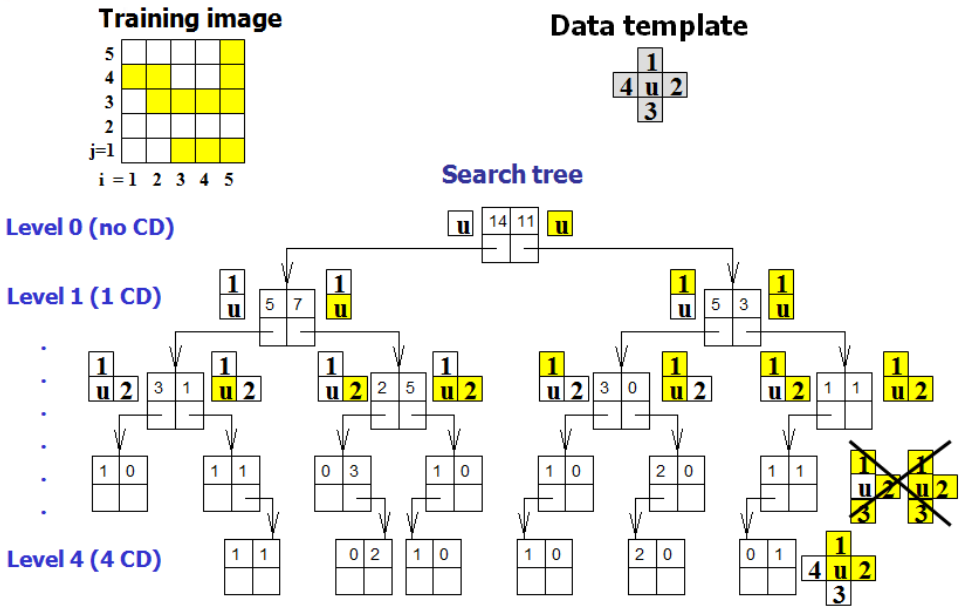

Figure 2. 4. Illustration of how a data template is used to scan a training image for the frequencies of occurrence of observed outcomes for the central nodal value (Caers, 2002)

In MPG the hard data are fixed at their nodal locations and they are never changed. Then the unsampled nodes are sequentially visited and simulated conditional to the previously simulated values as well as the hard data (Figure 2.5). In the case of soft (e.g. seismic) data conditioning the MPG simulation is performed in two steps (Liu, 2003; Liu et al., 2005). First, the soft data are extracted and stored in the search tree each in its location as in the case of hard data. Then, both the soft and hard data are

used as conditional data while performing the sequential simulation. SNESIM reproduces the structure of the training image and at the same time it honors the available hard and soft data. Figure 2.6 illustrates the workflow of MPG simulation conditional to both hard and soft data. The workflow then consists of three main parts: $P(A|B), P(A|C)$, and $P(A|B,C)$ where "A" stands for the value at location u to be simulated, "B" stands for geological information and hard data, and "C" stands for soft data (Liu, 2003; Liu et al., 2005). A more general and simplified illustration of MPG simulation workflow for such a case is given in Figure 2.7. For further details on SNESIM algorithm, the reader is referred to Strebelle (2000).

A user-friendly interface of SNESIM algorithm is available in an open-source computer package called "Stanford Geostatistical Modeling Software" (SGeMS). SGeMS is developed at Stanford University as its name implies and particularly by the Stanford Center for Reservoir Forecasting (SCRF). A description of the SNESIM algorithm parameters is given in Section 1 of Appendix A. SGeMS implements several geostatistics algorithms for modeling earth systems. Some of these algorithms are: Sequential Gaussian Simulation (SGSIM), Filter-based Simulation (FILTERSIM), and Training Image Generator (TIGENERATOR).

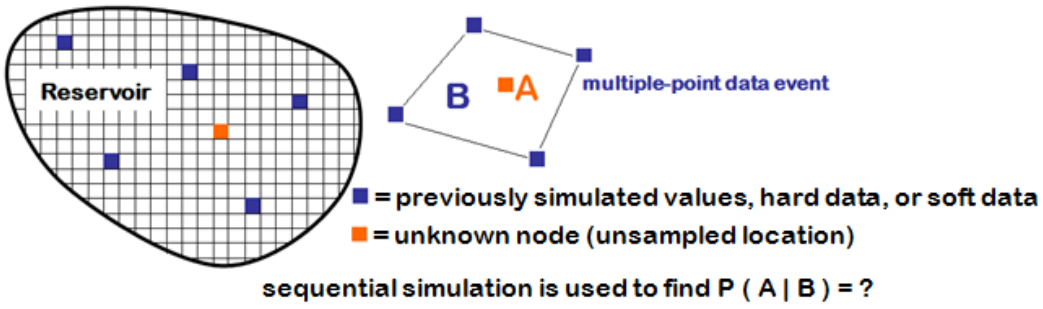

Figure 2. 5. Explanation of how unsampled nodes are simulated conditional to available data (Caers, 2002)

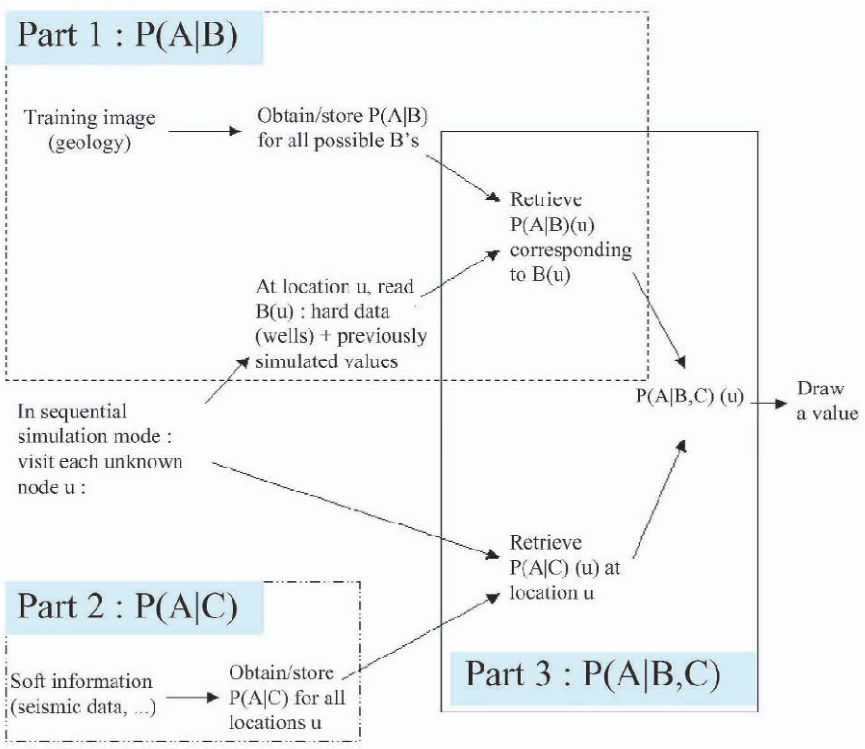

Figure 2. 6. A multiple-point simulation workflow (Liu, 2003; Liu et al., 2005)

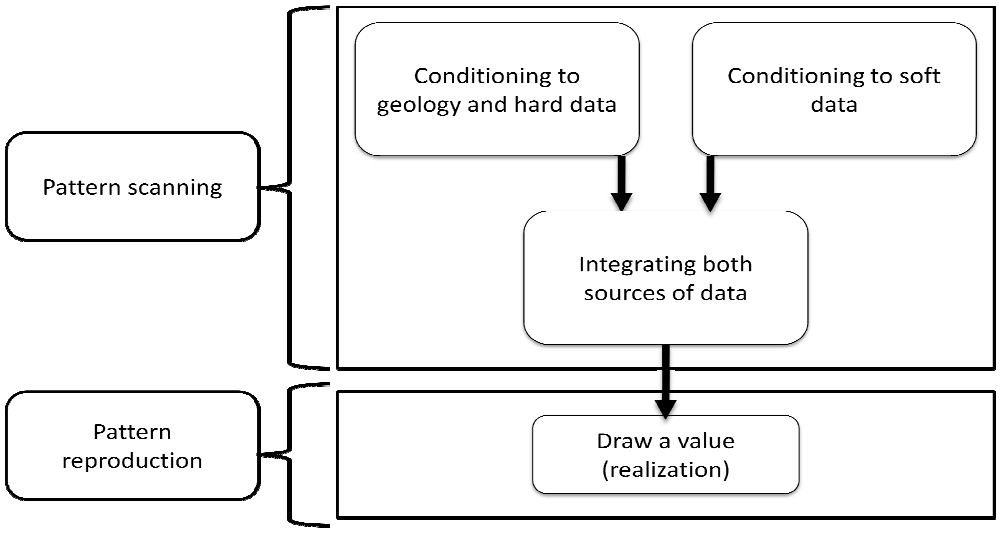

Figure 2. 7. Simplified multiple-point simulation workflow illustration

2.3 Previous Research Studies on MPG Simulation

Previous research studies on MPG simulation can be grouped into five main topics:

1. The use of non-stationary training images in MPG simulation (Caers and Zhang, 2004; Arpat, 2005; Mahraja, 2005; Strebelle and Zhang, 2005, Liu 2006; Strebelle, 2006; Wu, 2007; Chugunova and Hu, 2008; de Vries et al., 2009).
2. Development of new MPG simulation algorithms (Strebelle and Remy, 2005; Arpat, 2005; Arpat and Caers, 2007; Zhang, 2006; Straubhaar et al., 2011; Tahmasebi et al, 2012).
3. Applications of MPG (Liu et al.,2002; Harding et al., 2005; Okabe and Blunt, 2004; Feyen and Caers, 2005; Okabe & Blunt, 2005; Feyen and Caers, 2006; Zhang, 2008; Du et al., 2009; Hajizadeh et al., 2011; Mariethoz et al., 2011; Zhang et al., 2005; Comunian et al., 2011; Comunian et al., 2012; dell'Arciprete et al., 2012).
4. Reduction of RAM and CPU demand (Huysmans and Dassargues, 2011; Huysmans and Dassargues, 2012; Zhang et al., 2012).
5. Generation and selection of training images (Arslan, 2005; Boisvert et al., 2007; Boisvert et al., 2008; Huysmans and Dassargues, 2010; Eskandari, 2008).

Some of these studied are summarized in the following paragraphs.

Caers and Zhang (2002) in their work illustrated the differences between the traditional variogram and MPG techniques. Then, they pointed out the basic concepts in which reservoir modeling and thus MPG are based on. Briefly, these concepts are Stationarity and Ergodicity. Stationarity is the similarity repetition of the data to be collected. The Ergodicity, on the other hand, explains the expected fluctuation of the collected data (statistics) and the effect they have on the model building. Finally, the authors considered a very important point which is non-stationary models. As they have cited, actual reservoirs may contain non-stationary elements such as vertical proportion variations. Thus, the need for non-stationary reservoir models arises.

Then, they illustrated how to construct a non-stationary reservoir model from a stationary training image.

Liu et al. (2002) presented a methodology for generating stochastic models of fracture systems in reservoirs. In their work it was proven that the most important characteristics of the patterns corresponding to different classes of fracture systems can be reliably detected using multiple point statistical measures. Then, it was suggested to perform a detailed geological characterization of fracture outcrops. The essence of the fracture patterns described in those outcrop exposures are captured through multiple point statistical measures. Then, when modeling a target reservoir the analog model suitable for that reservoir can be constructed using the multiple-point statistical measures characteristic for that system. These patterns are then imposed on the model for the target reservoir using a growth-based stochastic simulation technique. The stochastic models can be constrained to all available information in the form of conditioning well data, seismic maps, rock mechanical strength data etc.

Strebelle et al. (2002) stated that deepwater turbidite reservoirs represent a growing number of hydrocarbon targets for major oil companies. Due to the high drilling and production costs associated with such reservoirs, however, the need for reliable architecture modeling increased. Thus, integration of geological information beyond two-point variogram reproduction becomes critical in order to quantify more accurately heterogeneity and assess realistically the uncertainty of oil recovery. Then, they proposed a practical approach to integrate large-scale seismic amplitude data into a finer scale geological model. They generated a TI depicting sinuous sand bodies using a non-conditional object-based simulation algorithm. Disconnected sand bodies are interpreted from seismic amplitude data using a principal component cluster analysis technique. In addition, a map of local sand probabilities obtained from a principal component proximity transform of the same seismic is generated. MPG then simulates multiple realizations of channel bodies constrained to the local

sand probabilities, partially interpreted sand bodies, and well-log data. The resulting model reflected the prior geologists' vision of the subsurface architecture while honored the well and the seismic data. Moreover, the authors proved that computer RAM and the time needed to run the resulting model are comparable to those of the traditional variogram-based algorithms.

Chevron Texaco's earth science community by using real case example proved that MPG method results in models that represent complex reservoir facies very well (Harding et al., 2004). They followed a four-step-procedure that can be summarized as follows:

- MPG algorithm has been improved to permit a single training image, which is constructed for a particular geological environment to model multiple stratigraphic zones.
- A relatively large number of facies have been employed; this enabled them to represent the complexities of the reservoir in the model.
- A workflow has been used which allowed the integration of geological facies' geometry, associations and heterogeneity with varying azimuth, and facies proportions.
- The workflow allows distinctly different geological scenarios to be modeled, permitting an improved understanding of the impact of uncertainty in facies distribution on the reservoir continuity and pore volume.

In their work Strebelle and Remy (2005) stated that the flow performance of reservoir heterogeneity is primarily controlled by the spatial distribution of the depositional facies. Thus, it would be better to model these depositional facies first, then populating each simulated facies with its corresponding specific porosity and permeability distributions. They also presented a new version of the MPG simulation algorithm; SNESIM, with integrated post-processing. In that newly proposed algorithm, the method used to gather local conditional facies probability distributions was modified to increase the number of conditioning data which were actually used

in that gathering process. This new estimating method has removed a great number of anomalies from MPG models. In other words, it has removed simulated patterns that were not present in the training image. Then a post-processing technique is proposed to reduce the number of the remaining anomalies. Finally, by applying the post-processing technique to a 2D horizontal section of a fluvial reservoir the authors proved that computer RAM and the time needed to run the new modified SNESIM are comparable to those of the original SNESIM, though the number of anomalies decreases dramatically.

Feyen and Caers (2005) indicated that MPG technique's potential to characterize subsurface heterogeneity for hydrogeological applications in a wide variety of complex geological settings is very high. Geological structures or features such as sand channels or clay lenses often constitute preferential flow paths or obstacles to flow. Thus, it is very important to accurately represent and locate these structures when predicting flow and transport in porous media. However, the authors claimed that further analysis is needed to systematically evaluate and quantify the effects of the different levels of geological uncertainty on groundwater flow and transport predictions in multi-modal settings.

Okabe and Blunt (2005) used MPG simulation on a 2D thin section image to generate a 3D pore space image with an assumption of isotropy for orthogonal planes. The method is tested on sandstone and carbonate samples. Permeability is predicted directly on the 3D image using the Lattice Boltzmann Method (LBM). This method is an extended version of MPG approach that was developed by Strebelle et al. (2002). It provides an important input for the creation of geologically realistic networks for pore-scale modeling to predict multiple flow properties. The major extension of this method is the rotation of the measured statistics by 90 degrees, which allowed the authors to generate a 3D structure. This process consists of three steps:

- Extracting multiple-point statistics from a training image,
- Probability calculation for each orthogonal plane using conditioning data,

- Pattern reproduction using the probability weighted by number of conditioning data on each plane.

The LBM provides a good approximation for the solutions of Navier-Stokes equations using a parallel and efficient algorithm that readily accommodates complex boundaries as encountered in porous media. This method is a suitable way to assess the structures if no microtomographic image of the rock is available.

In addition, Feyen and Caers (2006) studied the problem of quantifying the geological uncertainty for groundwater flow and transport modeling in complex geological settings. A two-step procedure was employed to generate realizations of the hydraulic property distributions. In the first one the realizations of the facies architecture were generated using MPG techniques. In the second the facies were populated with hydraulic property distributions generated using two-point geostatistical methods. In both steps they accounted for the uncertainty inherent in the selection of the statistical model and in the estimation of global statistics. Spatial bootstrap was used to estimate the uncertainty of unknown statistical parameters. With a comprehensive numerical analysis the authors evaluated the effect of different geological uncertainty scenarios on the predictions of a groundwater flow and transport model. Their results indicated that the level of facies uncertainty affected the variability of the head predictions largely.

Du and Zhang (2009) simulated porosity data using the continuous MPG algorithm; FILTERSIM of Zhang (2006). FILTERSIM simulates both continuous and categorical variables based on filters. In their proposed method Du and Zhang used nine filters to scan a 3D training image. The local patterns captured by the filters at the locations of each node in the 3D space are characterized by nine score values corresponding to the nine filters used. The patterns with close filter scores are stored in a group called “prototype”. The prototype of each group of patterns is given a score equal to the average of the filters’ scores that fall in that group (Wu et al., 2007; Zhang, 2006). After that and during simulation, the prototype with the score closest to

the conditioning data event is extracted. Then, a training pattern is drawn randomly from that prototype and pasted back onto the simulation grid. The results showed that this method generates the structures and characteristics of porosity in the used training image well and more accurately than the SGSIM results.

Huysmans and Dassargues (2010) gave details on how a training image can be constructed based on geological and hydrogeological field data. Besides, they explained how MPG can be applied to determine the impact of complex geological heterogeneity on ground water flow and transport in a real aquifer. In addition, the significant effect of small-scale sedimentary heterogeneity on the calculation of a contaminant concentration distribution was confirmed by a hypothetical case. The outputs showed that using a homogeneous model to predict the contaminant plume emigration and concentration would yield erroneous results. So, it was concluded that heterogeneity encountered in ground water contamination studies should be taken into account.

Hajizadeh et al. (2011) proposed a stochastic method that uses MPG technique for the construction of a 3D pore structure from a 2D thin section training image. In this method, the 3D porous media is constructed layer by layer using successive 2D MPG simulations coupled with multi-scale conditioning data extraction procedure. SNESIM algorithm is utilized as the simulation tool. Application of the method for a sample Berea sandstone confirmed that the obtained 3D realization preserved the pore space patterned of the thin section training image. The advantage of this method is its computational efficiency when compared with other similar methods such as that of Okabe and Blunt (2004). However, this method can only be applied to media with repeated multiple-point statistics. In other words, the training image used must be stationary because SNESIM algorithm relies on the assumption of stationary statistical properties.

Huysmans and Dassargues (2011) applied a method that uses MPG to perform a direct simulation for edge properties in order to model irregularly shaped surfaces

such as clay drapes. The edge properties in this method are used instead of pixel values. The proposed method allowed modeling reservoirs of aquifers having irregular shapes with considerable computational time reduction when compared with the traditional MPG. In other words, it decreased the demand for CPU and RAM significantly. Thus, this method is very valuable for 3D application of MPG.

Mariethoz et al. (2011) proposed a multiple-point super-resolution mapping method. This method requires an image of a coarse scale structure as the only input parameter. This image is treated as the training image; therefore, it should be large enough to contain a diversity of patterns. Then, MPG method is used to infer the fine scale structure from the coarse ones based on the scale invariance properties' assumption. This method generated images having the same properties as their coarse ones, both in terms of fractal dimensions and reproduction of spatial statistics. In addition, it is able to deal with both continuous and categorical variable and even can be generalized to multivariate problems. The only limitation of this method is that it only produces self-similar structures, but that is not always the case for natural images.

Huysmans and Dassargues (2012) used a combined approach of MPG and edge properties to include clay drapes in a flow model. Instead of representing clay drapes by pixels they were represented as grid cell edge properties. This allowed the reduction of CPU and RAM needed for modeling large grid cell sizes. The proposed method also allowed the simulation of realistic spatial distribution of the clay drape occurrence based on a field-based training image. Besides, it was proven to be efficient for integrating field-structures in a larger scale model.

Tahmasebi et al. (2012) proposed a methodology that utilizes MPG but without the need for pattern database and a small data event. This method works with both categorical and continuous training images. In addition, it is based on a cross-correlation function for the similarity of the generated pattern and the used training image. To apply this method a newly developed algorithm; cross-correlation simulation (CCSIM), is used. CCSIM algorithm is tested with different training

images and the results indicated its significant reduction of CPU and RAM demand when compared to previous algorithms. In addition, CCSIM is able to generate realizations of reservoirs with accurate conditioning and continuity.

Zhang et al. (2012) also developed a method that decreased the CPU and RAM demand when simulating reservoirs using MPG. A compact search tree containing the same information as the first search tree proposed by Strebelle (2000) was developed. However, it reduced memory cost by one order of magnitude. That is because the compact tree decreases the long non-branching sequences to only their essential information such as the common properties and number of repeating nodes. Due to that the proposed method accelerates MPG simulation significantly. Thus, allows the simulation of field-scale and complex 3D facies models.

A lot of work was conducted to improve MPG simulation techniques. The work conducted concentrated mainly on: the use of non-stationary training images (TIs) in MPG simulation, development of new MPG simulation algorithms, applications of MPG, reduction of RAM and CPU demand, and the generation and selection of training images. However, the generation and selection of training images have not been thoroughly studied yet. In other words, the literature addressing the issue of training image generation and the uncertainty associated is very limited. One part of the present study is devoted to analyze and quantify the impact of such uncertainty on reservoir models.

2.4 Uncertainty in the Hard Data

The hard data have some sorts of uncertainty (Figure 2.8). These uncertainties are either due to the physical phenomenon that is inherently random or errors in the predictions and estimations of the real world conditions (Ang and Tang, 1984). The inherent uncertainty is a state of nature so it cannot be decreased. However, the estimation (or modeling) uncertainty is possibly reduced by the use of more accurate

models or the acquisition of more data (Ang and Tang, 1984). The error in model prediction is subdivided into systematic error and random error. The systematic error or simply the bias is due to factors that are not taken into account in the predicting model that are likely to affect the estimation somehow (Duzgun, 2004). The estimations based on core samples analyzed in laboratory have systematic error, because they do not represent the in situ properties of the considered structure. The random error, on the other hand, is due to lack of knowledge. The sampling error that depends on the sample size is an example of such error. The description of the errors can be made by the use of the mean or median and the standard deviation or coefficient of variation.

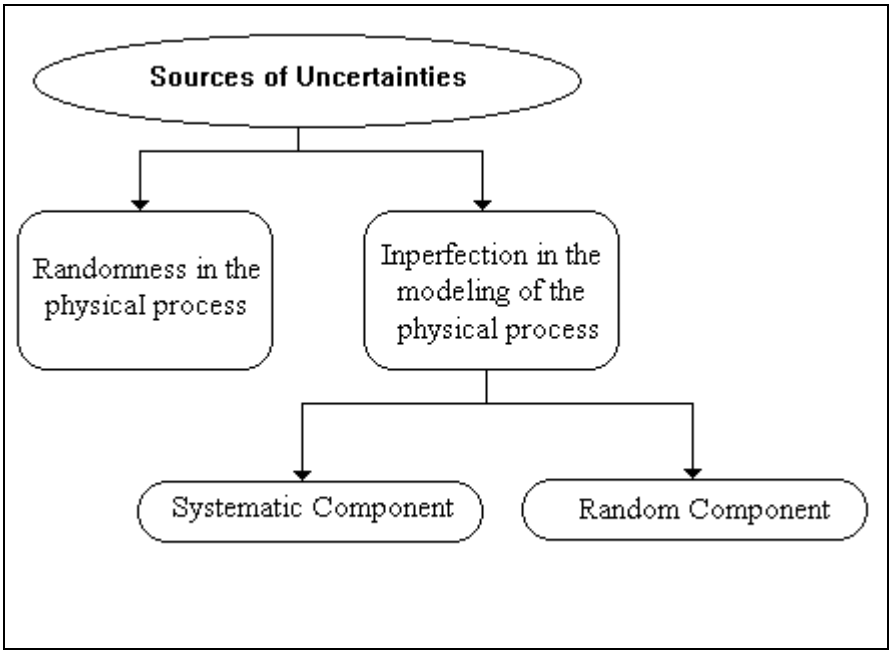

Figure 2. 8. Sources of uncertainties (Duzgun, 2004)

2.4.1 Analysis of Hard Data Uncertainties

The types of uncertainties explained in the previous section can be analyzed in a unified manner using the following model. Suppose that the true but unknown state of nature is X, a model denoted by $\hat{X}$, may be used. $\hat{X}$ is a model of the real world, therefore, it contains a certain degree of error and needs to be corrected by a factor, denoted by N. Thus, the true state is expressed as follows (Ang and Tang, 1984):

$$X = N\hat{X} \tag{2.1}$$

Then, if the state of nature is random, the model $\hat{X}$ should also be a random variable. As a result, the necessary correction factor N can also be considered as a random variable, whose mean value ν indicates the mean correction of the systematic error in the estimated mean value ($\bar{x}$), while the c.o.v of N, denoted by (Δ), represents the random error in the estimated mean value ($\bar{x}$). The inherent variability, denoted by (δ_x), on the other hand, is quantified utilizing the estimated mean value ($\bar{x}$) and variance (σ_x^2) of $\hat{X}$ as follows:

$$\delta_x = {}^{\sigma_x}/_{\bar{x}} \tag{2.2}$$

After assuming that N and $\hat{X}$ are statistically independent, Ang and Tang (1984) calculated the expected value of X by:

$$\mu_x = \nu\, \bar{x} \tag{2.3}$$

Where,

$\bar{x}$ = Estimate of the true mean value (i.e. the estimated mean value)

ν = Bias correction for systematic error in the estimated mean value $\bar{x}$

After assuming the statistical independence, Ang and Tang (1984) suggested that the total uncertainty (Ω_{total}) in the estimated value of a given variable X (such as porosity) is calculated by:

$$\Omega_{\text{total}} = \sqrt{\Omega_{\text{inherent}}^2 + \Omega_{\text{estimation}}^2} \tag{2.4}$$

Where,

Ω_{total} = the total coefficient of variation (uncertainty) in the predicted mean value

$\Omega_{inherent}$ = the coefficient of variation due to the inherent error

$\Omega_{estimation}$ = the coefficient of variation due to the estimation error

CHAPTER 3

STATEMENT OF PROBLEM

There are three main objectives of this study. The first one is to provide a tool to parameterize channelized training images. The parameterization is performed by means of a mathematical function (i.e. the Sine function). This function is used to represent the channel structure of a training image in two dimensions. Then, the parameters of the mathematical function are modified to generate different 2D training images. Next, 3D training images of these 2D training images are generated. The second objective of this study is to analyze the impact of training image parameters uncertainty on an original reservoir model. Thus, the generated 2D and 3D training images are used to remodel an original reservoir utilizing a proposed multiple-point geostatistics methodology. The third objective of this study is to investigate the impact of hard data uncertainty on the original reservoir model.

CHAPTER 4

METHODOLOGY

The main objectives of this study are: 1) providing a tool to parameterize training images, 2) investigating the impact of modifying training image parameters on an original reservoir model, 3) investigating the impact of hard data uncertainty on the original reservoir model. In order to perform the intended investigations, a MPG modeling methodology is proposed. Then, a synthetic fluvial channel reservoir model (Original Reservoir) is generated utilizing a given dataset and its training image. Next, a sensitivity analysis of the MPG modeling Algorithm and the methodology proposed is carried out.

A Sine function is employed to model the geological structure (i.e. channels) of the original training image. The Sine function is used to represent the channel structure of the training image in two dimensions. So, the training image becomes a function of four parameters. These parameters are the number of channels, the number of waves in each channel (i.e. in the Sine function), the amplitude level of waves, and the number of Z direction slices in the training image. After that, different 2D and 3D training images are constructed by modifying the four parameters defined. These developed training images are then employed to model reservoirs by utilizing the same methodology followed in the generation of the original reservoir. Next, the uncertainty due to the modification of training image's parameters is analyzed by comparing the developed reservoir models with the original reservoir.

In the present study, the impact of hard data uncertainty on the original reservoir model is investigated by considering only the uncertainty of the porosity data. This investigation is performed in three steps as follows. First, different realizations of the

original porosity data are generated through Monte Carlo Simulations using coefficients of variation of similar studies in literature. Then, the original reservoir is remodeled using the generated realizations instead of the original porosity data. Finally, the impact of porosity uncertainty on the reservoir model is analyzed.

4.1 The Proposed MPG Modeling Methodology

In this study, a MPG modeling methodology is proposed. This methodology is summarized as follows (Figure 4.1):

- Develop 2D and 3D training images by modifying the parameters of the training image defined. Then, import into Stanford Geostatistical Modeling Software (SGeMS) (This step is used while studying the impact of training image uncertainty on the original reservoir).
- Generate a reservoir facies realization using the facies hard data and MPG simulation algorithm; the Single Normal Equation Simulation (SNESIM) of SGeMS.
- Calculate the experimental variogram (in 3D) of the generated realization.
- Fit a variogram model to the experimental variogram
- Generate the corresponding porosity file (in 3D) using the Sequential Gaussian Simulation (SGSIM) of SGeMS
- Extract the porosity data out of SGeMS
- Upscale the porosity data
- Calculate the corresponding permeability values using defined logarithmic relations
- Construct a reservoir Model using the Builder tool of CMG software then input the porosity and permeability data calculated to the model
- Run the model by IMEX tool of CMG software

- Extract the Cumulative oil production (Q) versus time (T) plot and data, Original Oil In Place (OOIP) and Recoverable Oil In Place (ROIP) values

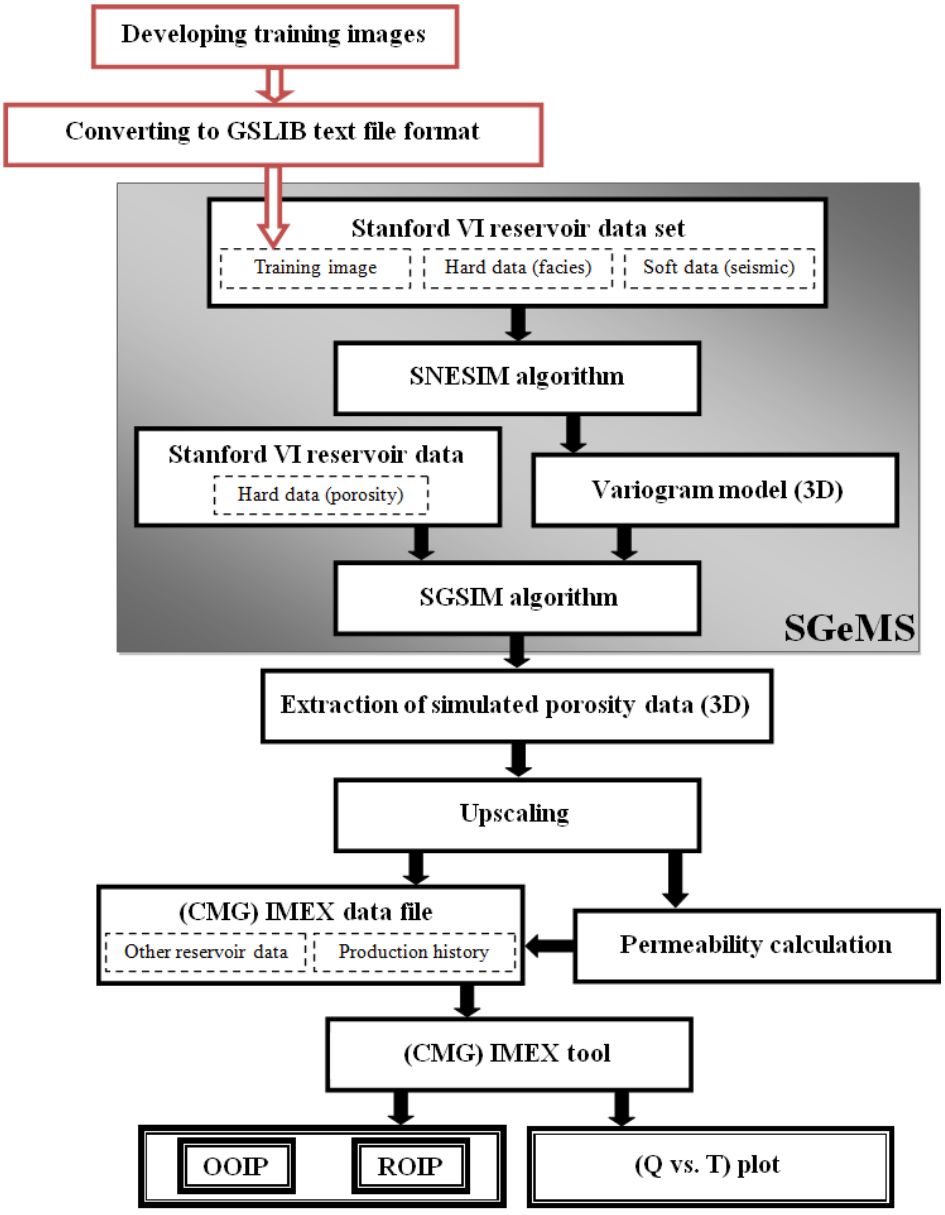

Figure 4. 1. A flowchart of the proposed MPG modeling methodology.

4.2 3D Dataset

The dataset used in the modeling process of this dissertation is acquired from Stanford VI, a synthetic dataset of a fluvial channel reservoir (Castro, 2007). The SGeMS project of this dataset is given by Remy et al. (2009). Three objects of this dataset are used in this study: *grid*, *training-image*, and *well-simple*. The *grid* object is a Cartesian grid consisting of 150 x 200 x 80 nodes, with its original point at the (0,0,0), and a unit cell size in each direction (Remy et al., 2009). The seismic or the facies probability data (p(sand|seis) and p(mud|seis)) are the only properties used in the *grid* object (Figure 4.2). The mud represents the shale (i.e. non-channel) structure. The training image of size 200 x 200 x 5 that is used in the MPG simulation is available in the *training image* object (Figure 4.3). This training image has a sand (channel) proportion of 0.271 and a shale (non-channel) proportion of 0.729.

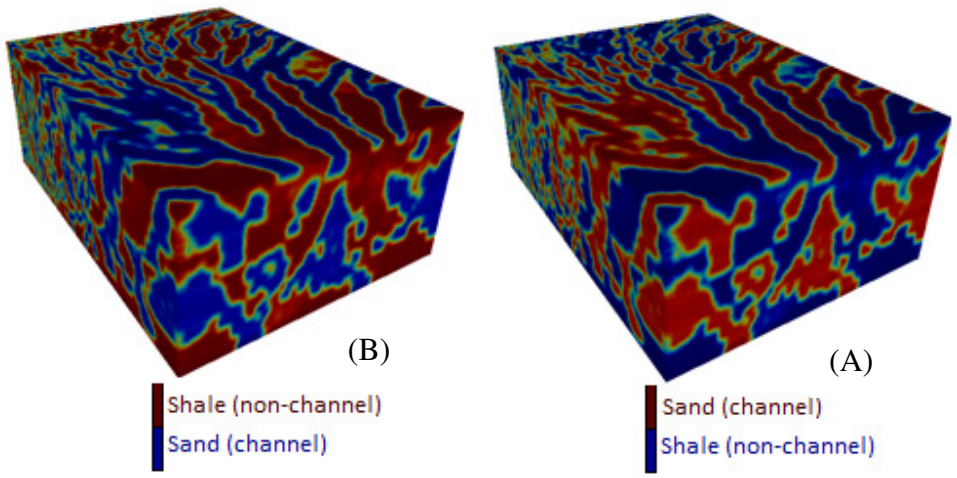

Figure 4. 2. Seismic (i.e. facies probability) data (p(sand|seis); (A), and p(mud|seis)); (B)

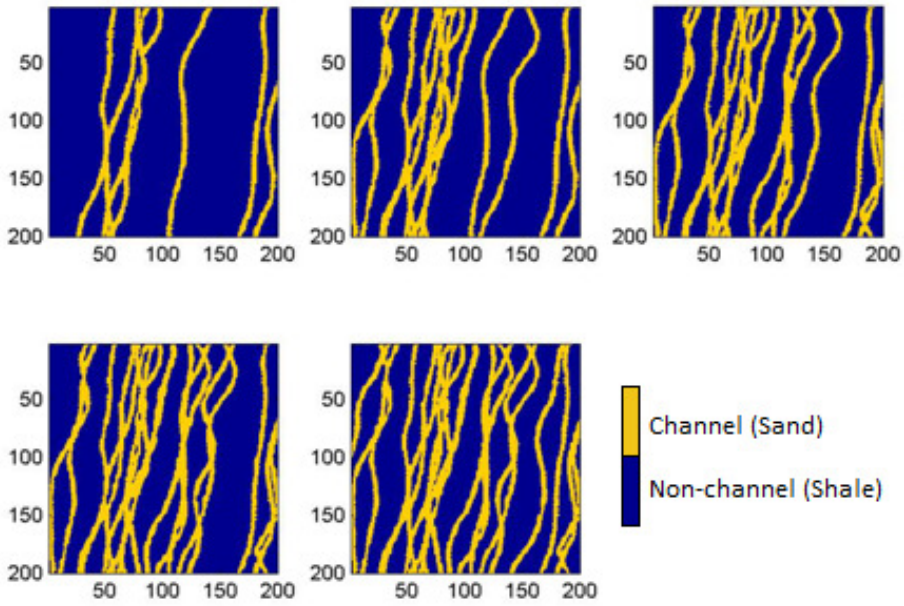

Figure 4. 3. Original training image used for modeling the original reservoir. The size of the training image is 200 × 200 × 5, each slice in the z – direction is shown here from top to bottom (Castro, 2007)

In this dataset (in the *well-simple* object) there are 46 vertical wells and six properties (density, facies, P-impedance, P-velocity, permeability, and porosity) that are associated with these wells. In the present study only three of these properties are used. These properties are 1) facies (binary indicators for the sand channel and shale having proportions of 0.4540 and 0.546, respectively), 2) porosity (Figure 4.4), and 3) permeability. Each of these properties has got 4320 data. Figure 4.5 shows the histograms of porosity, and permeability properties.

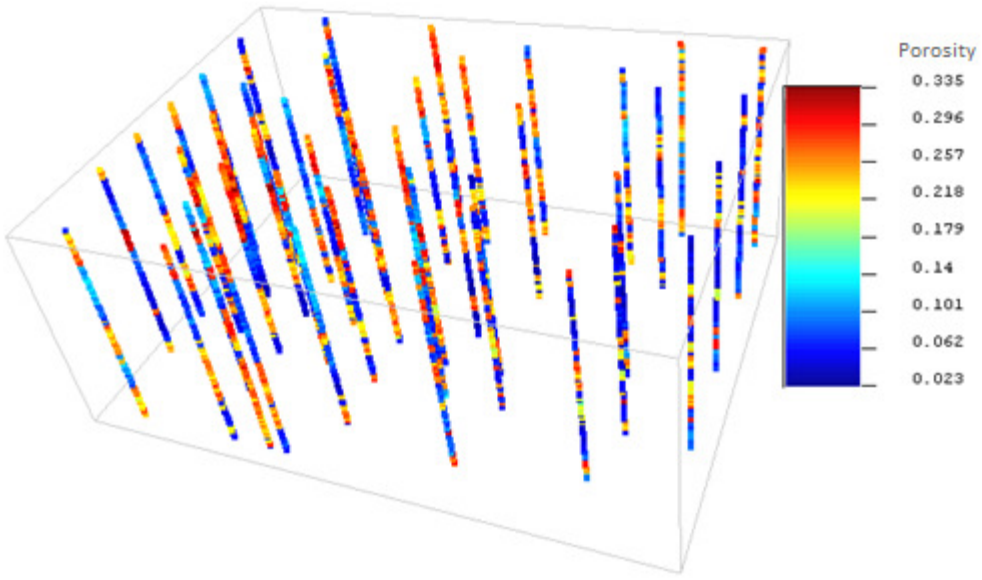

Figure 4. 4.The 46 wells of Stanford VI dataset showing the porosity property

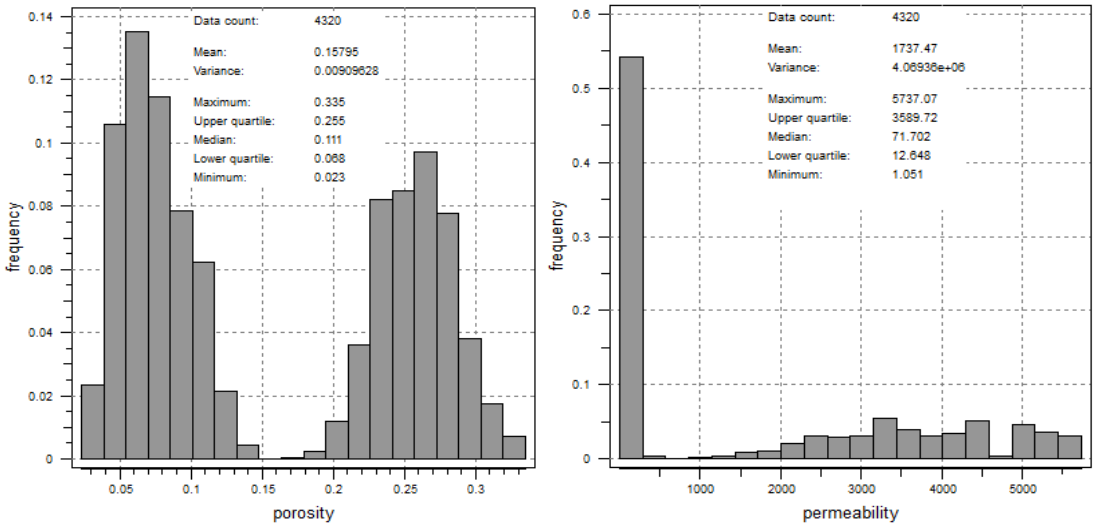

Figure 4. 5. Histograms of the porosity and permeability data of Stanford VI data set

4.3 Original Reservoir

4.3.1 Simulation with SNESIM Algorithm

The original hypothetical reservoir model is generated using the Stanford VI dataset objects defined in the previous section. The first step in this process is the utilization of the MPG simulation algorithm, SNESIM, to generate a categorical (facies) model (Figure 4.1). The parameters required by SNESIM for the present study are described in Section 1 of Appendix A. The values of these parameters are reported in Table 4.1. The "Target Marginal Distribution" values in Table 4.1 are the proportions of shale and channel categories in the facies hard data. These proportions are calculated as follows:

- The facies data (4320 data) are extracted to Excel spreadsheet
- Sorted
- Separated into shale (with "0" category) and channel (with "1" category)

Then the proportions are calculated by:

$$Proportion_i = \frac{number\ of\ data\ for\ category_i}{the\ total\ number\ of\ data} \tag{4.1}$$

In order to find the ranges of the "Search Template Geometry" the variogram of the hard data (facies) is computed in SGeMS (the details of this variogram computation are given in Section 1 of Appendix A). The Omni-directional variogram is calculated since the directional Variography is assumed to be isotropic (Figure 4.6 and Table 4.2). Thus, the angles of the search template were set to 0. As a rule of thumb, the ranges of the searching ellipsoid should have a value more than twice the range of the conditional data variogram. Therefore, all ranges were set as 21.

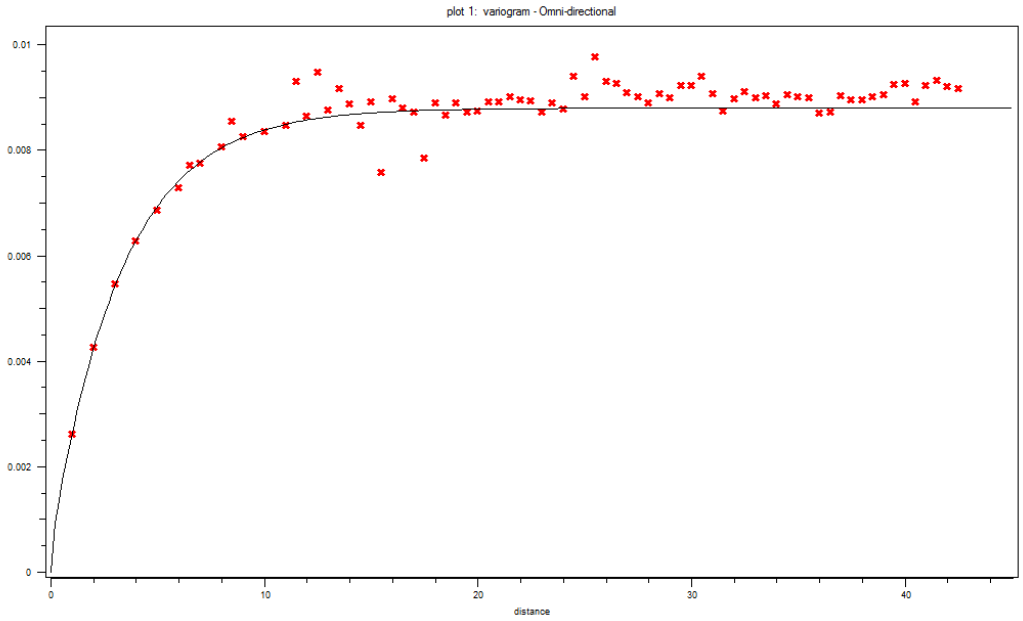

Figure 4. 6. Variogram model of the hard data

Table 4. 1. Variogram model fitted to the experimental variogram of the hard data. Ranges are shown in feet

Type	Exponential
Nugget	0.0005
Sill	0.0083
Ranges	10/9/8
Angles	0/0/0

The Global Affinity Change values are set as "2 1 0.5" indicating the corresponding change of the channels' width in the X, Y, and Z directions, respectively (Remy et al., 2009). Finally, the used search template is big enough to reproduce the structure of the training image therefore the number of Multigrids is set as 1.

Table 4. 2. Values of the parameters used by SNESIM algorithm to model the original reservoir

Parameter	**Value**
Seed	519175
# of Categories	2 (non-channel and channel)
Target Marginal Distribution	0.546 0.454
# of Nodes in Search Template	80 (default for a 3D training image)
Search Template Geometry (ranges and angles)	21, 21, 21 and 0, 0, 0
Hard Data (property)	Facies
Soft Data Probability	p(mud|seis) and p(sand|seis)
Tau Values for Training Image and Soft Data	1 1
Global Affinity Change	2 1 0.5
Min # of Replicates	1(default)
Servosystem Factor	0.5 (the default value which is the mean)
Re-simulation Threshold	-1 (default)
Re-simulation Iteration #	1 (default)
# of Multigrids	1
Previously Simulated Nodes	4 (default)
Template Expansion	Isotropic

The SNESIM parameter file including all these parameters is given in Section 1 of Appendix C. This file is loaded into SGeMS then SNESIM algorithm is run to simulate the original reservoir. Figure 4.7 shows the simulation output facies realization obtained. This realization honors both the hard data (compare the facies histograms in Figure 4.8), and the soft data (compare Figure 4.2 (A) with Figure 4.7).

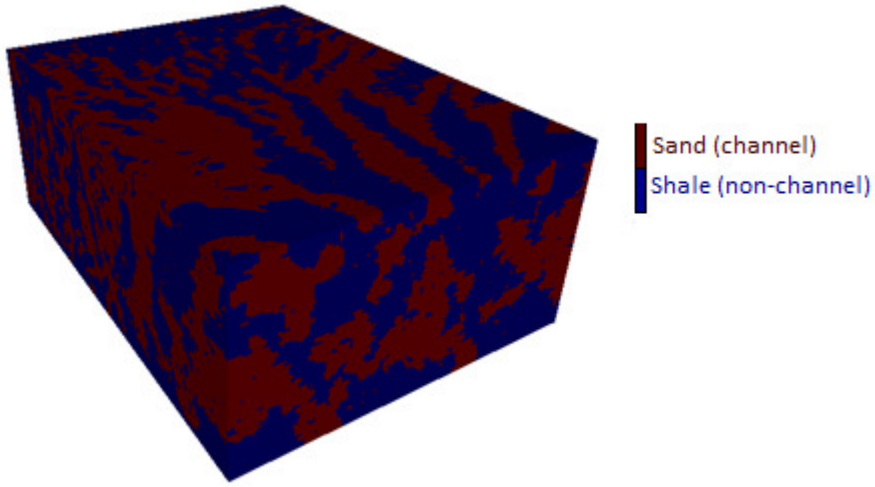

Figure 4. 7. Original reservoir's facies realization generated by SNESIM algorithm. The size of the model and the realization is 150 × 200 × 80

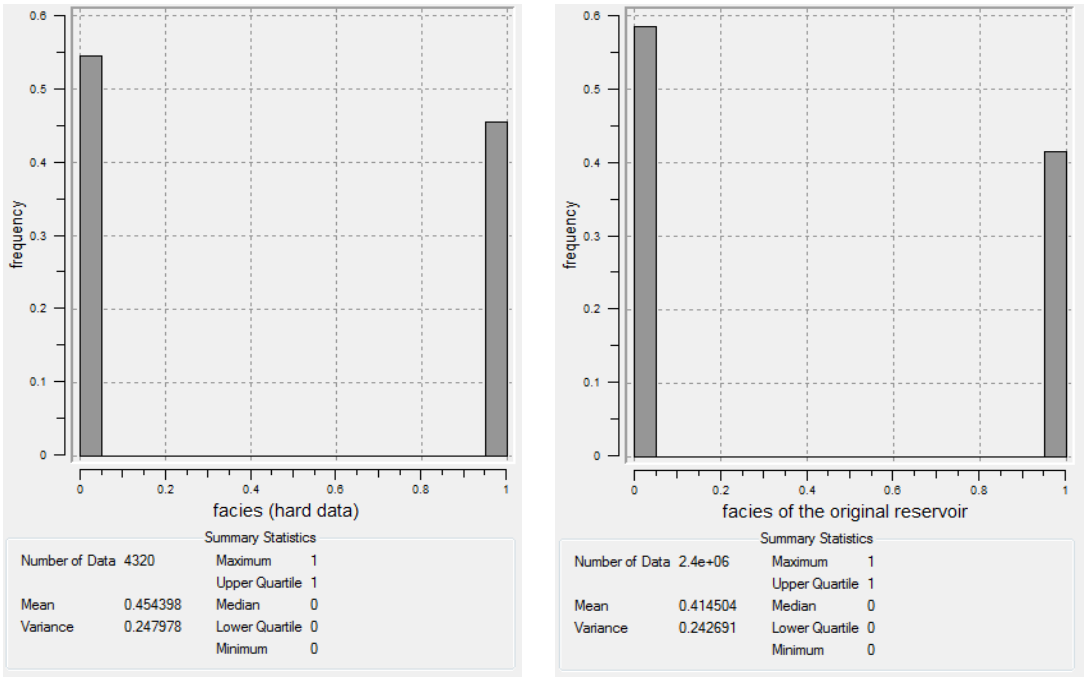

Figure 4. 8. The facies histograms of the hard data and the simulated reservoir realization illustrated in Figure 4.7

4.3.2 Simulation with SGSIM Algorithm

The next step after simulating the reservoir facies is to convert them into porosity numbers. In order to do that the Sequential Gaussian Simulation (SGSIM) algorithm of SGeMS is used (Figure 4.1). The parameters required by SGSIM are described in Section 2 of Appendix A. The values of these parameters are reported in Table 4.3 and their SGSIM parameter file is given in Section 2 of Appendix C. The variogram model used in SGSIM is that of the simulated facies realization given in Figure 4.7. The parameters and a plot of this variogram are shown in Table 4.4 and Figure 4.9, respectively (the details of this variogram computation are given in Section 2 of Appendix B). The calculated variogram is the Omni-directional since the directional Variography is assumed to be isotropic.

Table 4. 3. Values of the parameters used by SGSIM algorithm to convert the original reservoir facies into porosity numbers

Parameter	**Value**
Seed	14071789 (the default)
Kriging Type	Simple kriging
Hard Data (property)	Porosity
Max Conditioning Data	12 (the default)
Search Ellipsoid Geometry (ranges and angles)	80, 80, 80 and 0, 0, 0
Property with Reference Distribution	Porosity
Variogram	Variogram model of Table 4.4

Table 4. 4. Variogram model fitted to the experimental variogram of the simulated realization shown in Figure 4.7. Ranges are in feet

Type	Exponential
Nugget	0.04
Sill	0.1895
Ranges	22/21/8.1
Angles	0/0/0

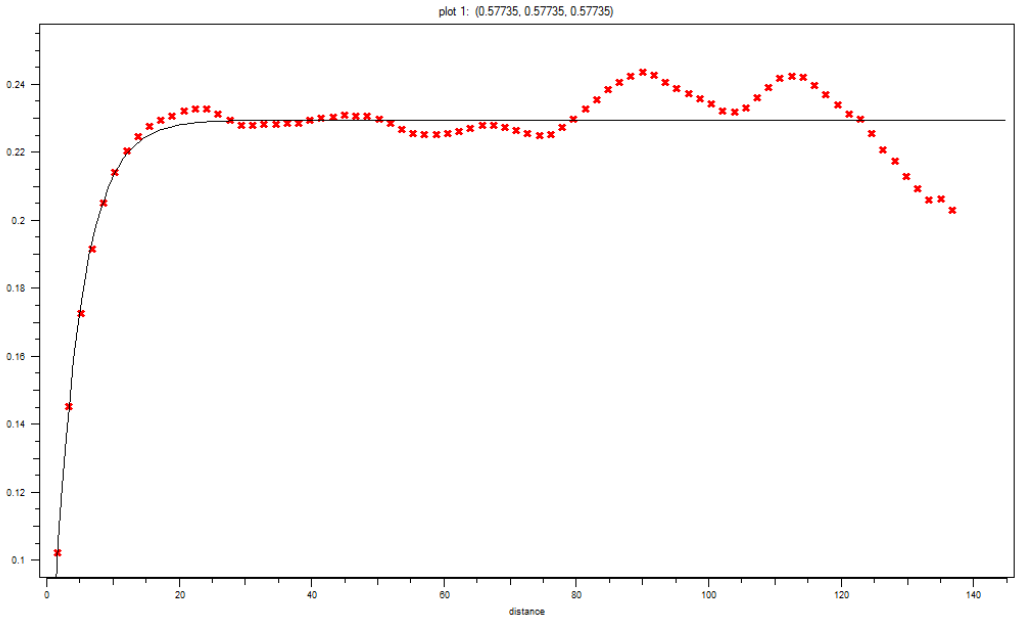

Figure 4. 9. Variogram model of the simulated realization shown in Figure 4.7

The porosity realization generated by the SGSIM algorithm utilizing the parameters defined above is shown in Figure 4.10. This realization honors the (porosity) hard data (compare the porosity histograms of Figure 4.11). However, the generated realization does not honor the soft data because SGSIM algorithm has no parameter that accounts for the probabilities of such data. Thus, the channel structure generated is not similar to that of Figures 4.2 (A) and 4.7.

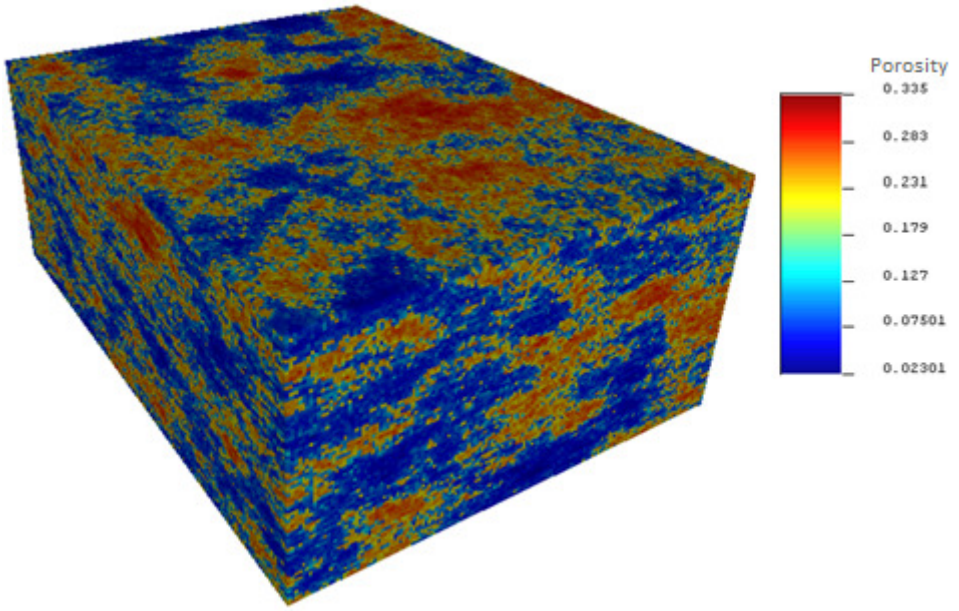

Figure 4. 10. Original reservoir's porosity realization generated by SGSIM algorithm

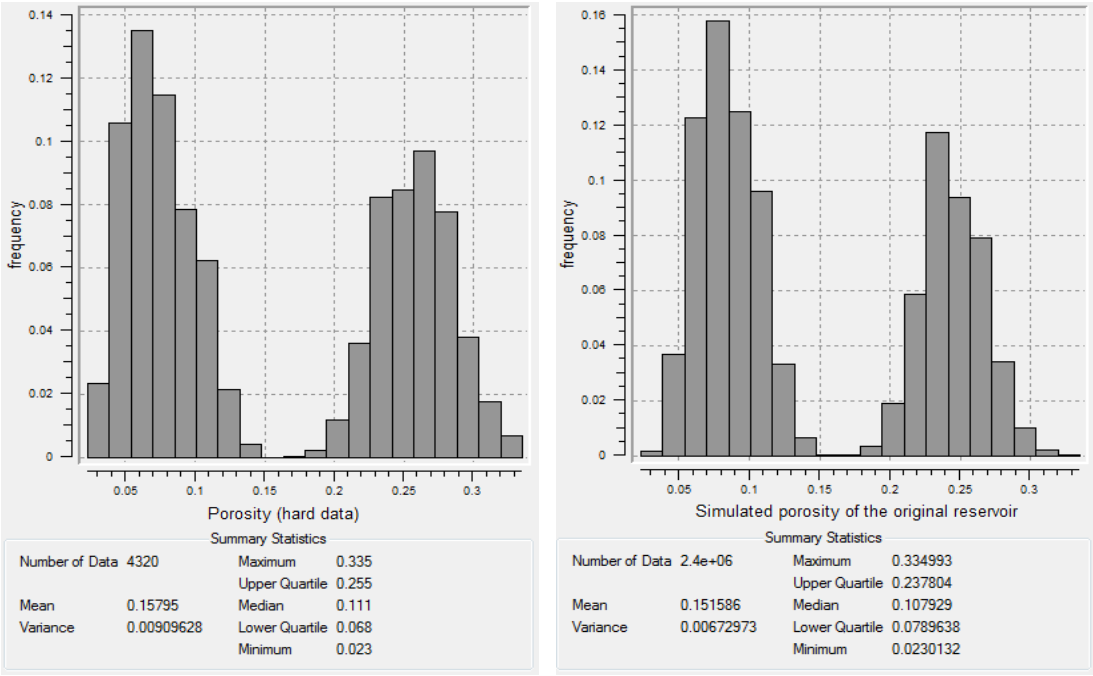

Figure 4. 11. The porosity histograms of the hard data and the simulated reservoir realization illustrated in Figure 4.10

4.3.3 Exporting Simulated Porosity Data

The data of the simulated porosity realization are exported out of SGeMS by means of a python code (Figure 4.1). This code is given in Section 1 of Appendix D. The code exports the data from the original grid (150 x 200 x 80 feet) to 1000 different ASCII files each corresponding to a block with a size of 15 x 20 x 8 feet. Each of the obtained 1000 files contains 2400 (i.e. 15 x 20 x 8) porosity data. The code exports the data block by block and Z-slice by Z-slice. In other words, the code loops through the X axis first, then the Y axis, and finally the Z axis.

4.3.4 Upscaling the Porosity Data

The size of real world geological models used for reservoir description exceeds by several orders of magnitude the capabilities of the available computer-based reservoir simulators. In other words, such models are too detailed to be used directly for reservoir simulation. Thus, upscaling is required. The main idea of upscaling is to replace some fine grid blocks of the same property with one equivalent coarse grid block. So, in general the main concept of upscaling is averaging. Upscaling therefore reduces the sizes of the simulation models so that they can be handled by simulators and within acceptable time frame.

Many upscaling approaches are available, but the simplest and the most widely used one is the arithmetic upscaling approach. This approach is the one used in the present study. So, the 1000 ASCII files of porosity data exported out of SGeMS in the previous section are arithmetically upscaled (Figure 4.1). In order to do that a Visual Basic code is developed. This code is given in Section 2 of Appendix D. The code averages the data in the 1000 ASCII files so that each file yields one porosity datum instead of 2400 data. As a result, the data are upscaled into 10 x 10 x 10 grid (i.e. only 1000 data) instead of 150 x 200 x 80 (i.e. 2.4 x 10^6 data). Both the exporting and upscaling processes are summarized in Figure 4.12.

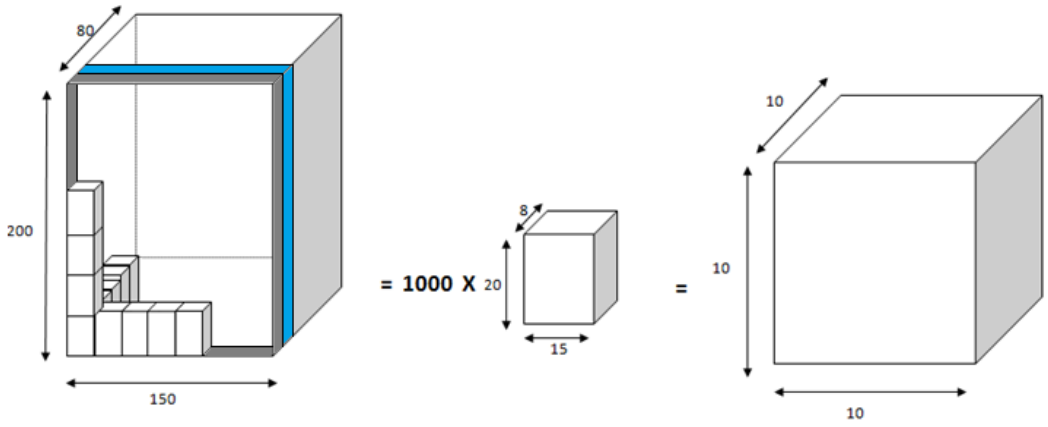

Figure 4. 12. The method followed in exporting and upscaling the simulated porosity data

4.3.5 Permeability Calculation

The next step in the proposed methodology is to calculate the permeability data corresponding to the porosity data of the previous section (i.e. the 1000 upscaled data) (Figure 4.1). In order to do that, the permeability and porosity hard data of Stanford VI dataset are plotted. Then, their logarithmic relations are obtained. Due to the bimodal distribution of the porosity data, corresponding to the channel and non-channel structures, the data are clustered into two groups. Thus, two logarithmic relations connecting porosity and permeability are found (Figure 4.13). These relations are tested using the F test and found to be highly significant. Next, they are utilized by means of an Excel spreadsheet to calculate the intended permeability data.

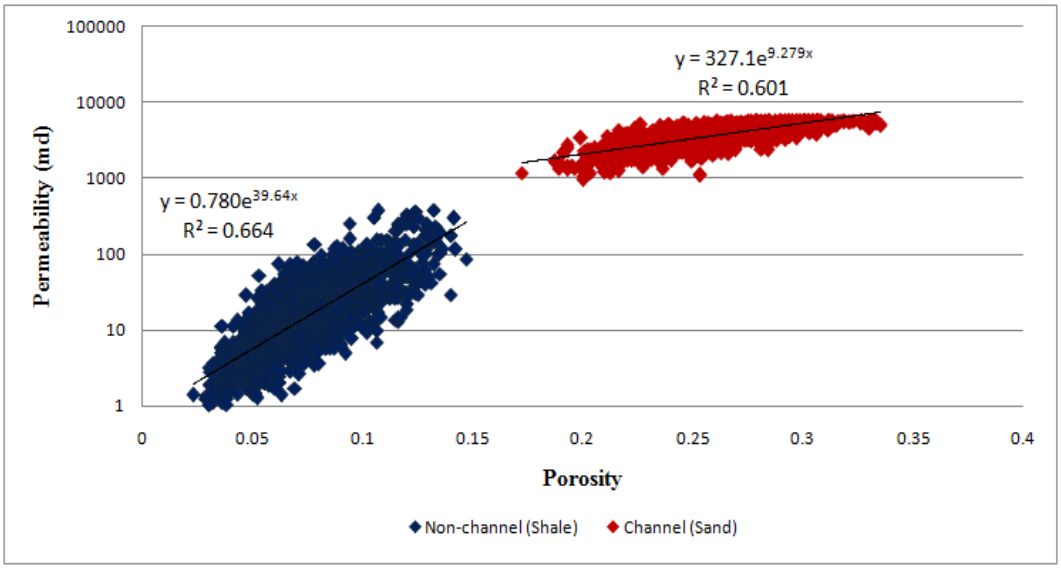

Figure 4. 13. The logarithmic relations between porosity and permeability hard data

4.3.6 Building the Synthetic Original Reservoir

4.3.6.1 Model Construction Steps

The original reservoir simulation model is a black oil model and constructed using the CMG's Builder tool. A Cartesian grid that consist of 1000 blocks; that is 10 x 10 x 10 is used for this purpose. The dimensions of each block are 500 ft, 1640 ft, and 8ft in the X, Y, and Z directions, respectively. The top of the formation is set at a depth of 5000 ft. The initial reservoir pressure and the bubble point pressure are defined as 4800 and 4014.7 psi, respectively. The Capillary effects are ignored and the relative permeability curves shown in Figure 4.14 are used. The gas is kept out of the calculation for simplicity; therefore, the gas oil contact (GOC) is set at a depth of 4000 ft. The water oil contact (WOC) is specified at 5064 ft. So, the first 8 K layers of the model make up the pay zone which is 64 ft thick. In addition, the previously simulated 1000 porosity and their corresponding permeability data are added to the model. Other model data as well as the CMG data file are given in Appendix E.

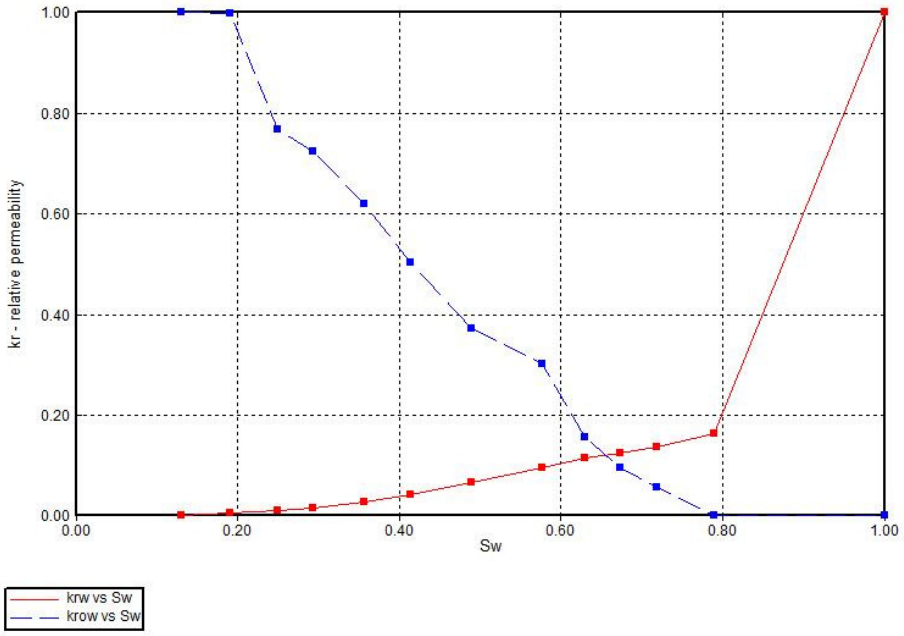

Figure 4. 14. Relative permeability curves used in modeling the original reservoir

After that, three production wells are added to the model. These wells are placed as shown in Figure 4.15. Then, the OOIP is calculated in order to define the production rates for three wells. The OOIP calculation details are shown below.

First the bulk volume is calculated:

$$V_b = (500 \times 10) \times (1640 \times 10) \times (8 \times 8) = 5{,}248{,}000{,}000\ cuft \quad (4.2)$$

$$= (5{,}248{,}000{,}000) \times (0.178108) = 934{,}710{,}784\ rbbl \quad (4.3)$$

Then, the OOIP is calculated:

$$OOIP = V_b \times \phi_{avg} \times (1 - S_w) \quad (4.4)$$

Where,

ϕ_{avg} = The average porosity value of the 1000 simulated porosity data found as 0.151586

S_w = The Connate Water Saturation of the relative permeability curves shown in (Figure 4.14)

Then,

$$OOIP = 934{,}710{,}784 \times 0.151586 \times (1 - 0.13) = 123{,}269{,}490\ rbbl \quad (4.5)$$

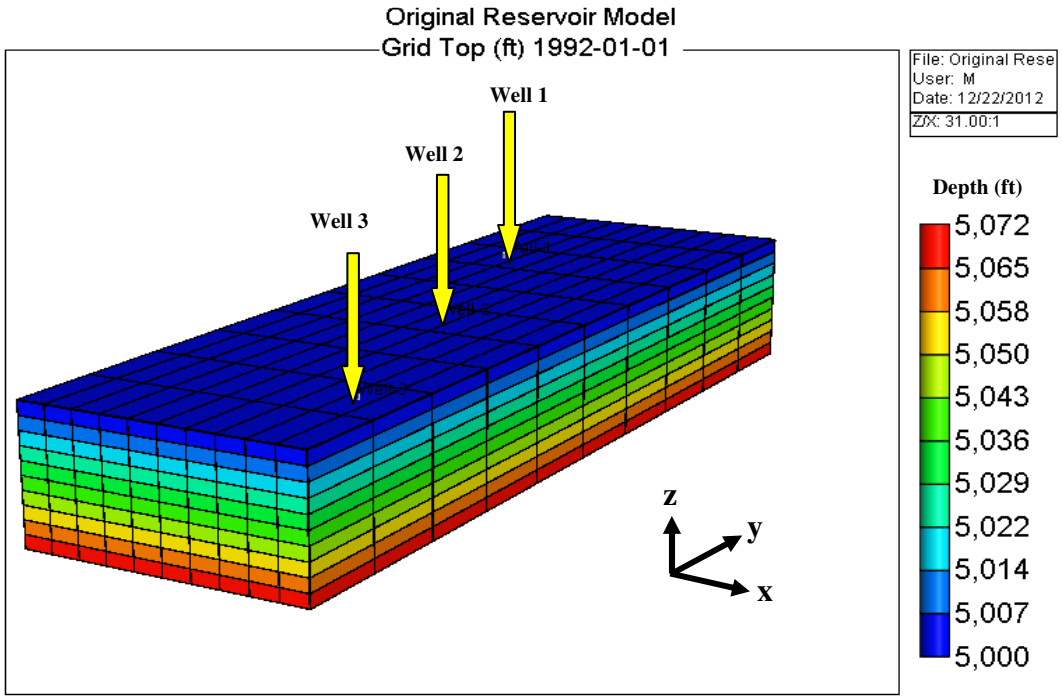

Figure 4. 15. 3D view of the reservoir constructed in CMG Builder tool showing the positions of the three wells used. The depth is given in feet

20-year-constant and continuous production (from 1992 to 2012) is planned for the reservoir model. Then, the production rates for the three wells are specified as 20%, 30%, and 50%, respectively. Next, using the calculated OOIP value (see Equation 4.5), well_1, well_2, and well_3 are set to produce 3377, 5066, and 8443 rbbl/day, respectively. The rates are calculated by Equation (4.6) given below. However, these rate values are later reset to 1478, 2217, and 3694 rbbl/day (see Section 4.3.6.2). The wells were perforated in all the eight K layers (Figure 4.16).

$$production\ rate\ (rbbl/day) = \frac{(production\% \times OOIP(rbbl))}{20\ year \times 365(day/year)} \quad (4.6)$$

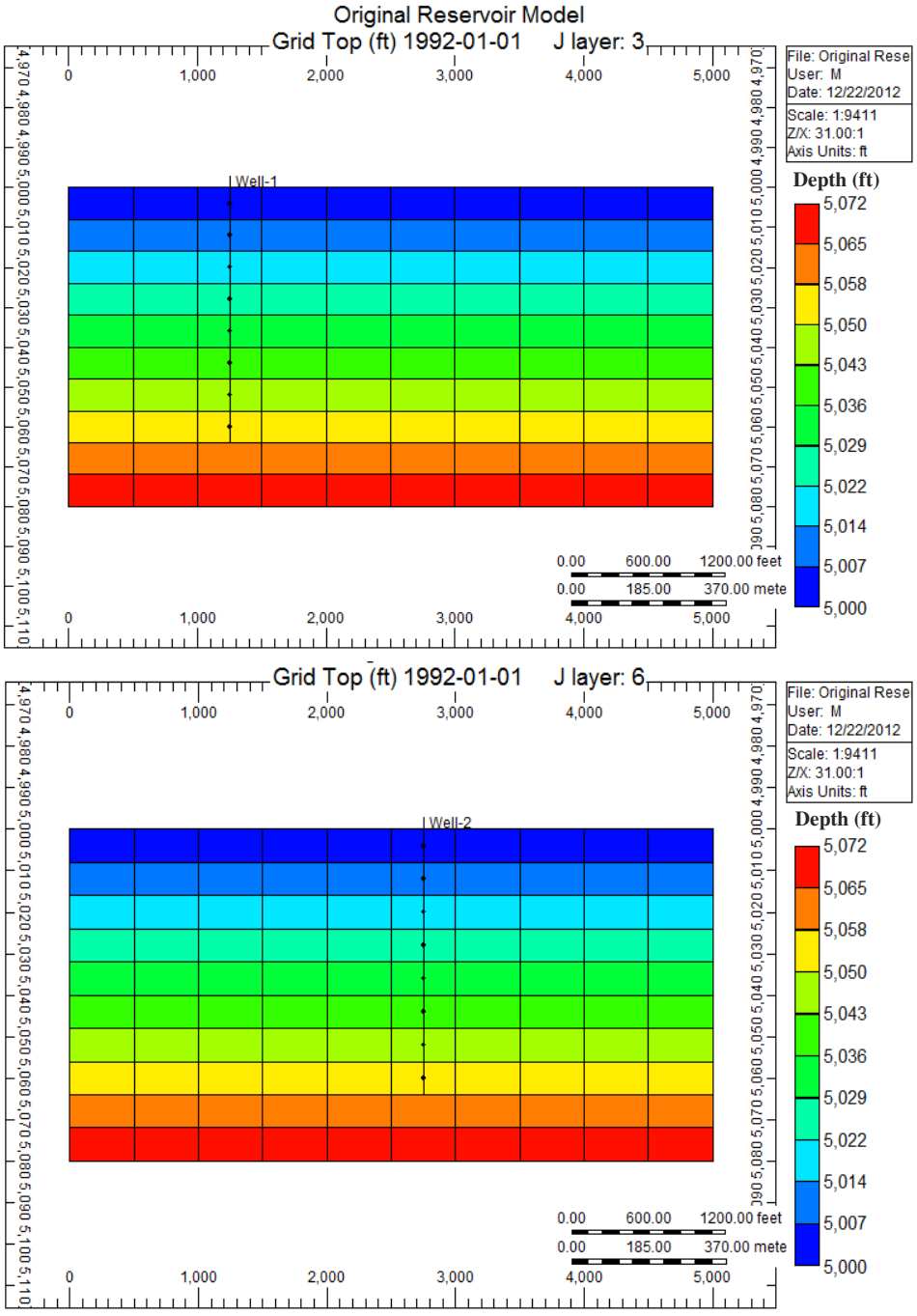

Figure 4. 16. Perforation of the eight K layer in wells 1 and 2. The depth is given in feet

The wells are initially operated on rate constraint. If the borehole pressure fails to produce the rate specified or violates the minimum bottomhole pressure (BHP) specified (i.e. min BHP = 50 psi) for a well, the BHP constraint becomes the operating constraint of that well. As a result, the simulator calculates the pressure difference value (i.e. grid block pressure – wellbore pressure) and uses it to calculate a new production rate for each timestep.

4.3.6.2 Running the Model in CMG (IMEX Tool)

When the model constructed in Section 4.3.6.1 is initialized in IMEX tool, it yields OOIP and ROIP of 71,212 M STB and 53,941 M STB respectively (Figure 4.1). The ROIP value obtained is used to recalculate the production rates of the wells since the original values are very high; therefore, they deplete the reservoir in a short time. That happens because the original production rates are calculated based on the amount of the OOIP which was calculated using the average porosity value (see Equation 4.5). Equation (4.6) is used to calculate the new production rates 1478, 2217, and 3694 rbbl/day. Plots of the production rate verses time and cumulative oil production versus time of the reservoir are given in Figures 4.17 and 4.18, respectively. The time when each of the wells is switched from constant rate constraint to bottomhole pressure constraint is shown by an arrow in Figure 4.17. The switching time of the wells is different because the grid blocks around each well have different pressure values than those around the others.

The complete methodology followed in the construction of the original reservoir model is summarized in Figure 4.19. Besides, the CMG data file of the reservoir is given in Appendix E.

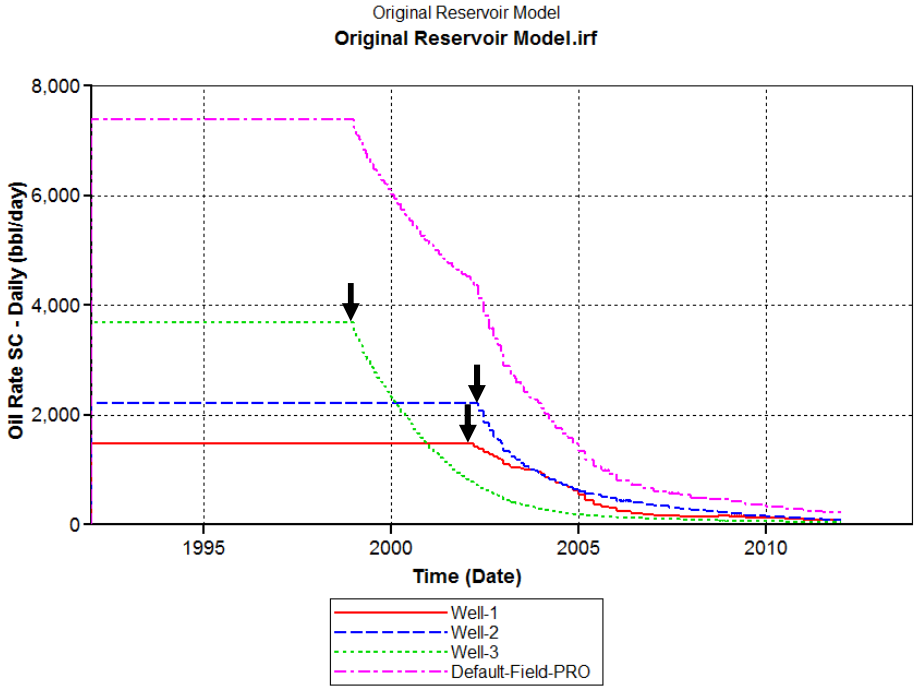

Figure 4. 17. Production rate verses time plot of the original reservoir

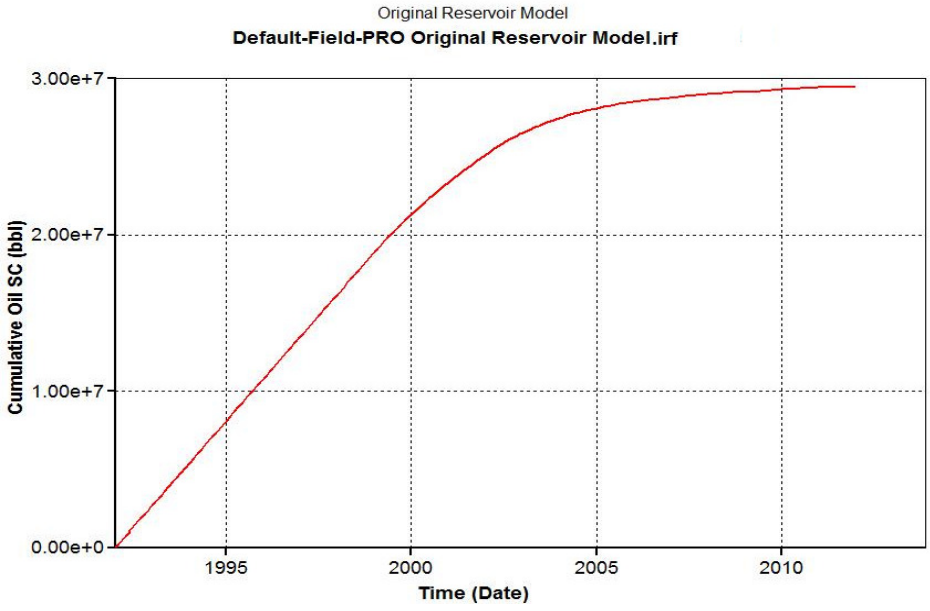

Figure 4. 18. Cumulative oil production verses time plot of the original reservoir

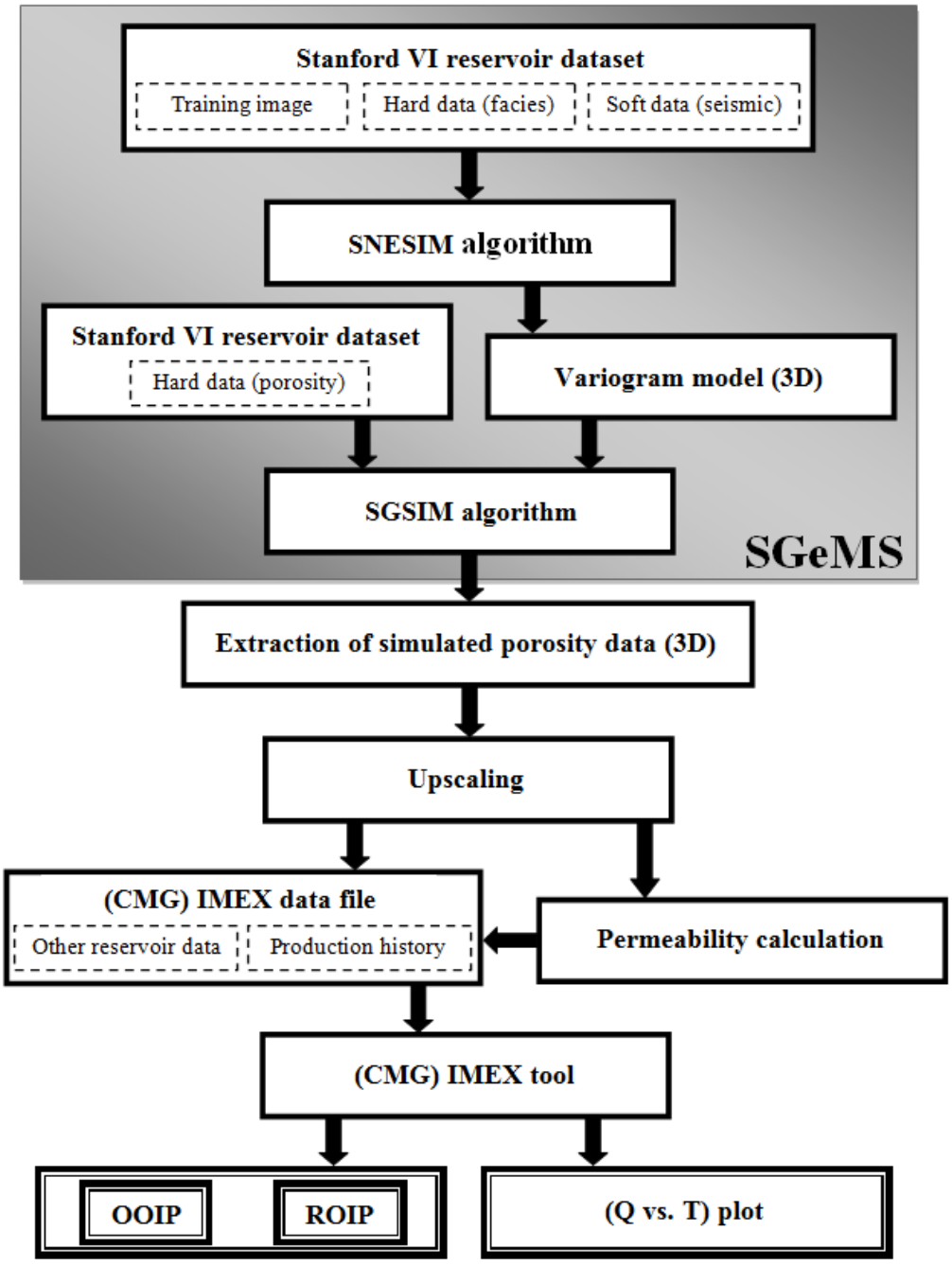

Figure 4. 19. Summary of the methodology followed in the generation of the original reservoir model. Where, OOIP = original oil in place, ROIP = recoverable oil in place, Q = cumulative oil production, and T = Time

4.4 Sensitivity Analysis of the SNESIM Algorithm and the Methodology Proposed

4.4.1 Simulation of the Original Reservoir

The sensitivity of the SNESIM algorithm and the methodology proposed is investigated by the generation of 50 equiprobable models of the original reservoir. The simulation performed utilizing the same SNESIM parameters of section 4.3.1 except for the seed. The seed is set to 211175 which is the default value. The seed number is changed in order not to generate the realization of the original reservoir (shown in Figure 4.7) again. After generating the 50 realizations, 50 variogram models are constructed as reported in Section 2 of Appendix B. These variogram models are given in the attached CD.

The corresponding porosity data of the 50 realizations are simulated by the SGSIM algorithm using the same parameters of Section 4.3.2 except for the variogram model. The variogram model of each realization is used to simulate its porosity data. These porosity data are exported, upscaled, and used to calculate their corresponding permeability data as explained in Sections 4.3.3, 4.3.4, and 4.3.5, respectively. The simulated porosities and the calculated permeabilities are input into the CMG data file given in Appendix E and run by the IMEX tool to get the OOIP and ROIP values.

4.4.2 Analysis of the Results

In order to study the sensitivity of the SNESIM algorithm and the proposed method the OOIP and the ROIP of the 50 generated models are plotted. In addition, the percentage errors for both parameters are calculated and plotted. The percentage errors are calculated by the following formula:

$$percentage\ error = \frac{X_{simulated} - X_{observed}}{X_{observed}} \times 100 \quad (4.7)$$

Where,

$X_{simulated}$ = OOIP or ROIP value for the simulated 50 reservoir models

$X_{observed}$ = OOIP or ROIP value for the original reservoir

Following that, the reliability of the information obtained with only 50 simulations is investigated as follows:

- The EasyFit statistical tool is used to fit a distribution to the errors calculated.
- The probabilities of finding an error within the limits of the calculated distribution or beyond them are calculated.

4.5 Sensitivity Analysis of the Variogram Model

Variogram fitting is subjective; therefore, the impact of different variogram models on the OOIP and ROIP is investigated in this section. However, it is important to state that the visual fitting of the variograms used in this study is investigated by the sensitivity analysis of the previous section. So, this analysis is performed by setting different model types and ranges than those of the originally found variogram model. In other words, this analysis is executed by fitting the following models to the experimental variogram of the original reservoir:

- A Spherical variogram model
- A Gaussian variogram model
- An Exponential variogram model with lower ranges than those of the original variogram given in Table 4.2
- An Exponential variogram model with larger ranges than those of the original variogram

The same methodology is followed in order to obtain the OOIP and ROIP values (see Figure 4.19). However, the process starts with the simulation of porosity in SGSIM

where the variogram model is employed. So, only the porosity and the permeability data are changed in the methodology steps. The final results (i.e. OOIP and ROIP values) are then compared with those of the original reservoir in order to analyze the sensitivity of the result to the variogram model.

4.6 Analysis of Training Image Uncertainty Impact on Reservoir Model

4.6.1 Parameterization of Original Training Image Structure and Modeling of 2D Training Images

In order to study the impact of training image Uncertainty on the original reservoir model the Sine function is used to represent the fluvial channels structure of the original training image shown in Figure 4.3. The Sine wave or sinusoid in its most basic form is (Webshaker website, 2011):

$$y(t) = A \times Sin(\omega t + \varphi) \tag{4.8}$$

Where,

A = Amplitude

ω = Frequency = 2πf (rad/s), where f = 1/T, and T = period in seconds

t = Time (s)

φ = Phase (rad)

In the present study, the channels (i.e. Sine waves) are sketched utilizing the "SpeQ Mathematics" software (SpeQ Mathematics website, 2011). The Sine wave in this software is defined by:

$$y = A \times Sin\ (\theta \times x) \tag{4.9}$$

Where,

A = Amplitude

θ = An angle (in radian) that controls both the frequency and the phase parameters

x = A fixed-length x-axis as $x \in [-10,10]$ for the one and three-wave cases and $x \in [-15,5]$ for the two-wave cases

The flowchart of the methodology proposed for training image generation is given in Figure 4.20.

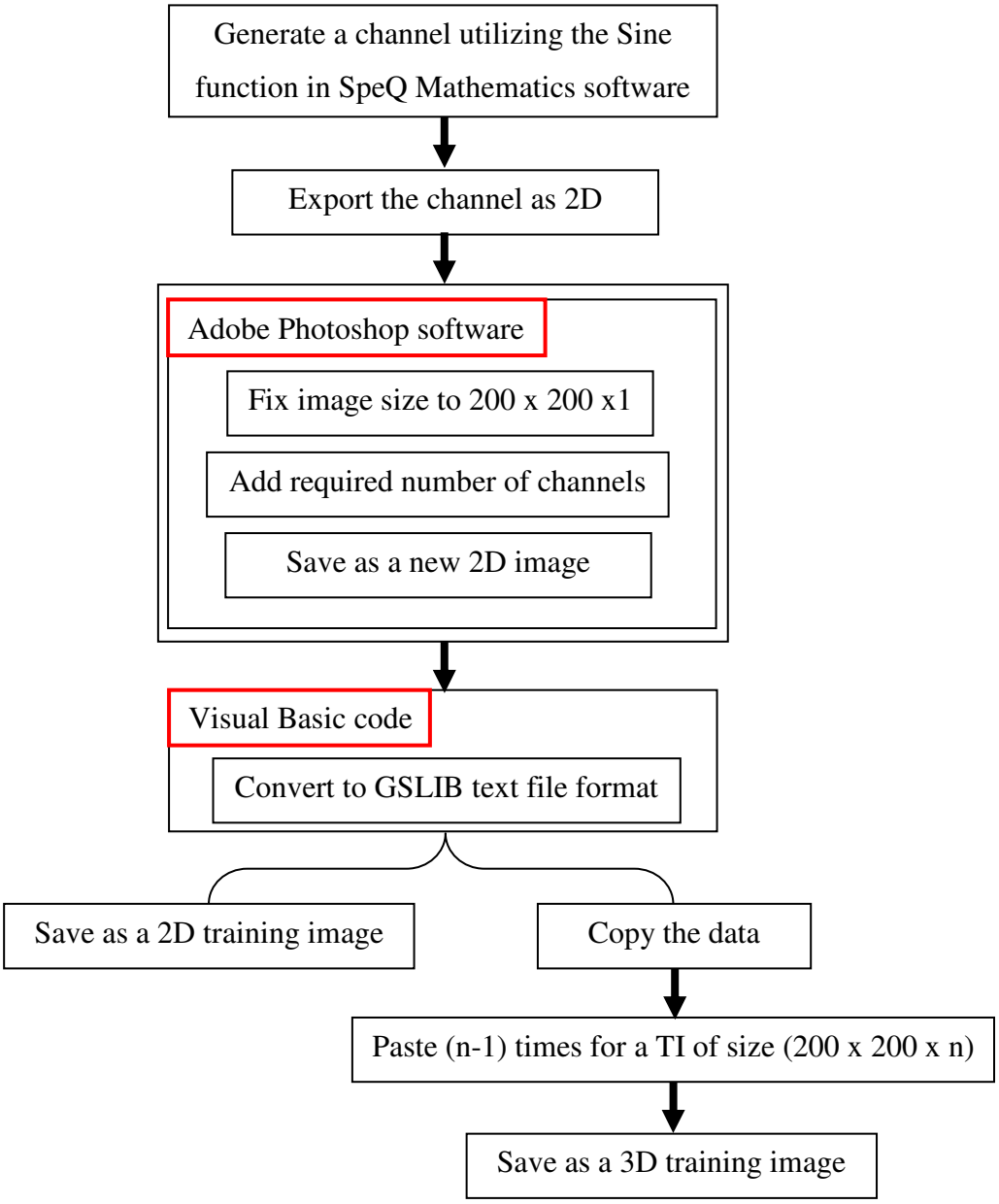

Figure 4. 20. Summary of the proposed methodology for training image generating

4.6.1.1 One-Wave Channel Cases

Using Equation (4.9) three one-wave channels having three different amplitudes are drawn. In order to get the one-wave channels $\theta = 0.315$ radian is used. The drawn channels are fixed-width and phase (Figure 4.21). The amplitudes used are high (i.e. 0.75), medium (i.e. 0.57), and low (i.e. 0.30). Each channel of Figure 4.21 is exported as a 2D image (Figure 4.20). Then, Adobe Photoshop Software is used to set the dimensions of each image to 200 x 200 x1 pixels (Figure 4.20). So, the amplitude and phase are converted into pixels, where, the phase is converted to 100 pixels for all the cases. The amplitudes are converted to 75 pixels, 57 pixels, and 30 pixels corresponding to the high, medium, and low cases, respectively (Figure 4.22).

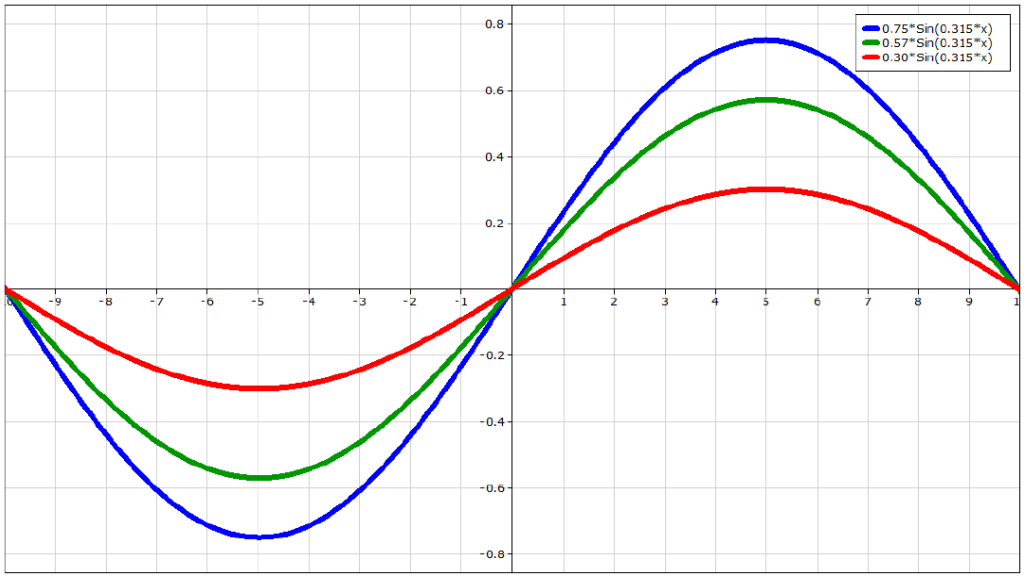

Figure 4. 21. One-wave channel cases having high, medium, and low amplitudes and a fixed phase value

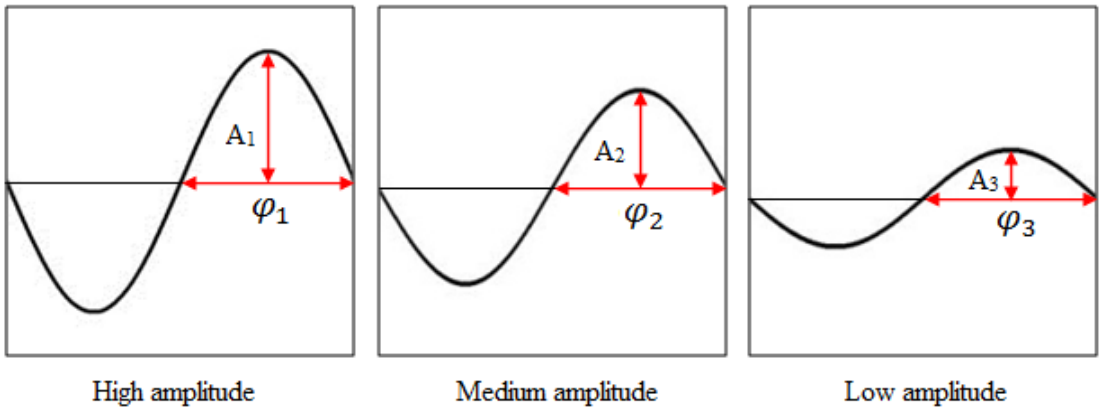

Figure 4. 22. Training images of size 200 x 200 x 1 pixels for the one-wave cases having high (A_1 = 75 pixels), medium (A_2 = 57 pixels), and low (A_3 = 30 pixels) amplitudes and an equal phase ($\varphi_1 = \varphi_2 = \varphi_3$ = 100 pixels).

4.6.1.2 Two and Three-Wave Channel Cases

The two and three-wave channel cases are drawn using Equation (4.9) too. However, the θ values for the two and three-wave channel cases are changed to 0.63 and 0.945, respectively (Figure 4.23 and 4.24). Each of these channels is exported as a 2D image and their dimensions are converted into 200 x 200 x1 pixels as in Section 4.6.1.1. In the two-wave channel cases the phase is 50 pixels, while the three-wave channel cases it is 33.33 pixels. The amplitudes are kept the same as in Section 4.6.1.1(Figure 4.19). So, they are 75 pixels, 57 pixels, and 30 pixels corresponding to the high, medium, and low cases, respectively (Figure 4.25 and 4.26). The phase and the numbers of waves in a channel are interrelated since the training image has a fixed size (Table 4.5). The amplitude and the wave number (corresponding to the phase) are the Sine function's parameters which are analyzed in this study.

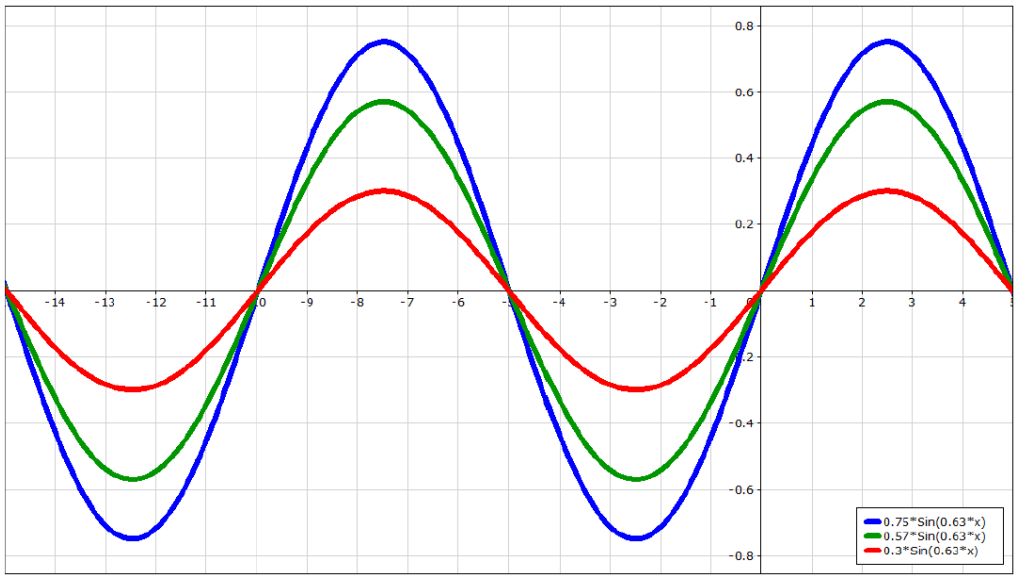

Figure 4. 23. Two-wave channel cases having high, medium, and low amplitudes and a fixed phase values

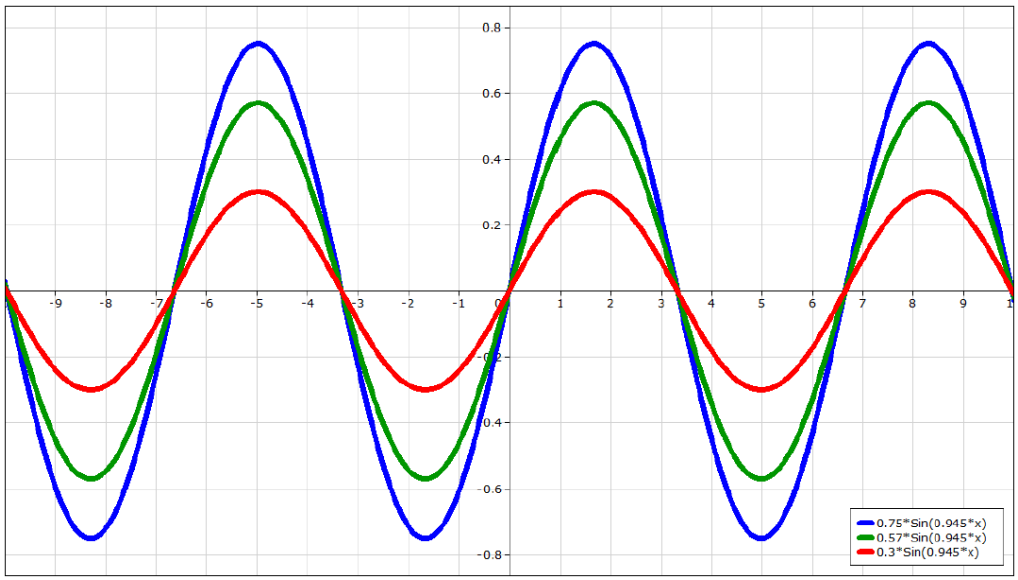

Figure 4. 24. Three-wave channel cases having high, medium, and low amplitudes and a fixed phase values

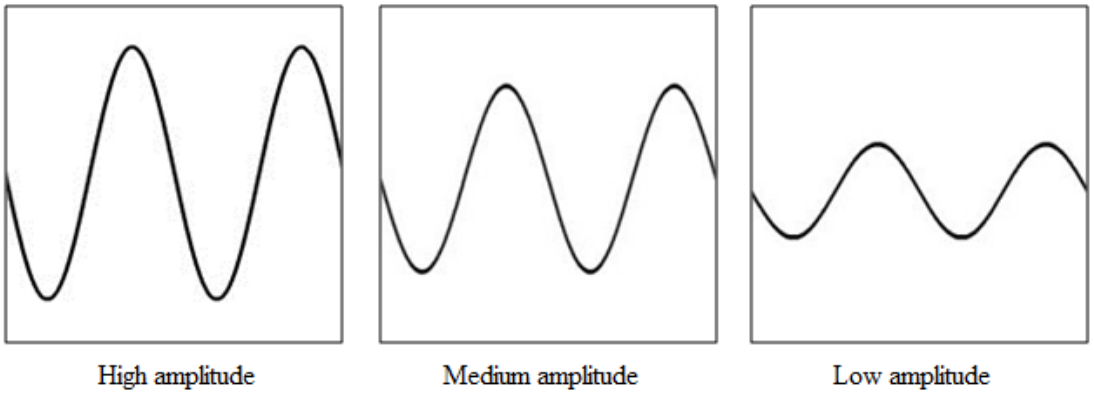

Figure 4. 25. Training images of size 200 x 200 x 1 pixels for the two-wave cases having high (A_1 = 75 pixels), medium (A_2 = 57 pixels), and low (A_3 = 30 pixels) amplitudes and an equal phase ($\varphi_1 = \varphi_2 = \varphi_3$ = 50 pixels)

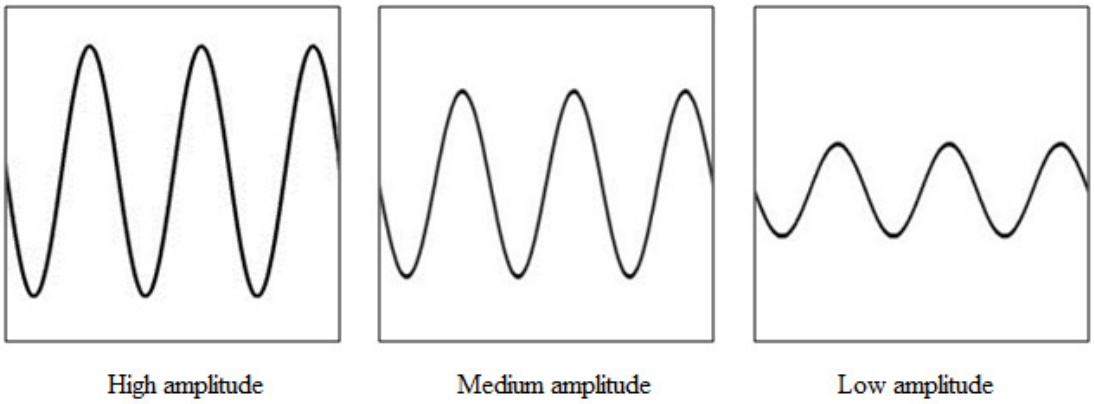

Figure 4. 26. Training images of size 200 x 200 x 1 pixels for the three-wave cases having high (A_1 = 75 pixels), medium (A_2 = 57 pixels), and low (A_3 = 30 pixels) amplitudes and an equal phase ($\varphi_1 = \varphi_2 = \varphi_3$ = 33.33 pixels)

Table 4. 5. The relation between the phase value and the number of waves in a channel

Phase value (pixel)	Number of waves in a channel
100	1
50	2
33.33	3

All the nine 2D training images generated so far are one channel training images (Figures 4.21, 4.23 and 4.24). In other words, each of these training images has only one channel. The channel number which a training image parameter is also analyzed in this work. Thus, other 2D training images containing different channel numbers are generated. Since, the number of channels in each training image is restricted by its fixed size (i.e. 200 x 200 x 1), amplitude level, and number of waves in each channel up to 8-channel training images are generated for the low amplitude cases. However, up to only 3 and 5-channel training images could be generated for the high and medium amplitude cases, respectively. So, the total number of the 2D training images generated is 46. Table 4.6 lists the modification of the considered parameters and the corresponding number of training images generated. Some of the generated training images are illustrated in Figures 4.27. The separation between channels in each training image is kept almost the same.

Table 4. 6. Modification of parameters and the corresponding number of the 2D training images generated

Number of Channels	Number of waves	Amplitude level	Number of generated training images
1, 2, and 3	1	High	3 x 1 = 3
1 and 2	2		2 x 1 = 2
1 and 2	3		2 x 1 = 2
1, 2, 3, 4 and 5	1, 2, and 3	Medium	5 x 3 = 15
1, 2, …, 7, and 8	1, 2, and 3	Low	8 x 3 = 24
Total number of 2D training images generated = 46			

The generated training images are converted into geostatistical software library (GSLIB) text file format by means of a developed Visual Basic code (Figure 4.20). That is made because SGeMS accepts files with GSLIB format. The developed code is given in Section 3 of Appendix D.

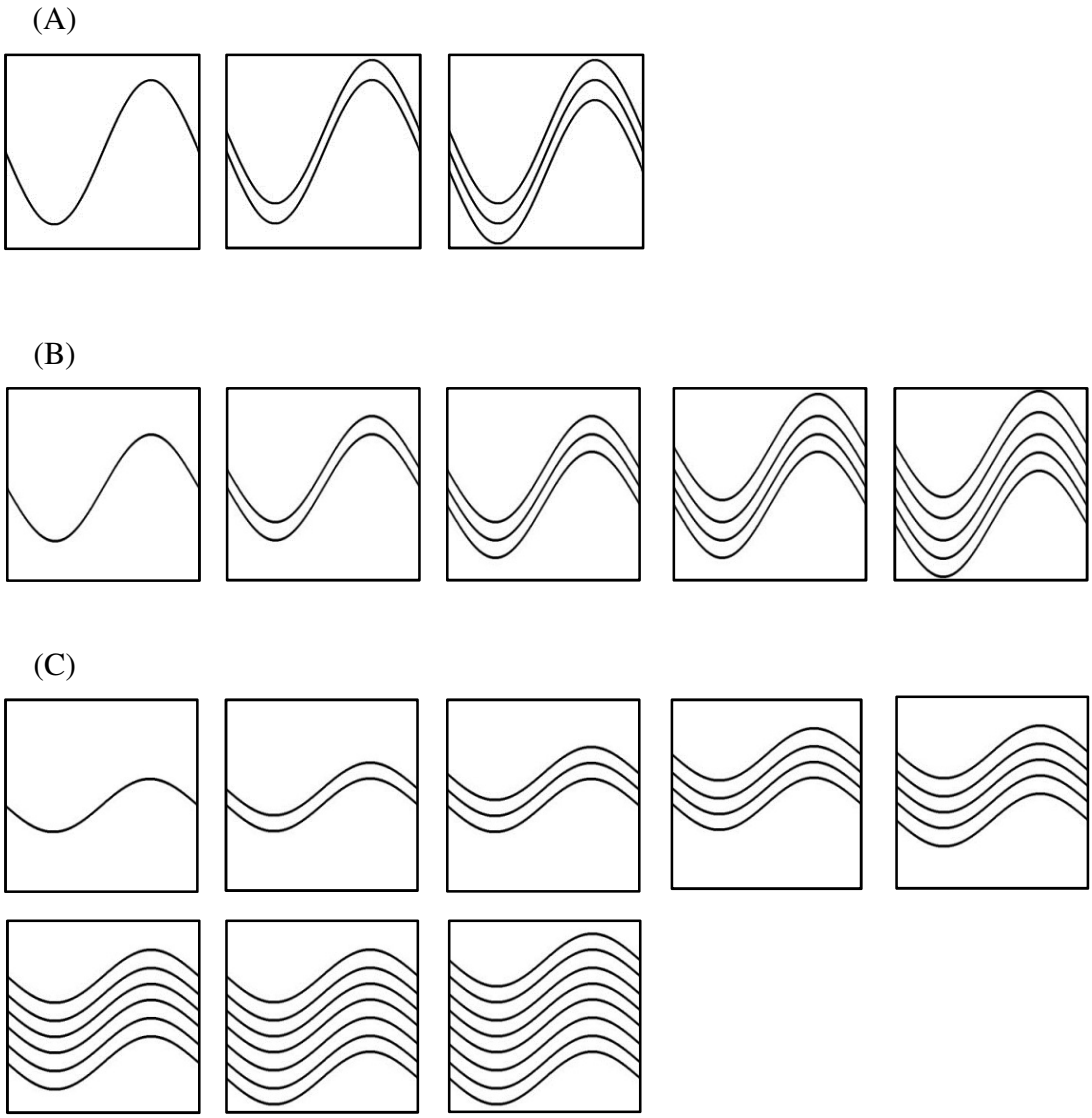

Figure 4. 27. Training images of the one-wave channel cases. The channel having high; (A), medium; (B), and low amplitudes; (C) are shown. Up to three, five, and eight channels could be fitted to the fixed size of the training image for the high, medium, and low amplitude cases, respectively

4.6.2 Modeling of 3D Training Images

After generating the 2D training images and converting them into GSLIB text files, the data in those files are used to add the third dimension slices (i.e. the Z slices) in order to generate the 3D training images. First, all the data (200 x 200 x 1= 40,000 data) in the GSLIB text file of the 2D training image are copied except the first three rows, which are the titles. Next, these data are pasted at the end of the first 40,000 data as many as the number of the required slices in the Z direction to generate the new 3D training image (Figure 4.20). In the present study, training images with up to eight Z direction slices are generated. Dissimilar to the original training image of Stanford VI dataset, all the slices in the Z direction of each training image are having the same number of channels as in the first one (i.e. the 2D training image). The training images are generated this way because the increase in number of channels with depth is not a general geological property and it depends on the sedimentation process as well as other factors (F. B. Rojay, personal connections, January 17, 2012). So, the generated training images in total (including both the 2D and 3D images) are 368 images. Table 4.7, which an extension of Table 4.6, lists these training images.

Table 4. 7. Modification of parameters and the corresponding number of training images generated

Number of Channels	Number of waves	Number of Z slices	Amplitude level	Number of TIs generated
1, 2, and 3	1	1, 2, …, 7, and 8	High	3 x 1 x 8 = 24
1 and 2	2	1, 2, …, 7, and 8		2 x 1 x 8 = 16
1 and 2	3	1, 2, …, 7, and 8		2 x 1 x 8 = 16
1, 2, 3, 4 and 5	1, 2, and 3	1, 2, …, 7, and 8	Medium	5 x 3 x 8 = 120
1, 2, …, 7, and 8	1, 2, and 3	1, 2, …, 7, and 8	Low	8 x 3 x 8 = 192
Total number of training images generated = 368				

4.6.3 Construction of reservoirs using the generated Training Images

All the 368 generated training images are input into SGeMS creating 368 reservoirs that are modeled following the same methodology used in modeling the original reservoir (see Section 4.3) by changing only three parameters:

1. The default seed values of the SNESIM algorithm (i.e. 211175) is used
2. One of the 368 generated training images of Sections 4.6.1 and 4.6.2 is used in SNESIM algorithm each time to generate a new facies realization. As a result, 368 different facies realizations are generated.
3. 368 experimental variograms are computed for the simulated 368 realizations using the parameters given in Section 2 of Appendix B. Then variogram models are fitted to them. These models are used in SGSIM to simulate the porosity values of the generated realizations.

These porosity values are used to generate 368 new reservoir models. The methodology followed in the generation of training images and their corresponding reservoir models is as summarized in Figure 4.1.

4.6.4 Analysis of Training Image Parameters Effects on Reservoir Model

4.6.4.1 Impact of Training Image Parameters on Cumulative Oil Production

In order to study the effect of the training image parameters on the cumulative oil production, the cumulative oil production versus time plots of the 368 generated reservoir models are compared with that of the original reservoir. The plots are grouped in order to study the effect of each training image parameter (i.e. # of Z slices, # of channels, # of waves in each channel, and amplitude level). Next, the results are used to define thresholds for the training image parameters defined to

assist in the construction of more representative reservoir models. Then, the effect of parameters' variation in the uncertainty is investigated.

4.6.4.2 Impact of Training Image Parameters on OOIP and ROIP

In this section the effect of each parameter is investigated. Then, the percentage errors of each case with respect to OOIP and ROIP of the original reservoir are calculated and plotted in order to find the uncertainty range of the methodology proposed. The calculation of the percentage errors is conducted as shown in Section 4.4.2. After that, the thresholds defined in the previous sections are utilized. In other words, the reservoir models not meeting the thresholds are eliminated. Then, the uncertainty range is reanalyzed.

4.7 Analysis of Porosity Uncertainty Impact on Reservoir Model

4.7.1 Modeling of Porosity Uncertainty

In this part, the effect of porosity uncertainty on the reservoir model is investigated. In order to do that the uncertainty related to the log-derived porosity (measurement uncertainty) and porosity derived from core samples analysis are both considered. With the aim of investigating the effect of porosity uncertainty on the predicted reservoir model, the uncertainty due to core sample analysis (i.e. laboratory uncertainty) is assumed to be the inherent uncertainty.

Logging tool reading uncertainty (5%) is obtained from the Century Geophysical Corporation website (2012) and assumed to be the coefficient of variation (c.o.v) for the log reading (Ω_{log}). On the other hand, a 0.26 coefficient of variation of a sandstone core analysis performed by Sanjay (2000) is considered as the inherent uncertainty (Ω_{core}). These two coefficients of variations are combined using Equation 2.4 to find the total uncertainty in the predicted porosity value, Ω_{total}, as shown below.

$$\Omega_{\text{total}} = \sqrt{0.26^2 + 0.05^2} = 0.265 \quad (4.8)$$

Since the porosity hard data of Stanford VI dataset has a bimodal distribution (see Figure 4.5), the porosity data are clustered into two different groups (Figure 4.28). Then, the standard deviation (σ) of each group is found using the Ω_{total} and the mean (μ) of that data group. Next, a Gaussian Monte Carlo Simulation (MCS) is performed to generate 50 realizations for each porosity datum using the calculated σ and μ by means of a developed Visual Basic code, which is given in Section 4 of Appendix D. These 50 realizations are extracted from Excel software into text files of GSLIB format by another Visual Basic Code. The details of the code are given in Section 5 of Appendix D. The generated 50 text files are then imported into SGeMS and named "Realization_i", where "i = 1, 2, 3, …, 50". Then, the distribution structure and the overall mean of the hard data are checked in order to verify that the introduced uncertainty has not disturbed them. In addition, the experimental variograms of the 50 realizations are computed and their best fitting variogram models are found. Then, the fitted models are plotted in order to investigate whether the introduced uncertainty have interrupted the autocorrelation (spatial correlation) of the real hard data or not.

Aiming at studying the effect of porosity uncertainty, the original reservoir is employed. In order to generate the reservoir models corresponding to the 50 generated porosity realizations, the methodology steps of Section 4.3 are repeated using the original reservoir. However, the only difference is in the porosity simulation part of the SGSIM algorithm. In the second page of the algorithm interface; "Data" (see Figure A.2), the "Hard Data" and the "Property with Reference Distribution" objects are selected as one of the 50 generated porosity realizations each time a new reservoir is modeled. For example, if the first reservoir is being modeled, the objects are selected as "Realization_1". As a result, the only factor affecting the reservoir models is the porosity uncertainty since the other parameters are constant. The investigation of this effect is the aim of this section.

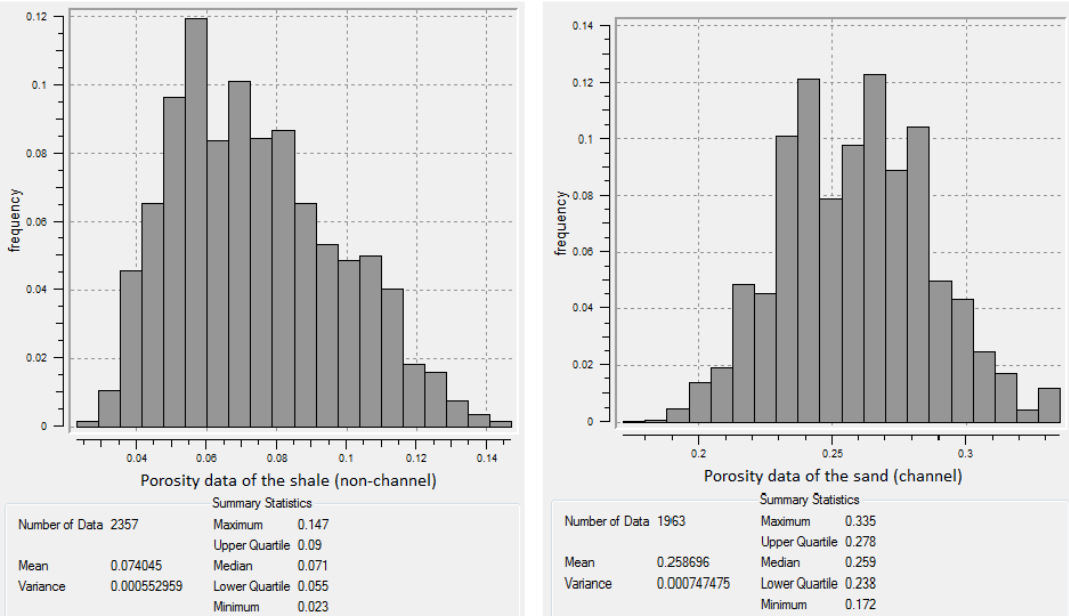

Figure 4. 28. Two groups of the porosity hard data

4.7.2 Analysis of Porosity Uncertainty Impact

The porosity uncertainty the OOIP and the ROIP of the 50 generated reservoirs corresponding to the MCS realizations of the previous section are plotted. In addition, the percentage errors of each case with respect to OOIP and ROIP of the original reservoir are calculated, plotted and analyzed. The calculation of the percentage errors and the investigation of the results' reliability are made as shown in Section 4.4.2.

In this section the effect of different Ω_{total} values on the percentage errors is investigated and compared with that of $\Omega_{hard\ data}$ (Table 4.8). The cases where Ω_{total} is 0.01, 0.02, 0.05, 0.10, and 0.15 are considered and 30 MCS are performed to generate 30 reservoir models for each case. The steps explained previously in Section 4.4.2 are followed here to generate the corresponding reservoir models.

Table 4. 8. Descriptive statistics of the porosity hard data

Original data	c.o.v	mean	StDev
Non-reservoir (Shale)	0.317578	0.074045	0.023515
Reservoir (Cannel)	0.105684	0.258696	0.027340

In addition, analysis of porosity uncertainty impact utilizing different upscaling method is carried out. In the previous parts of this study the arithmetic upscaling method is used. Although, the arithmetic upscaling method is widely used, it has a smoothing effect on the results. The median, on the other hand, is a more robust statistic (i.e. it is not affected with the number of small and large data). Thus, in this section the median upscaling method is employed and once again the total uncertainty ($\Omega_{total} = 0.265$) is used. In order to perform the upscaling using the median, the Visual Basic code of Section 4.3.4 is extended to include the option of "calculation method" which is either median or average. This code is given in Section 6 of Appendix D.

CHAPTER 5

RESULTS AND DISCUSSIONS

5.1 Sensitivity Investigation of the SNESIM Algorithm and the Methodology Proposed

In order to study the sensitivity of the SNESIM algorithm and the methodology proposed, the OOIP and ROIP values of the generated 50 equiprobable reservoirs as well as their corresponding percentage errors with respect to the values of the original reservoir are plotted (Figures 5.1 and 5.2). The OOIP and ROIP values of the generated reservoirs are in the ranges (71,233 – 71,195) M STB and (53,957 – 53,928) M STB, respectively. The percentage errors of these values with respect to those of the original reservoir are in the ranges (2.9% – -2.4%) and (3% – -2.4%), respectively. As expected the percentage error of the OOIP and ROIP are almost identical since the permeability is calculated from the porosity by means of logarithmic relations. These results verify that the SNESIM algorithm and the proposed method including its entire steps allow good reproduction of the original reservoir with confidence limits between 3% and -2.4%. In other words, the proposed method including SNESIM simulation, variogram fitting, SGSIM simulation, upscaling, and running the model in CMG (IMEX tool) is producing accurate results with accuracy of about ±3%.

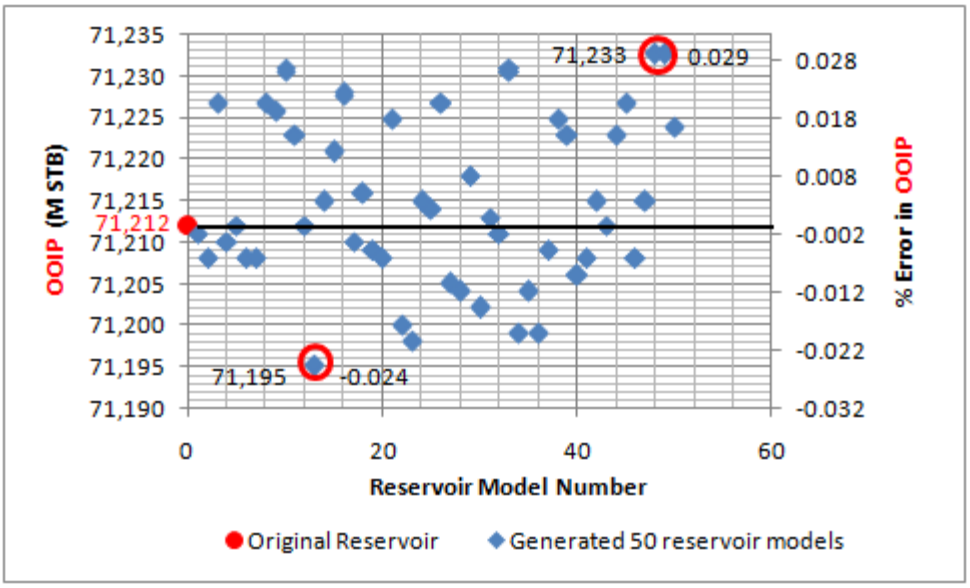

Figure 5. 1. The OOIP values of the 50 generated reservoir models and their percentage errors with respect to the OOIP of the original reservoir model

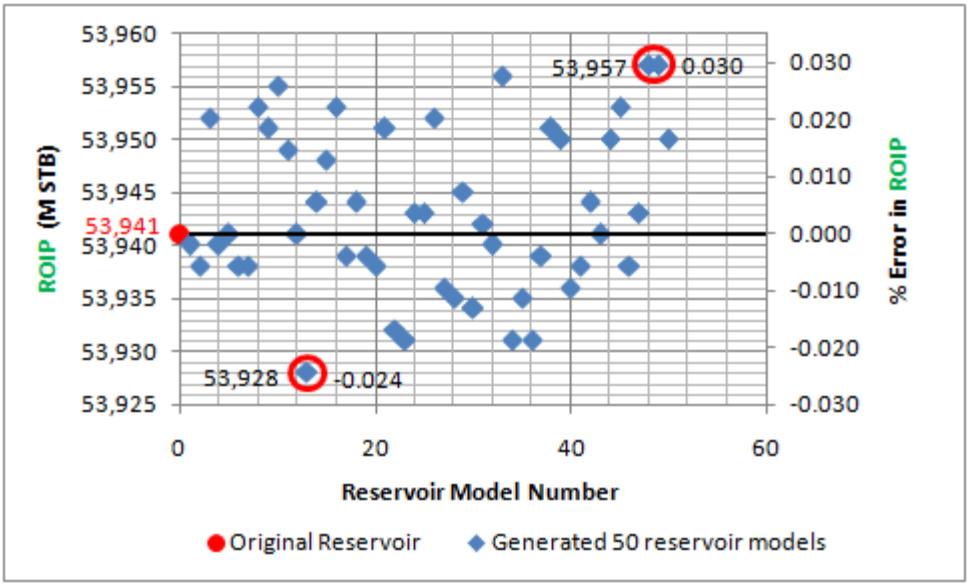

Figure 5. 2. The ROIP values of the 50 generated reservoir models and their percentage errors with respect to the ROIP of the original reservoir model

After that, the reliability of the information obtained with only 50 simulations is investigated by the utilization of the EasyFit statistical tool. The EasyFit tool is used to fit a distribution to the calculated percentage errors. As the error is normally distributed, a normal distribution is fitted to the errors. Then, the goodness of fit is checked by the same tool (Figure 5.3).

Normal [#27]					
Chi-Squared					
Deg. of freedom	4				
Statistic	1.8131				
P-Value	0.77009				
Rank	16				
a	0.2	0.1	0.05	0.02	0.01
Critical Value	5.9886	7.7794	9.4877	11.668	13.277
Reject?	No	No	No	No	No

Figure 5. 3. Goodness of fit details

In order to understand Figure 5.3 it is important to know the details of the EasyFit tool output. First of all, the null and alternative hypotheses being tested are:

H0 = the data follows the normal distribution.
H1 = the data does not follow the normal distribution.

Then, if the resulting p-value is less than the level of significance, the null hypothesis is rejected and within the required degree of certainty it cannot be stated that the data is normally distributed. In other words, if we would like to state within 95% certainty that the data can be described by the normal distribution, the resulting p-value must be greater than the level of significance. As the level of significance equals 1 minus the required degree of certainty, it is 0.05 in this case. In Figure 5.3 the resulting p-

value is 0.77 which is greater than the level of significance; therefore, the null hypothesis is not rejected. As a result, with at least 95% certainty it can be stated that the data is normally distributed, with N (0.00368, 0.01424).

Using the normal distribution fitted to the percentage errors, the reliability of the information obtained with only 50 simulations is investigated. First, the probabilities of finding an error within the limits of the calculated distribution or beyond them are calculated. Here only the OOIP error is considered as the error in the ROIP is almost identical. The probabilities P (x < -0.024) and P (x < 0.029) are calculated using the NORMDIST function in Excel software. The following equations show the calculation details:

$$P(x < -0.024) = 0.0260 \tag{5.1}$$

$$P(x > 0.029) = 1 - P(x < 0.029) = 0.0377 \tag{5.2}$$

$$\begin{aligned} P(-0.024 < x < 0.029) &= 1 - \big(P(x < -0.024) + P(x > 0.029) \big) \\ &= 1 - (0.0260 + 0.0377) = \ 0.9363 \end{aligned} \tag{5.3}$$

These probability values show that if more than 50 simulations are performed the chance of obtaining errors within the limits of the obtained normal distribution is 0.9363. Thus, it is almost sure that other simulations will provide the same information which obtained with only 50 reservoir models. In other words, the 50 reservoir models are enough to comment on the sensitivity of the methodology proposed.

5.2 Sensitivity Investigation of the Variogram Model

In order to perform this analysis the following variogram models are fitted to the experimental variogram of the original reservoir realization shown in Figure 4.7:

- A Spherical variogram model
- A Gaussian variogram model

- An Exponential variogram model with lower ranges than those of the original variogram given in Table 4.2
- An Exponential variogram model with larger ranges than those of the original variogram

The plots and parameters of these variogram models are shown in Tables 5.1 through 5.4 and Figures 5.4 through 5.7, respectively. After finding these variogram models, the corresponding reservoirs' porosities are generated. Then, the other reservoir modeling steps given in Section 4.3 are followed to get the corresponding cumulative oil production plots and their data.

Table 5. 1. The parameters of the Spherical variogram model fitted to the experimental variogram of the original reservoir. Ranges are shown in feet

Type	Spherical
Nugget	0.08
Sill	0.1485
Ranges	14/14/14
Angles	0/0/0

Table 5. 2. The parameters of the Gaussian variogram model fitted to the experimental variogram of the original reservoir.

Type	Gaussian
Nugget	0.095
Sill	0.135
Ranges	15/14/11
Angles	0/0/0

Table 5. 3. The parameters of the Exponential variogram model with lower ranges fitted to the experimental variogram of the original reservoir.

Type	Exponential
Nugget	0.04
Sill	0.1895
Ranges	20.9/19.95/7.7
Angles	0/0/0

Table 5. 4. The parameters of the Exponential variogram model with larger ranges fitted to the experimental variogram of the original reservoir.

Type	Exponential
Nugget	0.04
Sill	0.1895
Ranges	23.1/22.05/8.51
Angles	0/0/0

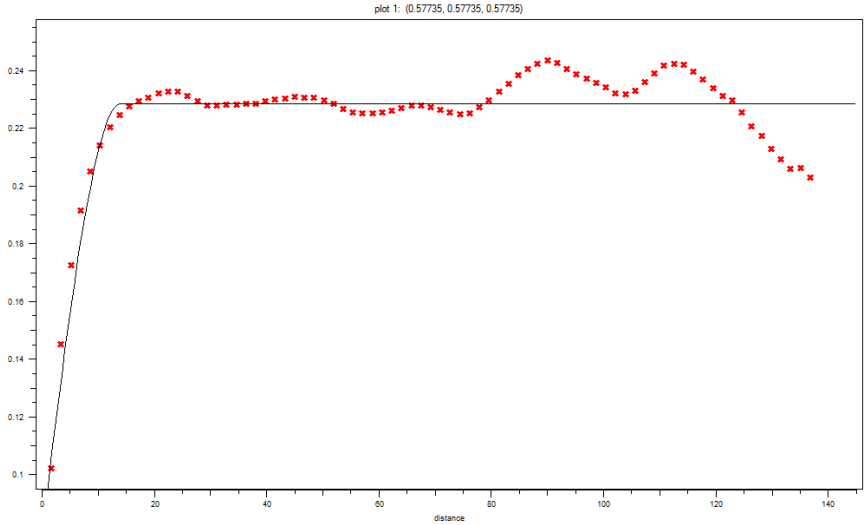

Figure 5. 4. The Spherical variogram model fitted to the experimental variogram of the original reservoir.

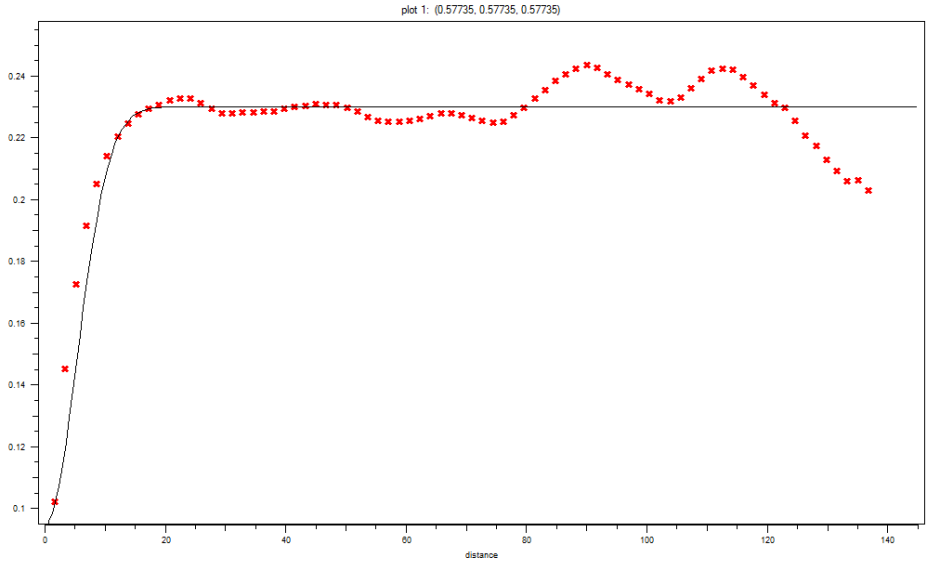

Figure 5. 5. The Gaussian variogram model fitted to the experimental variogram of the original reservoir

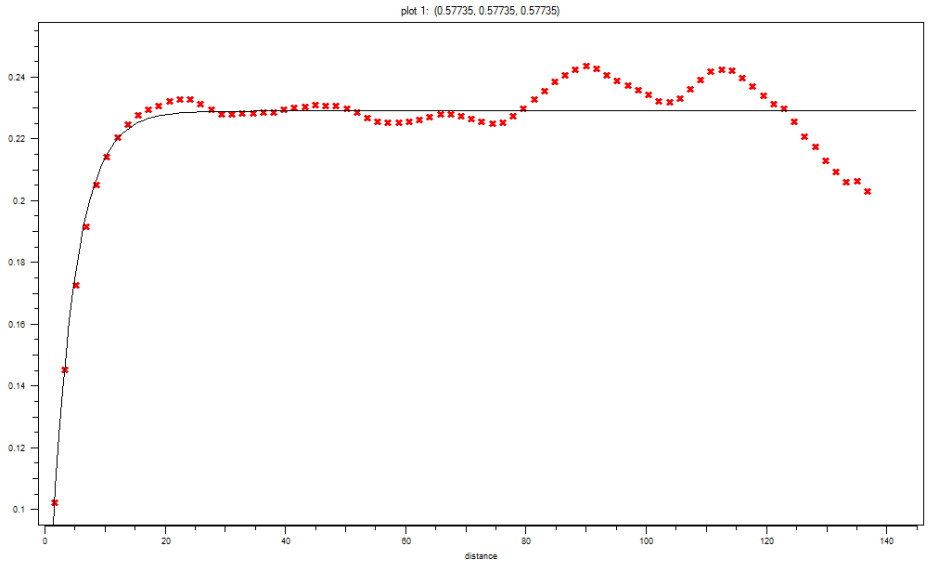

Figure 5. 6. The Exponential variogram model with lower ranges fitted to the experimental variogram of the original reservoir

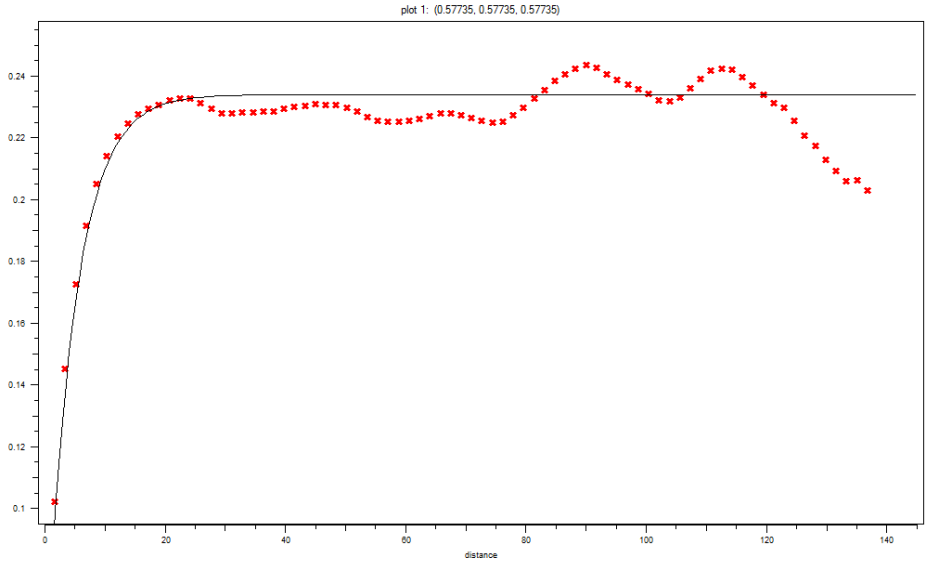

Figure 5. 7. The Exponential variogram model with larger ranges fitted to the experimental variogram of the original reservoir

To check the sensitivity of the reservoir model to the variogram model, the OOIP and ROIP of the generated reservoirs are compared with those of the original reservoir. None of the generated reservoirs output a value identical to that of the original reservoir (Table 5.5). For example, if the variogram used in modeling the original reservoir (see Table 4.4) is used, but with a 5% increase in the ranges it results in 0.16% change in the OOIP and ROIP values (Table 5.5). In addition, 5% decrease in the ranges of that variogram results in 0.19% change in the OOIP and ROIP values (Table 5.5). Although, the percentage differences are not very large, it is very clear that the reservoir model is sensitive to the variogram used in the simulation of porosity. As a result, it is advised to carefully select the appropriate variogram model when using the proposed modeling methodology.

Table 5. 5. Comparison of the reservoirs generated using different variogram models with the original reservoir

The variogram Model used	OOIP (M STB)	ROIP (M STB)	Difference in OOIP (M STB)	Difference in ROIP (M STB)	Difference (%)
Original variogram (Exponential)	71,212	53,941			
Gaussian model	72,202	54,691	990	750	1.39
Spherical model	72,475	54,897	1,263	956	1.77
Exponential with larger ranges	71,100	53,856	-112	-85	-0.16
Exponential with lower range	71,344	54,041	132	100	0.19

5.3 Impact of Training Image Parameters on Reservoir Model

5.3.1 Effect of Training Image Parameters on Cumulative Oil Production

In this section the effect of training image modification on the cumulative oil production is investigated. So, the effect of each training image parameter (i.e. amplitude, and number of waves in each channel, number of fixed-width channels, and number of slices in Z direction) on the cumulative oil production is studied individually. The following subsections illustrate this work.

5.3.1.1 Effect of Z slice number

From Figure 5.8 it is very clear that the number of Z slices has a great influence on the amount of the cumulative oil production. Figures 5.8 through 5.10 demonstrate that the values of the cumulative oil production obtained using training images having 1, 2, 3, and 4 Z slices do not represent the original reservoir. In contrast, the results of the simulations in which training images having 5, 6, 7, and 8 Z slices are used, yield

values closer to that of the original reservoir. Note that the increase in the number of Z slices beyond 5 has no noticeable effect on the cumulative oil production value. Thus, it can be said that training images having at least 5 Z slices are needed to simulate the considered reservoir accurately using the MPG technique proposed. This can be generalized to all 3D reservoirs if verified by applications to reservoirs with thicker and thinner grid sizes.

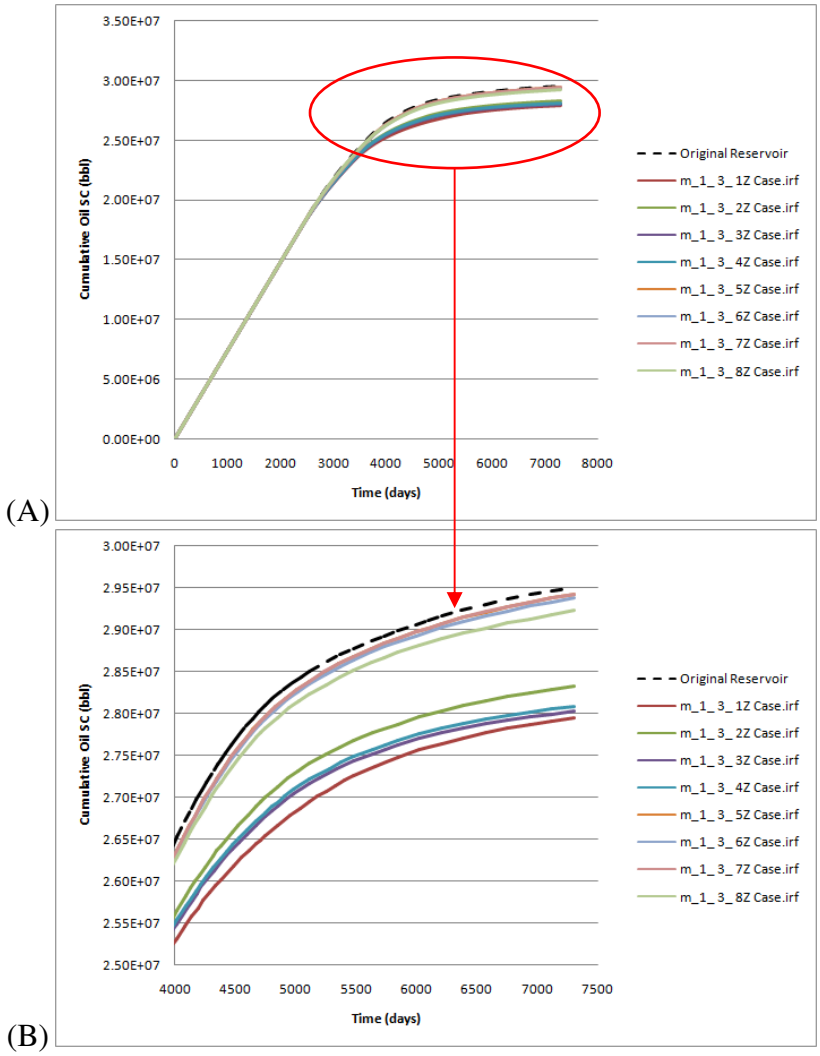

Figure 5. 8. Medium Amplitude_ One Wave_ Three Channels Cases; (A). Exaggerated plot of the highlighted part of A; (B)

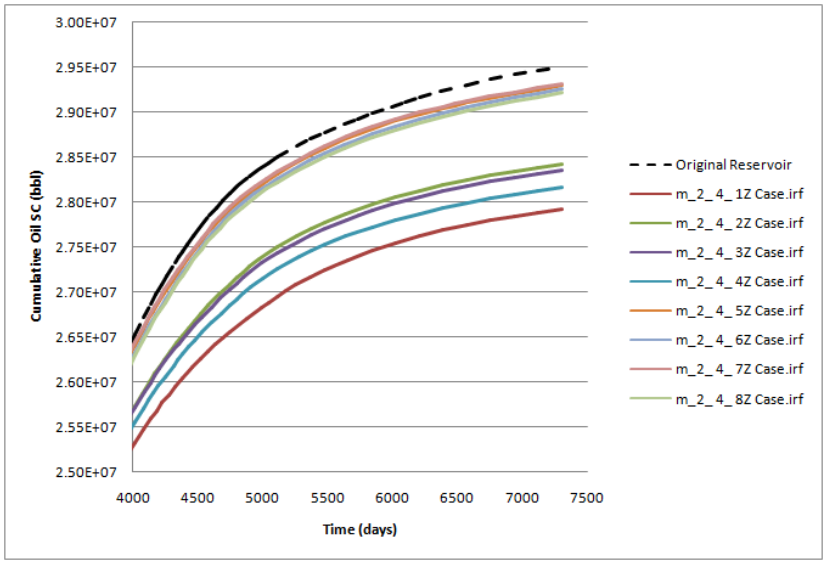

Figure 5. 9. Medium Amplitude_ Two Waves_ Two Channels Cases

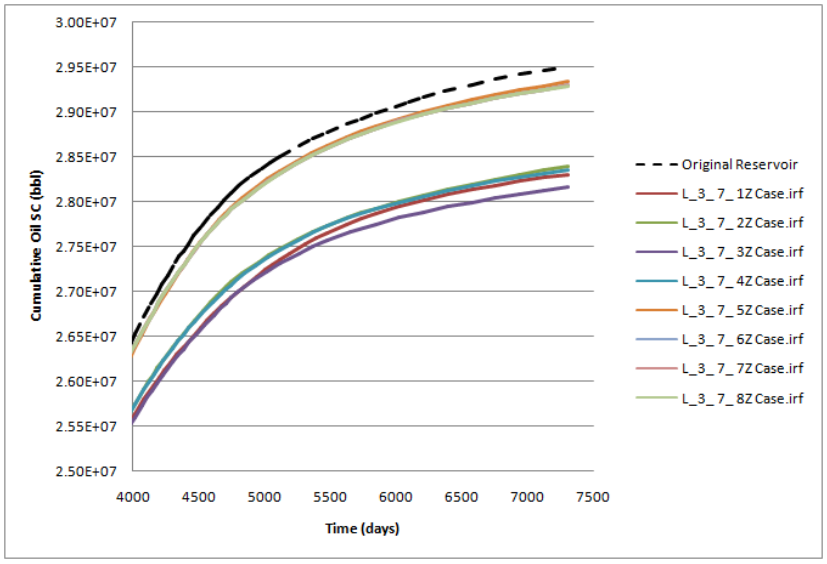

Figure 5. 10. Low Amplitude_ Three Waves_ Seven Channels Cases

The reason behind the differences between cumulative oil production values of reservoirs obtained using training images with 4 Z slices or less and the ones obtained with 5 Z slices or more is the extreme underestimation of the porosity. This extreme

underestimation of the porosity clearly occurs somewhere between the porosities obtained by the use of 4 and 5 Z slices (see Figures 5.8 through 5.10). When the porosity is significantly underestimated, the pore volume and therefore the OOIP are significantly underestimated too. As a result, the reservoir is depleted faster. In addition, the reservoir pressure drops faster and therefore the control of each production well is switched from constant rate constraint to BHP constraint. Thus, the value of cumulative oil production for such reservoir at the end of the production period is definitely less than that of a reservoir having a larger porosity value.

The results show that at least 5 Z slices are needed to perform a representative simulation of the original reservoir. However, the original reservoir model is synthetic and generated using the original training image which consists of 5 Z slices too. So, this might be the reason behind the defined 5 Z slices threshold. In order to investigate that, the original reservoir is remodeled four more times using different training images. These training images are generated using the Z slices of the original image (see Figure 4.3). The details of the training images generated are given below.

- The first training image is generated using the first four Z slice of the original training image (i.e. it contains 4 Z slices)
- The second training image consists of the first Z slice of the original training image repeated five times (i.e. it contains 5 Z slices)
- The third training image consists of the last Z slice of the original training image repeated five times (i.e. it contains 5 Z slices)
- The fourth training image consists of the original training image with its all Z slices plus the last slice repeated one more time (i.e. it contains 6 Z slices)

Note that the first Z slice has the least number of channels and therefore the least channel proportion. In contrast, the last Z slice has the most number of channels and therefore the most channel proportion (see Figure 4.3). The channels proportions of the generated training images are given in Table 5.6.

Figure 5.11 illustrates the (cumulative oil production vs. time) plots of the reservoirs generated using the four training images of Table 5.6. Figure 5.11 shows that training image number 1 (TI_1), which has 4 Z slices, outputs cumulative oil production value far from the original value (i.e. the values of the original reservoir). Note that training image number 2 (TI_2), which has 5 Z slices, have less channel proportion than TI_1, but it outputs a larger cumulative oil production value which is not close to the original value as well. Training images number 3 (TI_3) and 4 (TI_4), on the other hand, overestimate the channel proportion of the original training image (see Table 5.6), however, they result in cumulative oil production values that are very close to the original values. So, TI_2 and TI_3 resulted in very different cumulative oil production values, although both of them consist of 5 Z slices. As a result, the threshold of a 5 Z slices defined earlier is not related to the size of the original training image utilized in modeling the original reservoir. However, the higher the channels proportion in the training image the more reasonable the result.

Table 5. 6. Categories' proportions of the training images used to investigate the effect of Z slice number

Name and description of training image	**Channel (Sand) proportion (%)**	**Shale (Non-channel) proportion (%)**
Original training image	0.271	0.729
TI_1 (with the first 4 Z slices original training image)	0.251	0.749
TI_2 (with the first Z slice of the original training image repeated 5 times)	0.145	0.855
TI_3 (with the last Z slice of the original training image repeated 5 times)	0.349	0.651
TI_4 (original training image with the last Z slices repeated one time)	0.284	0.716

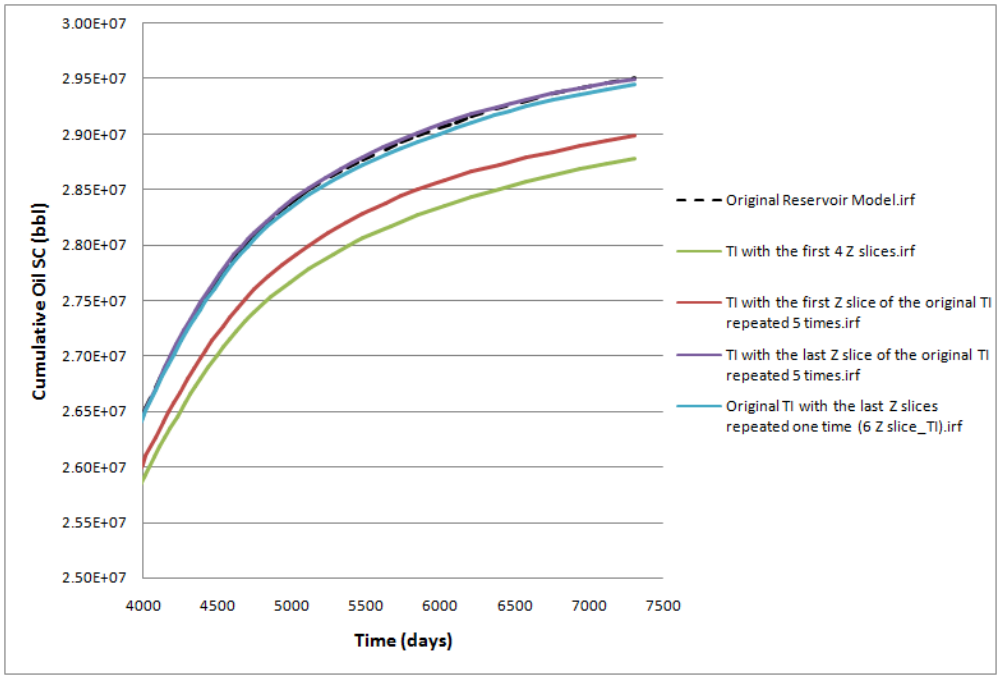

Figure 5. 11. Cumulative oil production versus time plots of the reservoirs generated using the four training images of Table 5.6

5.3.1.2 Effect of other parameters (channel number, wave number, and amplitude level)

The investigation of the channel number, wave number, and amplitude level effect on the cumulative oil production is performed in two steps. First, the reservoirs generated are grouped based on the parameters' values of the training images used. Then, the cumulative oil production values of the reservoirs in each group are plotted and compared.

The results of the previous section showed that the training images having 1, 2, 3, and 4 Z slices are not suitable for the simulation of the original reservoir. Thus, the reservoirs consider in this part are the ones modeled using 5, 6, 7, and 8 Z slices training images (in total 156 reservoirs) (see Table 4.7).

Figures 5.12, through 5.15 illustrate the results of the reservoirs generated using one, two, and three medium-amplitude-wave channels, respectively. In these figures the reservoirs generated using the one and two channels' training images having medium amplitude waves, output unrepresentative results. In Figure 5.12 the one channel training image produces a reservoir which overestimates the cumulative oil production of the original reservoir although it has less pore volume and therefore less OOIP and ROIP than those of the original reservoir (Table 5.7). The reason behind that is the dissimilarity between the grid blocks' pressure of the generated and the original reservoir. To clarify, the wells are initially operated on constant rate constraint, but if the borehole pressure in any well fails to produce the rate specified, the bottomhole pressure constraint becomes the operating constraint of that well. Then, the simulator (i.e. IMEX) calculates the pressure difference value (i.e. grid block pressure – wellbore pressure) and uses it to calculate a new production rate for each timestep. As a result, the cumulative oil production depends on the value of the pressure difference which is a function of the grid block pressure. However, the grid block pressure changes according to the value of its simulated porosity which is a function of the training images used. The arithmetic upscaling application has a smoothing effect on the cumulative oil production as well. However, its impact on all the reservoir models is the same; therefore, it does not cause a great change unless the porosity values are totally different. As a result, the one channel training image is not suitable for simulating the original reservoir as it does not produce representative reservoir. In addition, the two channels' training image in Figure 5.12 produces unrepresentative reservoir model since its cumulative oil production extremely underestimates that of the original reservoir. That happens due to the underestimation of the grid porosities which causes the grid pressure to be very low. As a result, the two channel training image is also not suitable for simulating the original reservoir. In Figures 5.13 through 5.15 the one channel training images also show unreliable results as their cumulative oil production curves are changing while the others are almost constant. The reason for that is also the unrepresentative porosity.

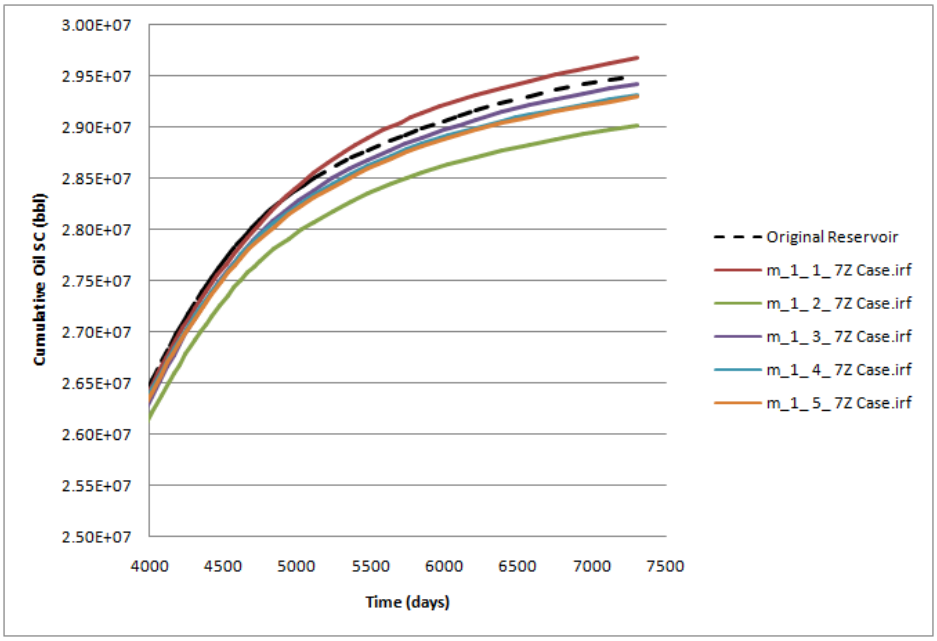

Figure 5. 12. Cumulative oil production for reservoirs generated using training images with different numbers of channels. The abbreviation (m_1_1_7Z) stands for medium amplitude_ one wave_ one channel_ 7 Z slices training image

Table 5. 7. Comparison of the reservoir models given in Figure 5.12

	Original	**m_1_1_7Z**	**m_1_2_7Z**	**m_1_3_7Z**	**m_1_4_7Z**	**m_1_5_7Z**
Reservoir pore volume (M rbbl)	179659	178373	178978	179194	179096	179121
OOIP (M STB)	71212	71158	71371	71223	71422	71431
ROIP (M STB)	53941	53900	54061	53950	54100	54107
Cumulative oil production (M STB)	29502	29681	29021	29429	29310	29294
Current oil in place (M STB)	41714	41476	42347	41793	42094	42131

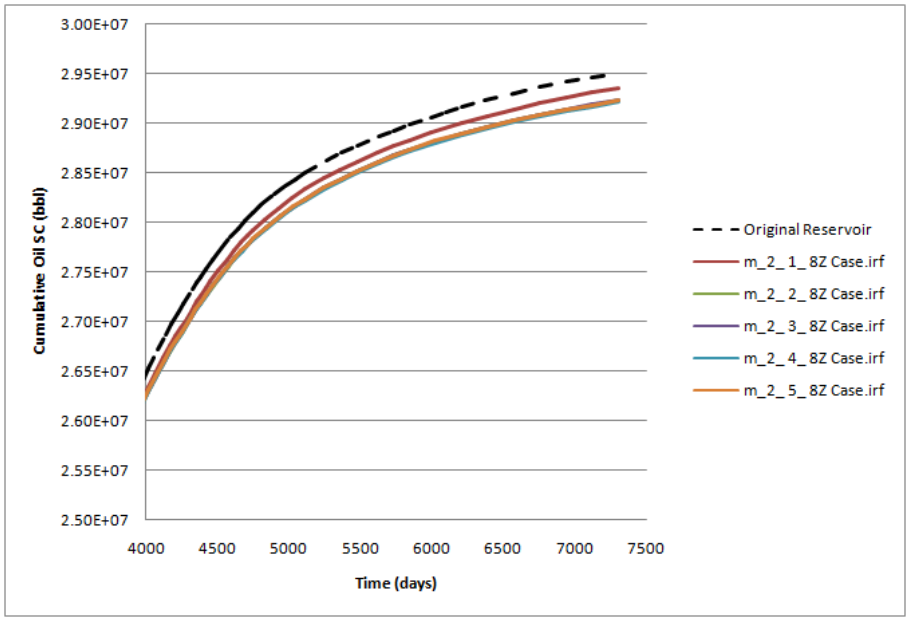

Figure 5. 13. Cumulative oil production for reservoirs generated using training images having different numbers of channels, two waves, medium amplitude, and eight Z slices

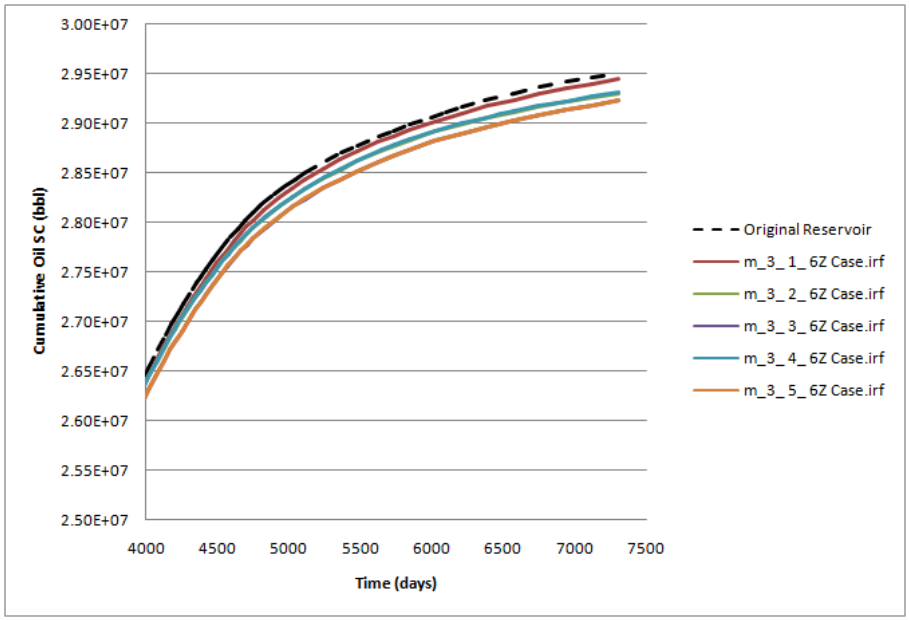

Figure 5. 14. Cumulative oil production for reservoirs generated using training images having different numbers of channels, medium amplitude, three waves, and six Z slices

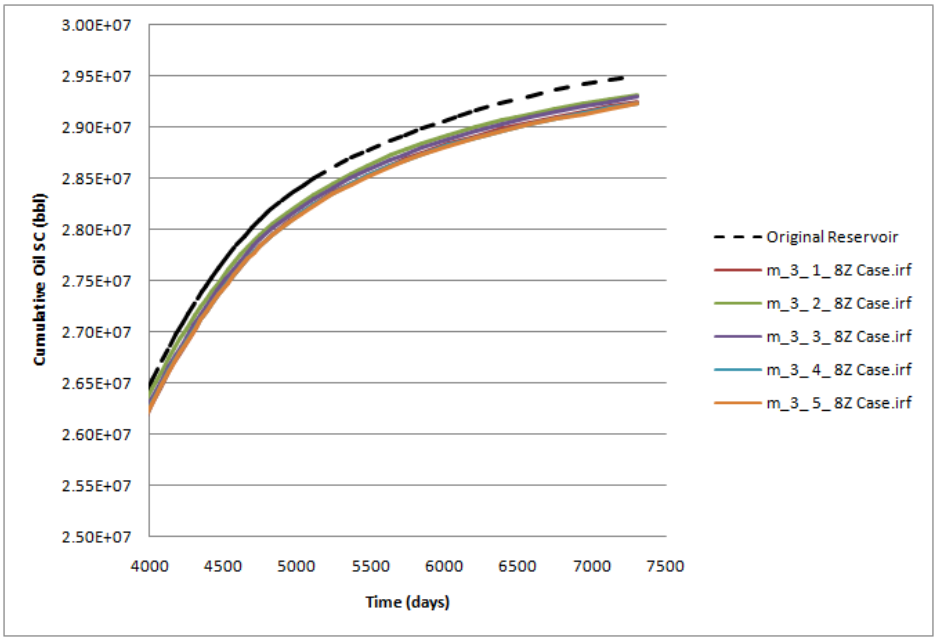

Figure 5. 15. Cumulative oil production for reservoirs generated using training images having different numbers of channels, medium amplitude, three waves, and six Z slices

Due to the same reasons the low-amplitude-wave channel cases produce completely unrepresentative results when one-wave-channel training images are used (Figures 5.16 and 5.17). However, in the 2 and 3 waves' cases at least 3 channels are needed to get fair results (Figures 5.18 and 5.19). As a result, training images having medium and low amplitude wave channels with less than 5 Z slices, 3 channels, and 2 waves in each channel produce reservoirs with porosity values that do not represent the original reservoir. Based on these findings and as a general rule, the training images having medium and low amplitude wave channels produce reservoirs with reliable cumulative oil production results when at least 5 Z slices, 3 channels and 2 waves in each channel are used in the training image (other results' plots are given in the attached CD).

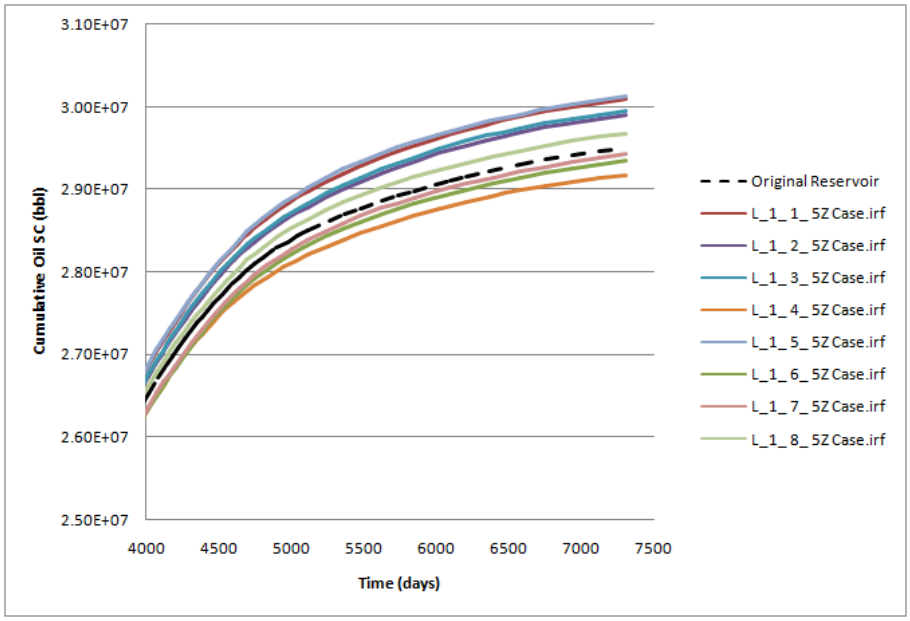

Figure 5. 16. Cumulative oil production for reservoirs generated using training images having different numbers of channels, low amplitude, one waves, and five Z slices

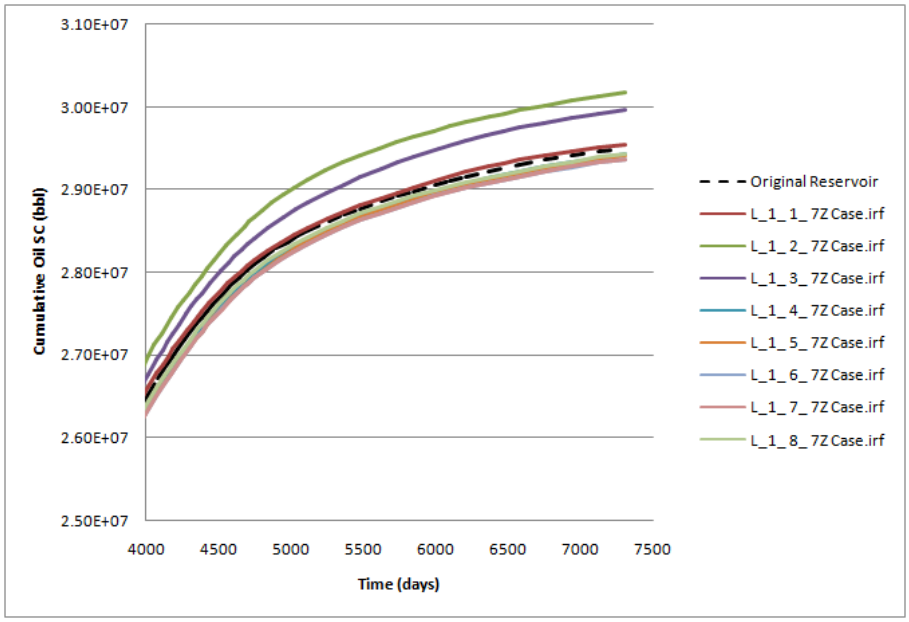

Figure 5. 17. Cumulative oil production for reservoirs generated using training images having different numbers of channels, low amplitude, one waves, and seven Z slices

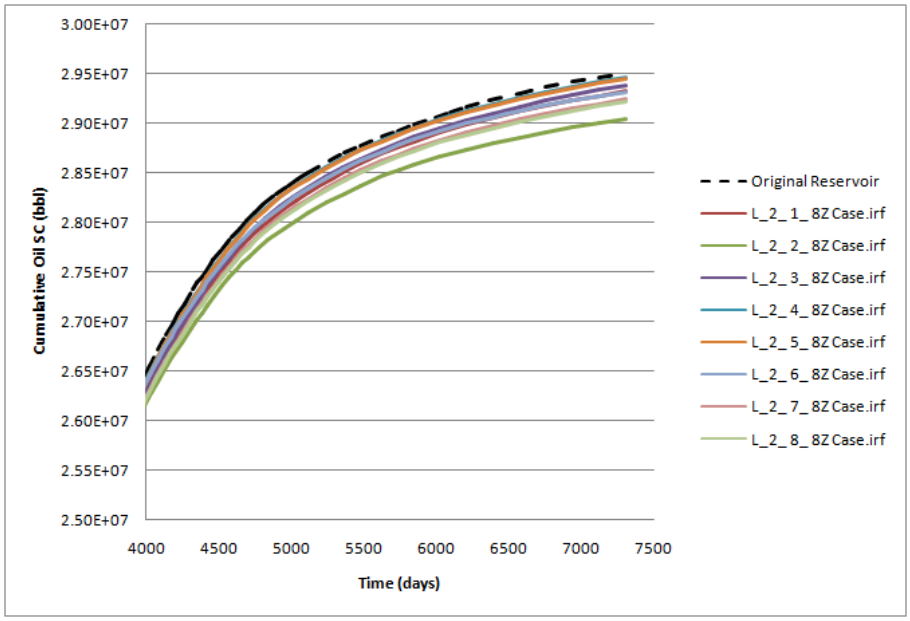

Figure 5. 18. Cumulative oil production for reservoirs generated using training images having different numbers of channels, low amplitude, two waves, and eight Z slices

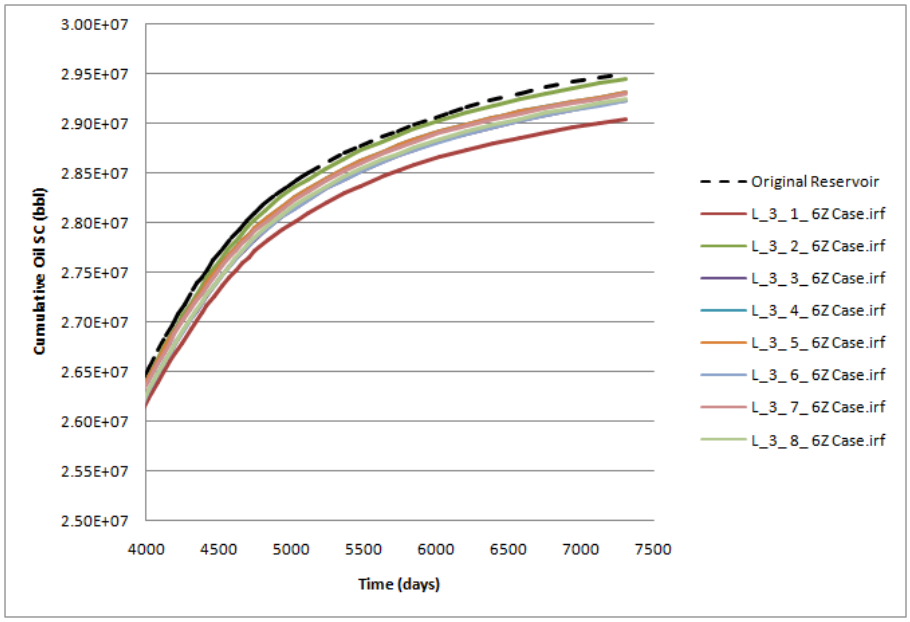

Figure 5. 19. Cumulative oil production for reservoirs generated using training images having different numbers of channels, low amplitude, three waves, six Z slices

The channels' number is limited by the size of the training image, number of waves in each channel, and the amplitude level of waves. In the high amplitude case it was not possible to fit more than 3 channels having one wave, or 2 channels having 2 and 3 waves into the training image (Figure 5.20). So, the number of cases generated is not large enough to mean anything statistically. Thus, the high amplitude cases are not considered in the present study.

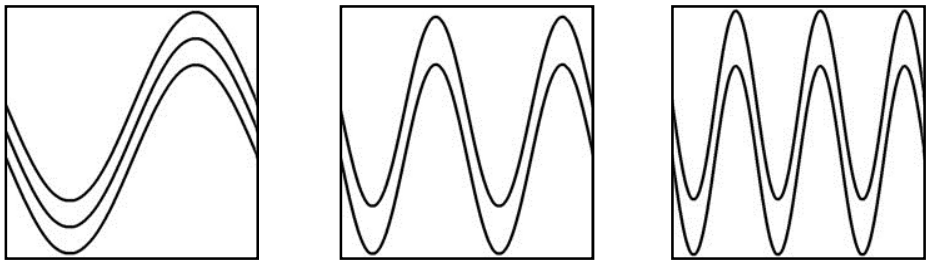

Figure 5. 20. The high amplitude cases fitted to the limited size training image

In general the pore volumes of the models developed in the present study underestimate the pore volume of the original reservoir (see Table 5.7). This is due to the underestimation of the porosity. That can either be because the training image is not pattern-rich or its sand (i.e. channel) proportion is not high enough. Strebelle, (2000) and Arpat (2005) indicated that when a training image is not large enough or when it is not pattern-rich the data events of that training image are not enough to condition to when simulating unsampled nodes. However, in the present case the same training image size is used, therefore, low channel proportion means pattern-poor. Thus, the underestimation of the porosity is due to the fact that all the cases have channel proportions less than that of the original training image (Table 5.8).

Although, SNESIM has a servosystem parameter that forces it to remain close to the global target proportions (or target marginal distribution) defined by the user (Strebelle, 2000), it still underestimates the value of the channel proportion.

Increasing the servosystem parameter value brings the simulated marginal probability closer to the target, but at a cost of losing the structural information of facies (Liu, 2006). So, the use of training image that is not pattern-rich leads to poor reproduction of pattern in SNESIM algorithm. In other words, when modeling fluvial reservoirs less continuity of sinuous channel patterns are obtained therefore porosity is underestimated. These lead to erroneous flow responds. So, the thresholds defined earlier are the ones below which the SNESIM algorithm fails to reproduce the closest marginal probabilities and patterns of the reservoir under consideration.

Table 5. 8. The sand and shale proportions of the original training image and the training image with the highest channel proportion among the developed training images

Training Image	**Channel (sand) proportion**	**Non-channel (shale) proportion**
Original image	0.271	0.739
Training image having 3 waves, 8 channel, and 8 Z slices	0.154925	0.845075

5.3.1.3 Effect of parameters' variation

The effect of the parameters variation is examined and the results show that:

1. As the number of channels and waves increase the uncertainty of the simulation decreases. For example, the uncertainty range decreases from 435 M STB to 70 M STB when the number of channels having medium-amplitude waves increases from 1 to 3 in an 8 Z slices training image (Figures 5.21). In addition, it decreases from 801 M STB to 237 M STB when the number of low-amplitude waves in channels increases from 1 to 3 in a 7 Z slices training image (Figures 5.22).
2. The increase in the number of Z slices from 5 to 8 and in the amplitude level from low (A_3 = 30 pixels) to high (A_1 = 75 pixels) have no noticeable effect on the uncertainty (Figures 5.23 and 5.24).

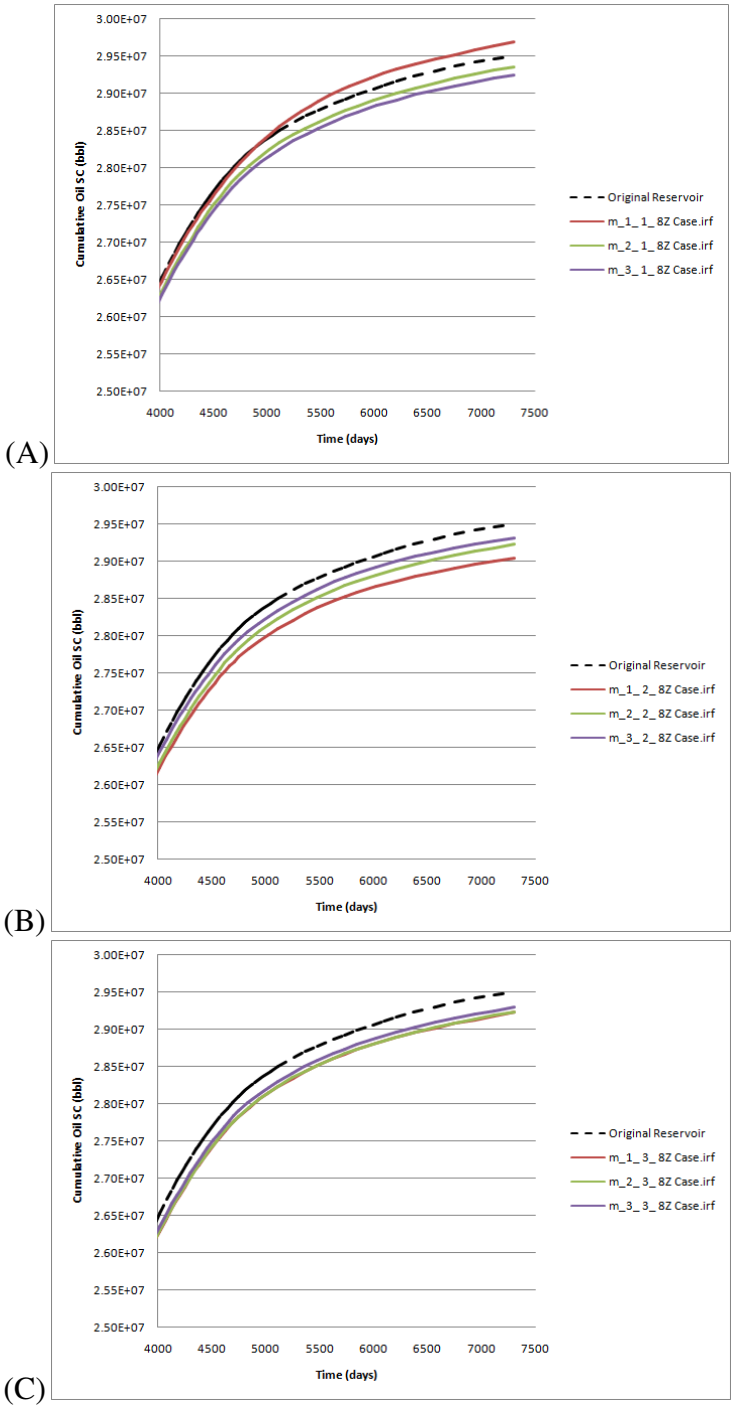

Figure 5. 21. (Effect of channel's number): medium amplitude_ **one channel**_ eight Z slices cases; (A), medium amplitude_ **two channels**_ eight Z slices cases; (B), medium amplitude_ **three channels**_ eight Z slices cases; (C)

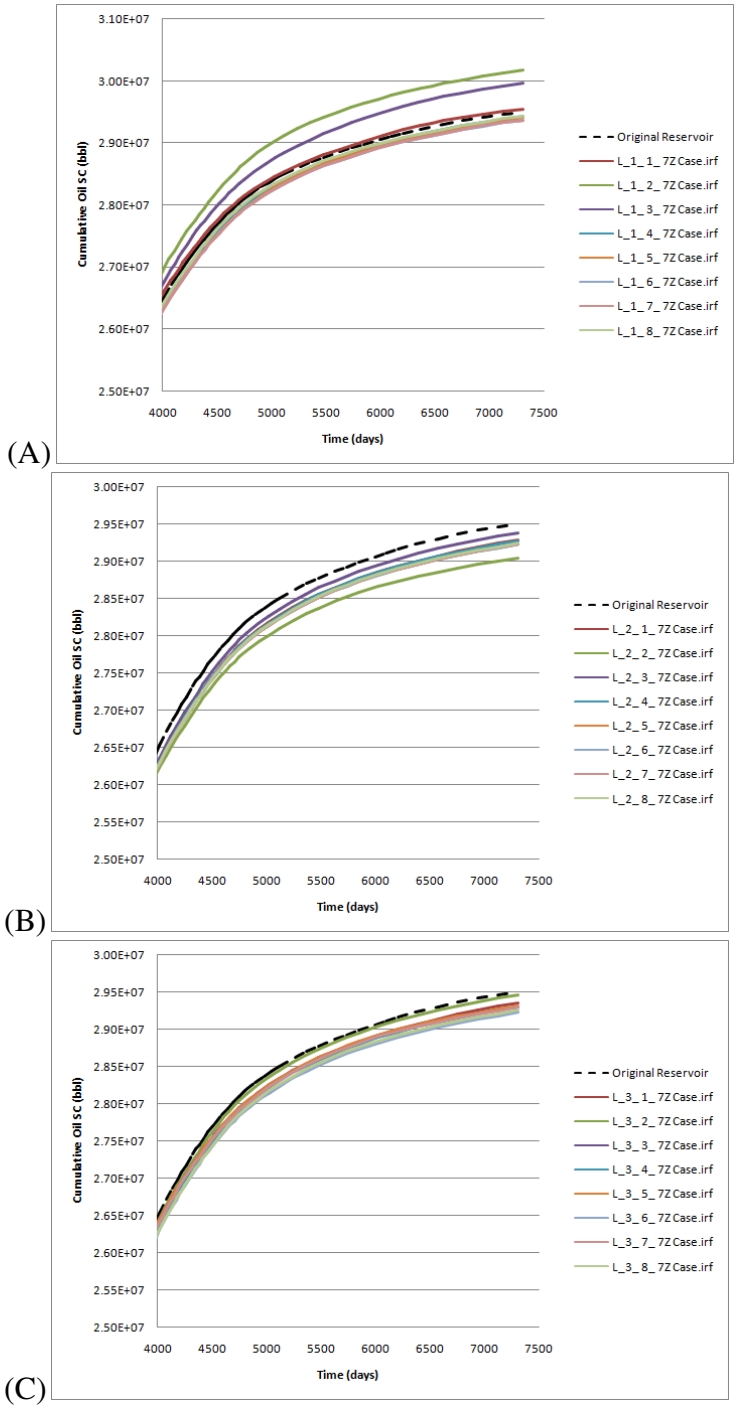

Figure 5. 22. (Effect of wave's number): low amplitude_ **one wave**_ seven Z slices cases; (A), low amplitude_ **two waves**_ seven Z slices cases; (B), low amplitude_ **three waves**_ seven Z slices cases; (C)

(A)

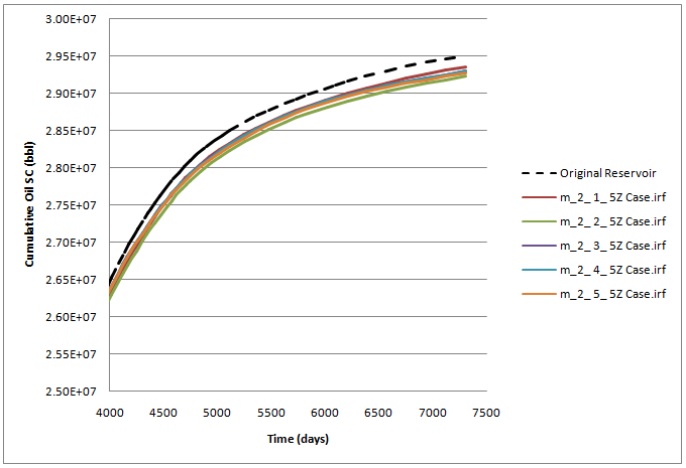

(B)

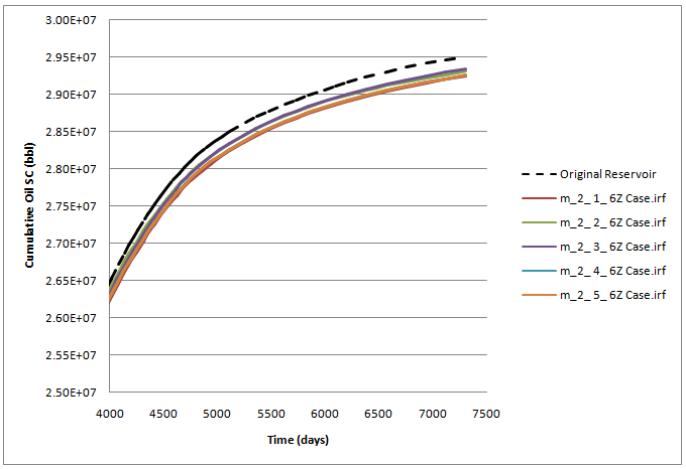

(C)

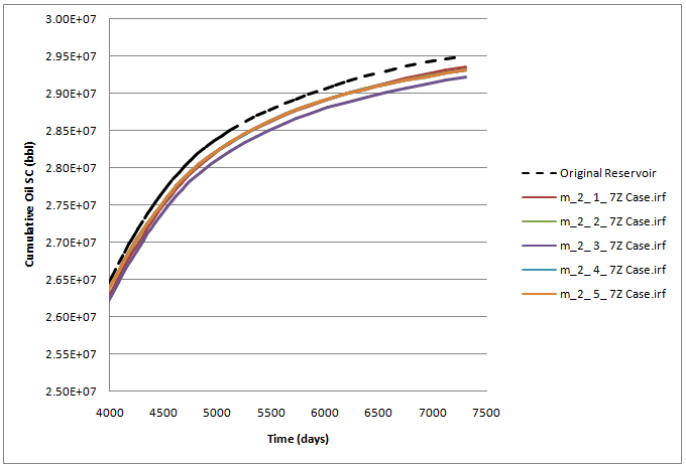

Figure 5. 23. (Effect of Z slices' number): medium amplitude_ two waves_ **five Z slices** cases; (A), medium amplitude_ two waves_ **six Z slices** cases; (B), medium amplitude_ two waves_ **seven Z slices** cases; (C)

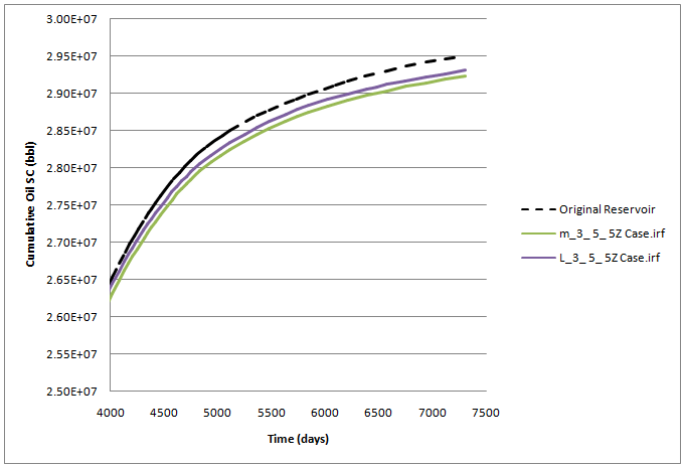

(A)

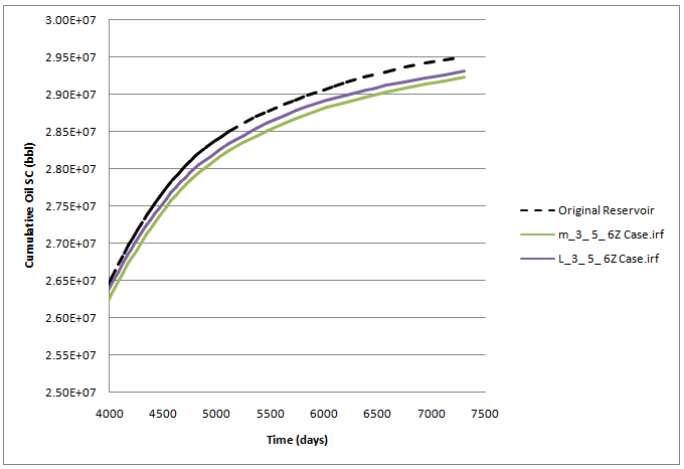

(B)

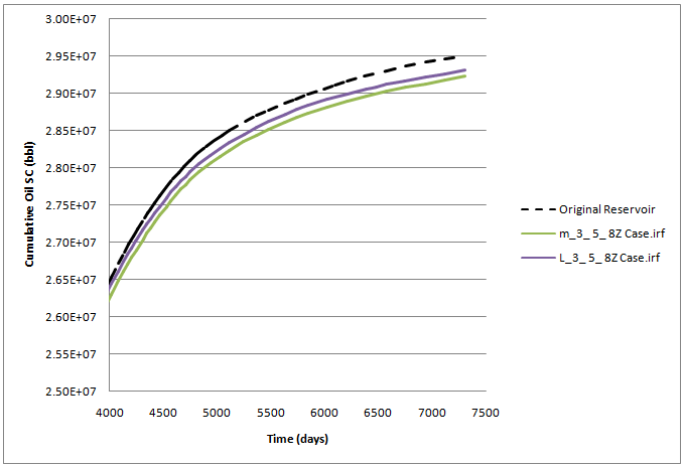

(C)

Figure 5. 24. (**Effect of amplitude**): three wave_ five channels_ five Z slices cases; (A), three wave_ five channels_ six Z slices cases; (B), three wave_ five channels_ eight Z slices cases; (C)

5.3.2 Effect of Training Image Parameters on OOIP and ROIP

In this section the effect of training image parameters on the OOIP and ROIP is studied. The effect of the parameters on both OOIP and ROIP are identical as expected because the permeability is calculated based on the porosity utilizing the logarithmic relations of Figure 4.13. The effect of the Z slice number shows no specific trend except for the 1 Z slice case. The training images having 1 Z slice always overestimates the OOIP and ROIP which clearly indicates that 2D training images are not suitable for 3D reservoir simulation (Figures 5.25 through 5.27). The smoothing effect of the arithmetic upscaling might be the reason behind the undefined trend of the change in OOIP and ROIP in the other cases of the Z slice number (i.e. 2, 3, …, 7, and 8 Z).

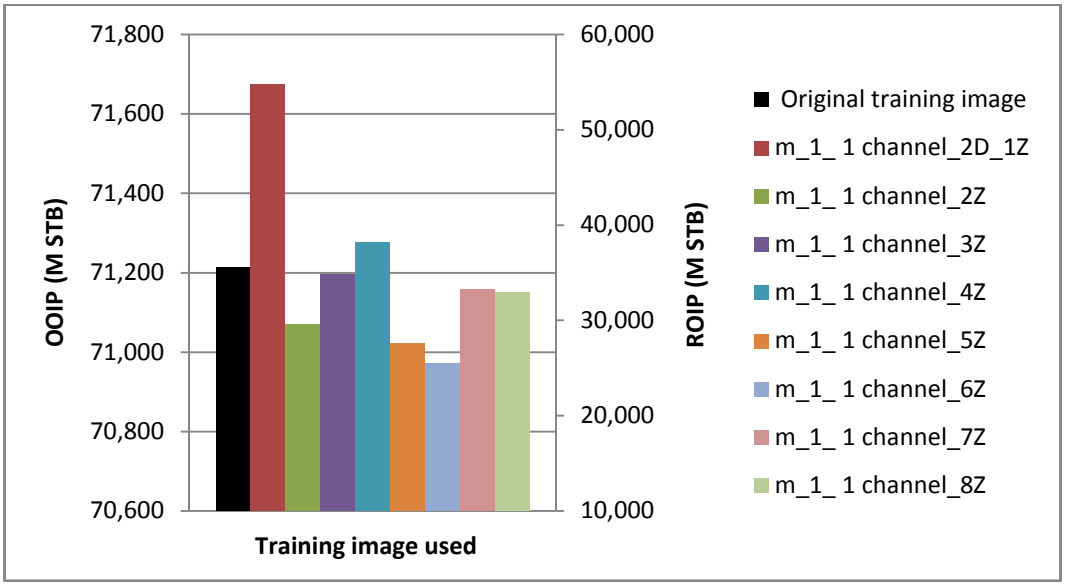

Figure 5. 25. OOIP and ROIP values for the reservoirs modeled using training images having different numbers of Z slices and one channel containing one wave having medium amplitude (m) level

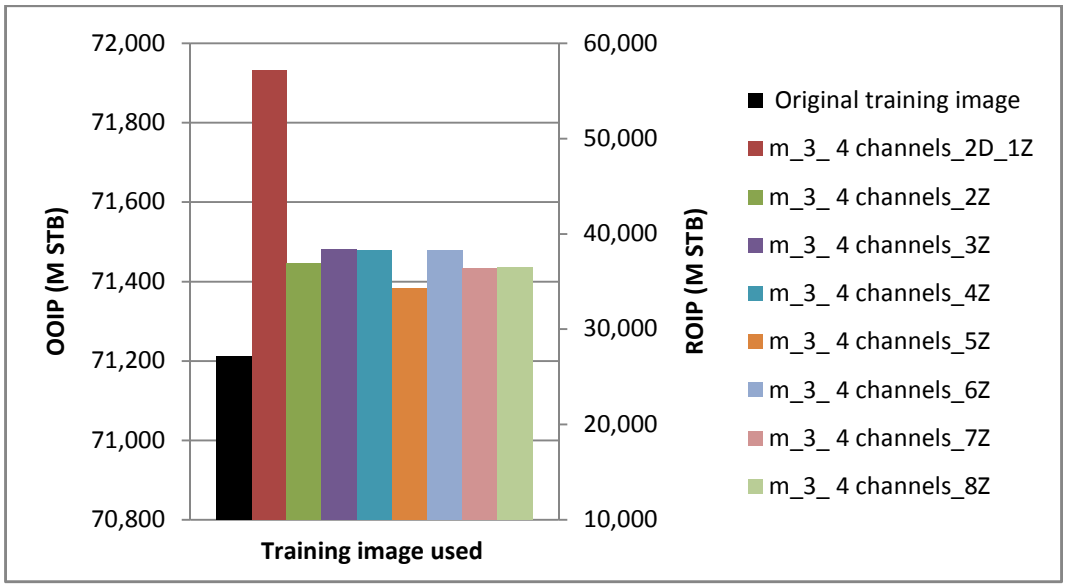

Figure 5. 26. OOIP and ROIP values for the reservoirs modeled using training images having different numbers of Z slices and four channels each contains three waves having medium amplitude (m) level

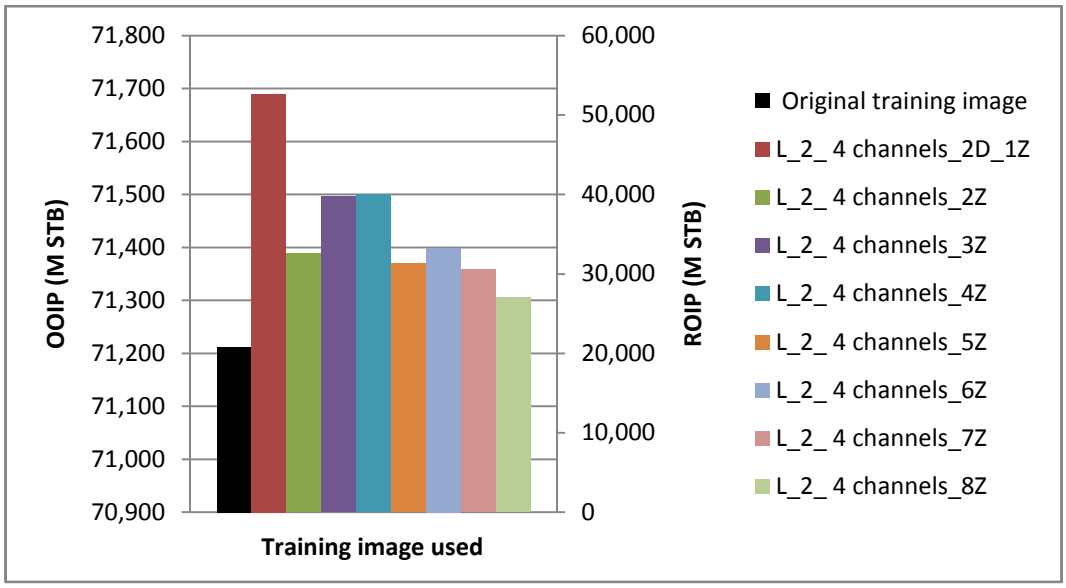

Figure 5. 27. OOIP and ROIP values for the reservoirs modeled using training images having different numbers of Z slices and four channels each contains two waves having low amplitude (L) level

The effect of training image channel number on the OOIP and ROIP is random (Figure 5.28 through 5.30). However, the amount of the OOIP and ROIP are directly proportional to the number of waves in the channels used (Figure 5.31 and 5.32). As in the case of the Z slice and channel number, the amplitude level of the wave has no specific effect on the OOIP and ROIP (Figure 5.33 and 5.34) (other results' plots are given in the attached CD).

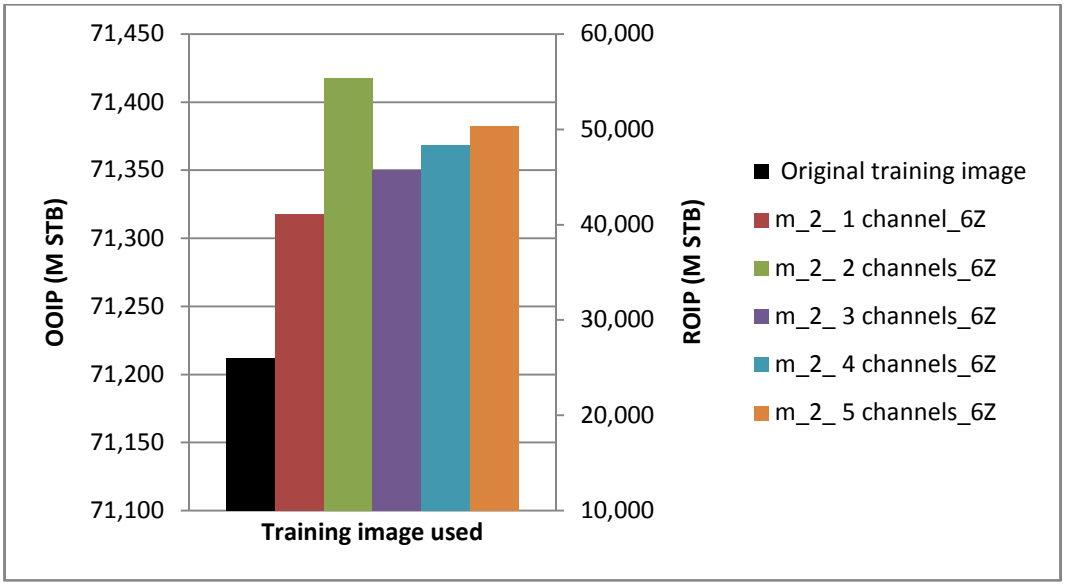

Figure 5. 28. OOIP and ROIP values for the reservoirs modeled using 6 Z slice-training images having different numbers of channels; each of these channels contains two medium amplitude waves

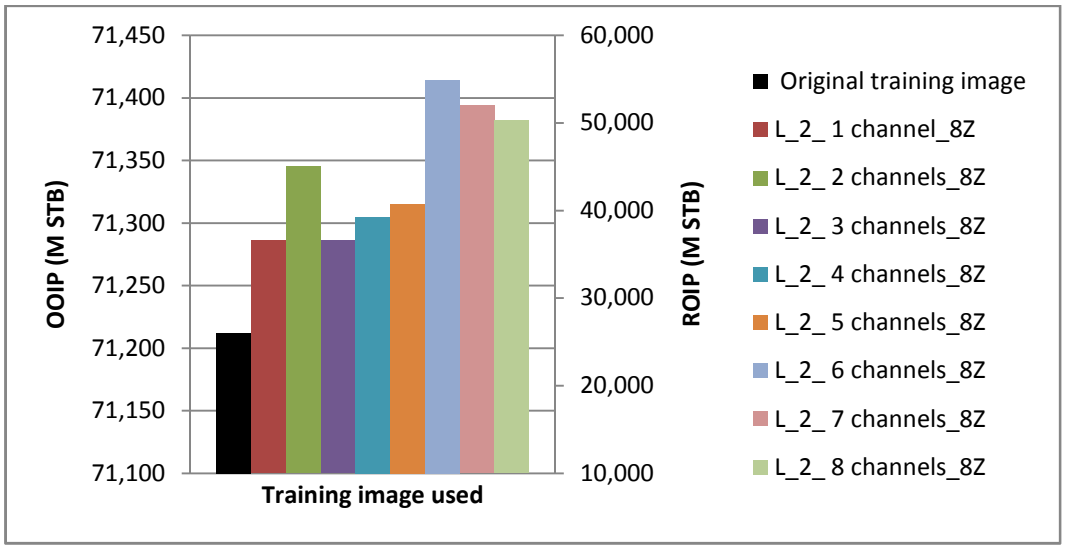

Figure 5. 29. OOIP and ROIP values for the reservoirs modeled using 8 Z slice-training images having different numbers of channels; each of these channels contains two low amplitude waves

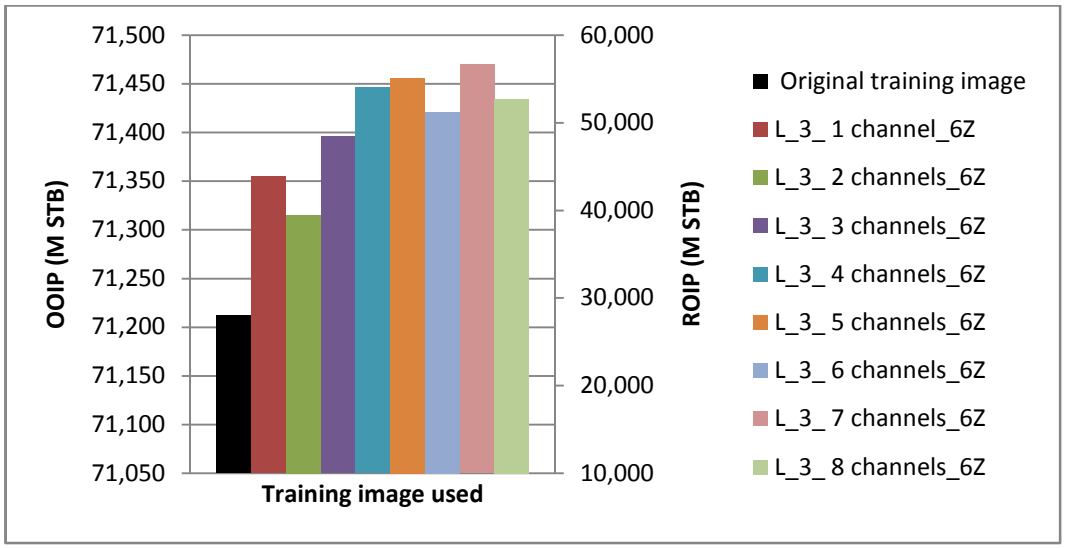

Figure 5. 30. OOIP and ROIP values for the reservoirs modeled using 6 Z slice-training images having different numbers of channels; each of these channels contains three low amplitude waves

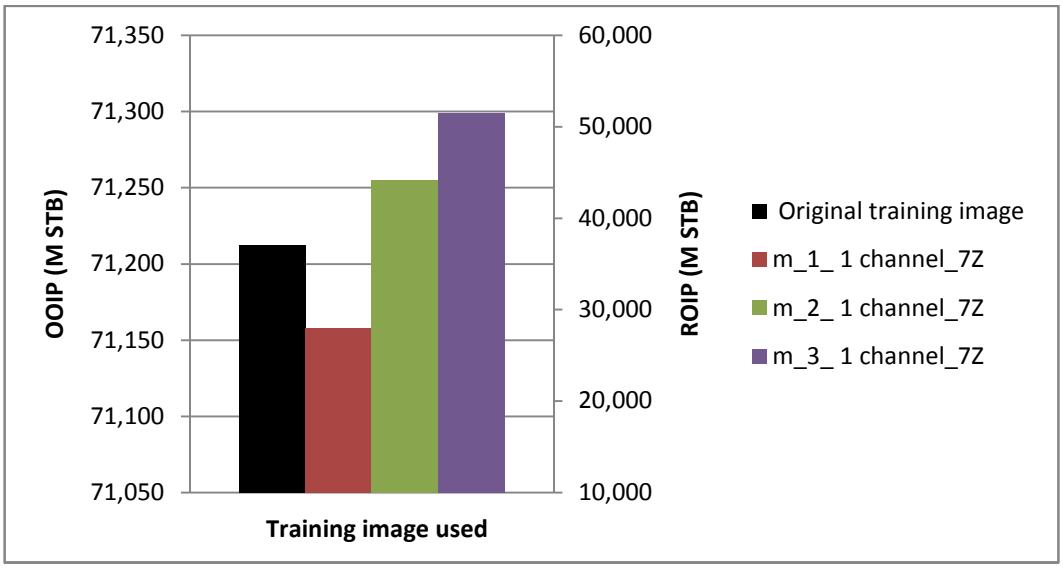

Figure 5. 31. OOIP and ROIP values for the reservoirs modeled using 7 Z slice-training images having a single channel with different numbers of medium amplitude waves

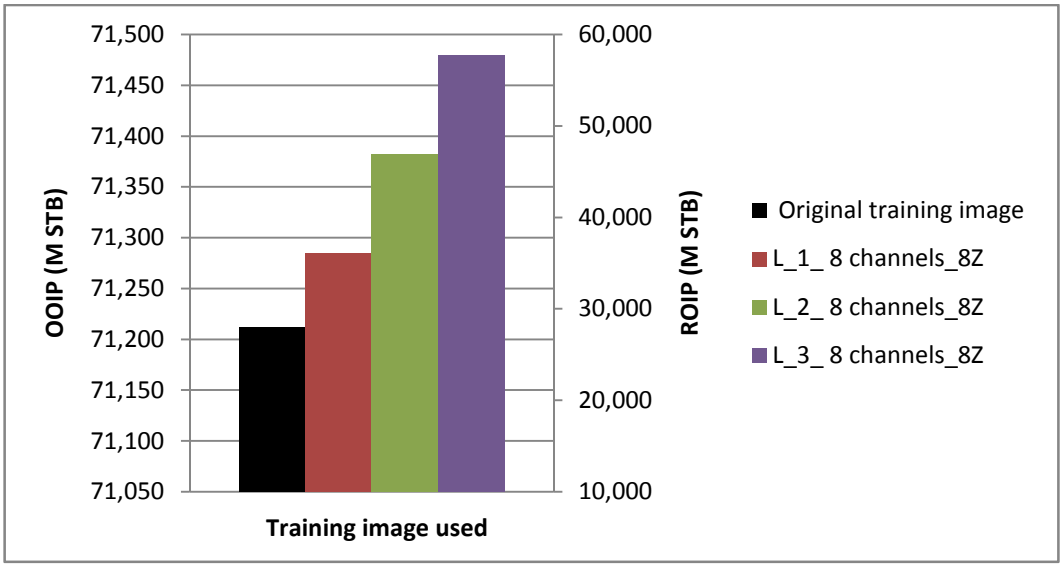

Figure 5. 32. OOIP and ROIP values for the reservoirs modeled using 8 Z slice-training images having eight channels; each of these channels contains different numbers of low amplitude waves

Figure 5. 33. OOIP and ROIP values for the reservoirs modeled using 5 Z slice-training images having three one-wave channels with different amplitude levels

Figure 5. 34. OOIP and ROIP values for the reservoirs modeled using 6 Z slice-training images having three two-wave channels with different amplitude levels

After analyzing the effect of each training image parameter on the OOIP and ROIP the percentage errors of each case with respect to OOIP and ROIP of the original reservoir are calculated using Equation 4.7. Next, the calculated percentage errors for the developed 368 reservoir models are plotted and analyzed. Figures 5.35 and 5.36 illustrate that the OOIP and ROIP can be predicted with an uncertainty range of +1.549% – -0.345%. Yet again the percentage errors of both OOIP and ROIP are identical as the permeability is calculated based on the porosity utilizing the logarithmic relations of Figure 4.11. However, this uncertainty range (i.e. +1.549 – -0.345) can be narrowed down by eliminating the cases that are not meeting the parameters thresholds defined in Section 5.3.1. As a result, the uncertainty range of the OOIP and ROIP prediction is reduce to 0.382% – 0.104% (Figures 5.37 and 5.38). This verifies that the defined thresholds provide the most representative reservoir models.

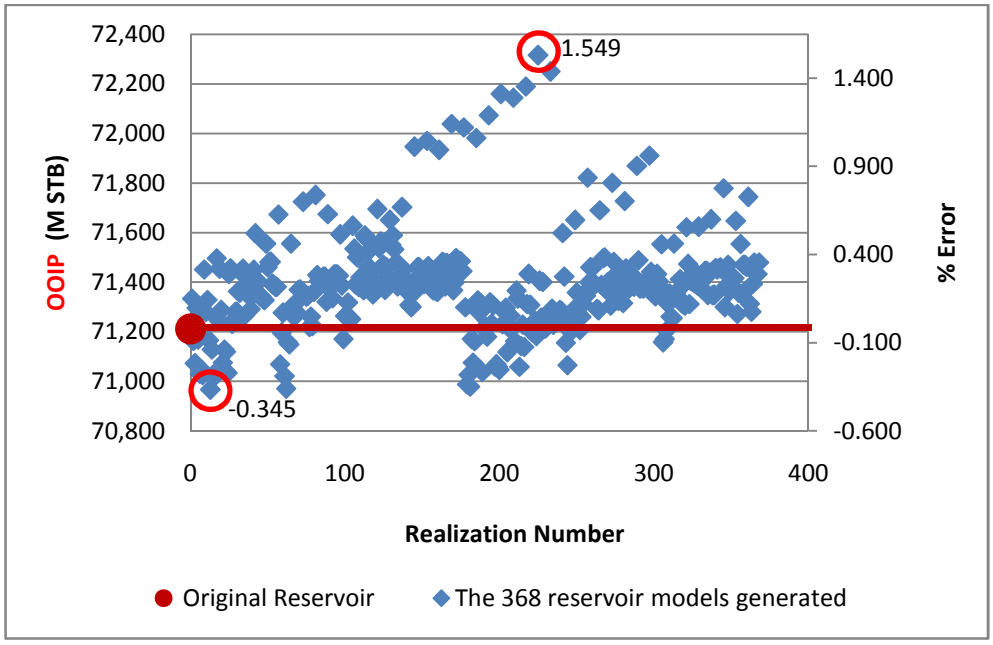

Figure 5. 35. The OOIP values of the reservoirs generated by using the developed 368 training images and their percentage errors with respect to the OOIP of the original reservoir

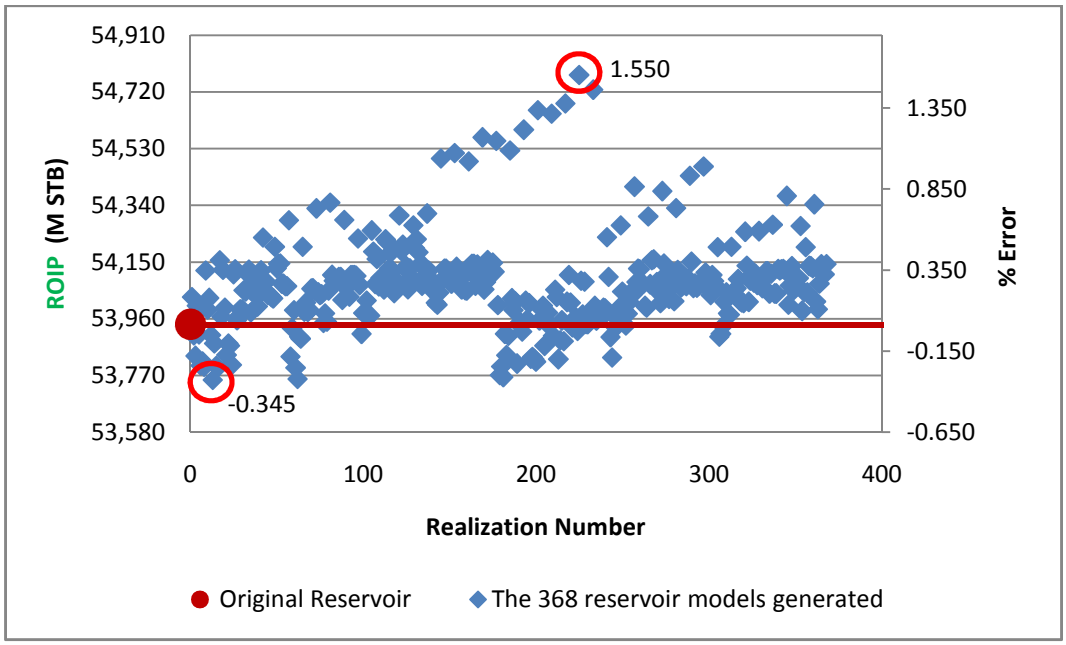

Figure 5. 36. The ROIP values of the reservoirs generated by using the developed 368 training images and their percentage errors with respect to the ROIP of the original reservoir

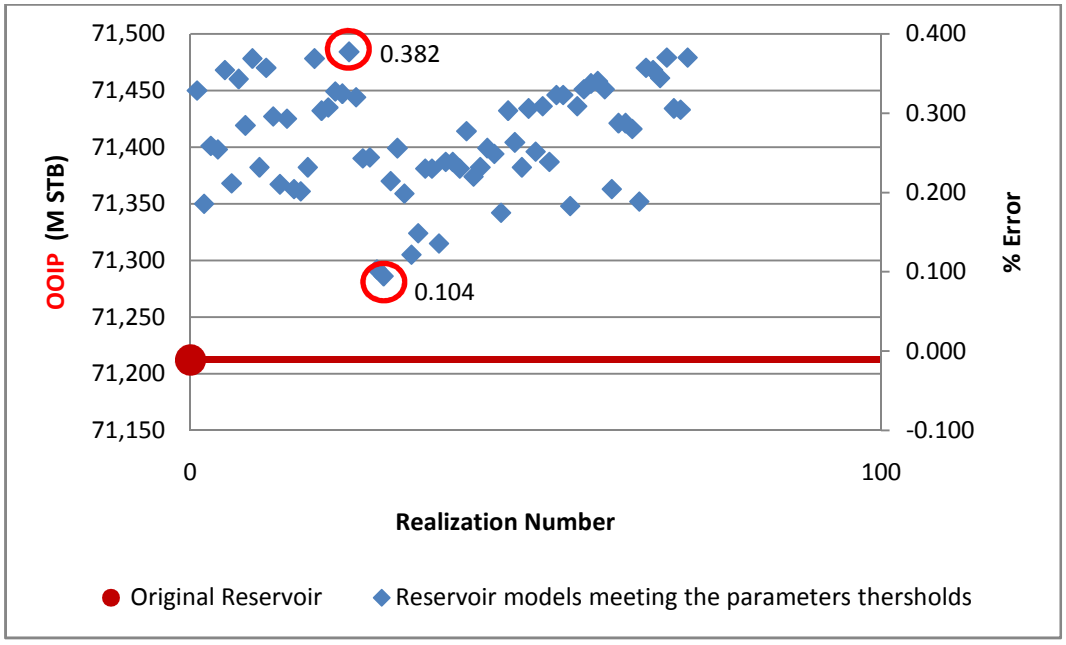

Figure 5. 37. Percentage error associated with the prediction of OOIP using the developed training images after excluding the cases that fail to meet the defined thresholds

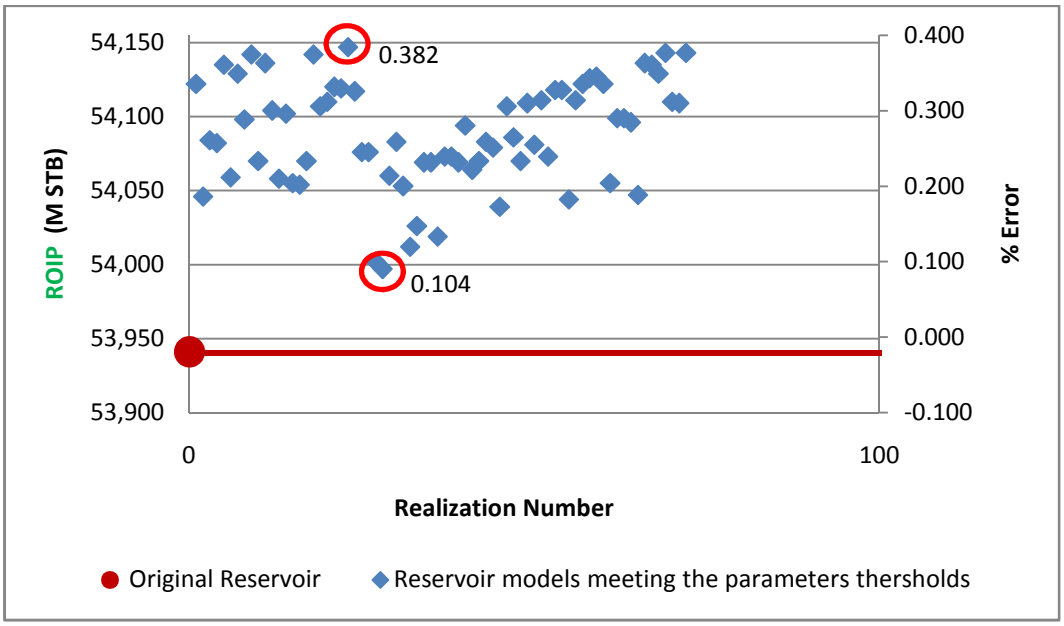

Figure 5. 38. Percentage error associated with the prediction of ROIP using the developed training images after excluding the cases that fail to meet the defined thresholds

The reservoir models illustrated in Figures 5.37 and 5.38 are the ones generated with training images that meet the thresholds of the parameters defined in Section 5.3.1 (Table 5.9). So, these models are the ones that represent the original reservoir the best. As a result, they can be used to history match the production data of the original reservoir.

Table 5. 9. The training images that meet the thresholds of the parameters defined

Number of Channels	Number of waves	Number of Z slices	Amplitude level	Number of TIs
3, 4 and 5	2, and 3	5, 6, 7, and 8	Medium	3 x 2 x 4 = 24
3, 4, 5, 6, 7, and 8	2, and 3	5, 6, 7, and 8	Low	6 x 2 x 4 = 48
Total number of training images = 72				

Based on these findings a history matching workflow can be established. So, in order to obtain the best history matching model for a fluvial channel reservoir the following

workflow is proposed. First, the 3D training images reported in Table 5.9 are generated as illustrated in Sections 4.6.1 and 4.6.2. Next, their corresponding reservoir models are developed and run utilizing the MPG methodology proposed (see Section 4.6.3). After that, an objective function for history matching is defined using the water cut and bottom-hole pressure (BHP) of the production wells (Li and Caers, 2011). After normalizing the water cut and BHP data the objective function is used to computes the sum of the square differences between the observed (original) and simulated data. The best matching model is the one with the smallest sum of the square differences.

5.4 Porosity Uncertainty Impact on Reservoir Model

5.4.1 Porosity Uncertainty Modeling

The developed 50 Monte Carlo simulation (MCS) realizations of the porosity data using the total coefficient of variation (Ω_{total}) of 0.265 are evaluated by plotting their histograms and variograms. This assessment is performed to confirm that the real hard data are not disturbed by the introduced error. In case the data are disturbed by the introduced error, the generated realizations do not represent the real hard data; therefore, analyzing such data would be of no use.

The results show that the overall mean (i.e. 0.157) and distribution structure (i.e. bimodal) of the real hard data are not disturbed by the uncertainty introduced (Figures 5.39 and 5.40, the other plots are given in the attached CD). In addition, the variogram models of the realizations and the real hard data are similar (i.e. exponential) (Figure 5.41 and 5.42, the other variograms are given in the attached CD). As a result, the introduced error did not interrupt the autocorrelation of the real hard data. So, the generated 50 MCS realizations represent the real hard data, therefore, can be used to analyze the impact of that data uncertainty on reservoirs modeled using the proposed MPG methodology.

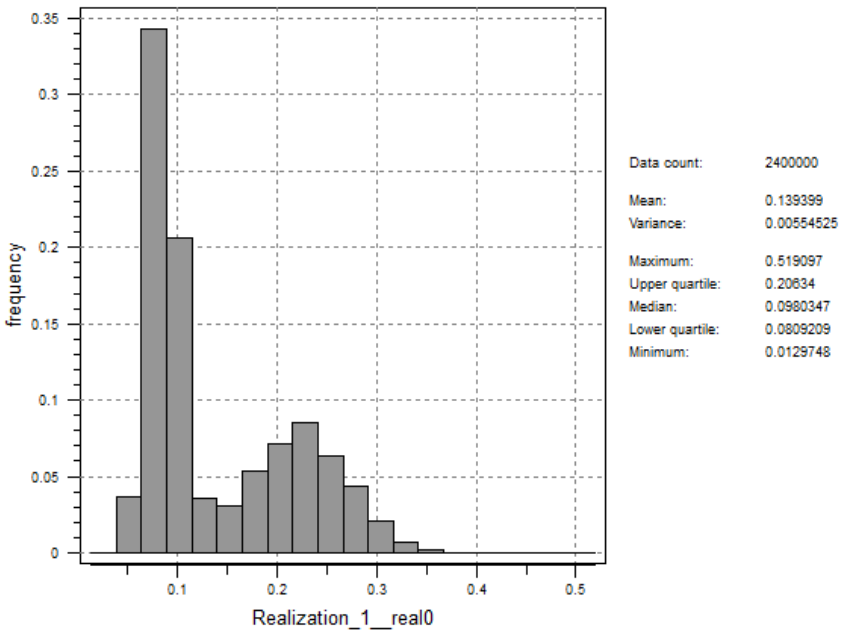

Figure 5. 39. Porosity histogram of the first MCS realization

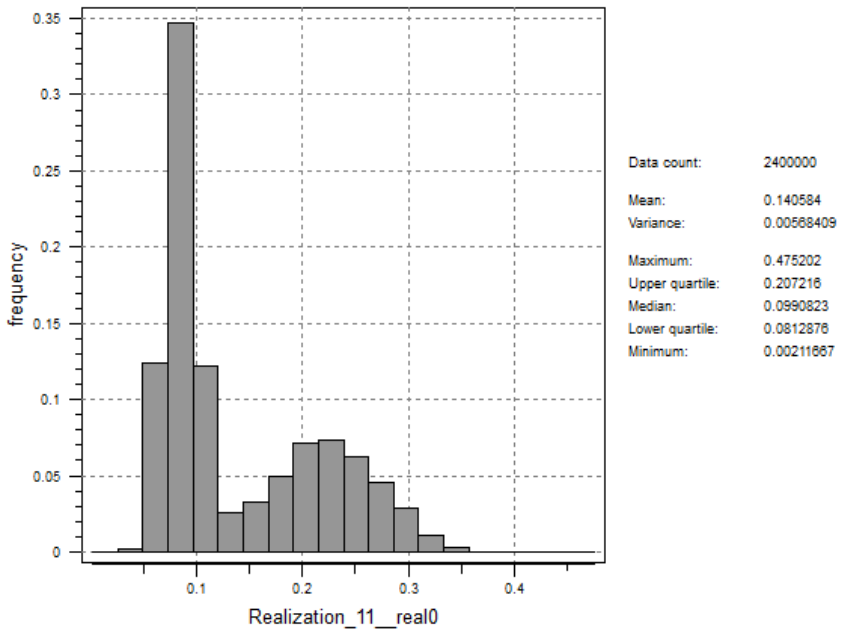

Figure 5. 40. Porosity histogram of the thirty-first MCS realization

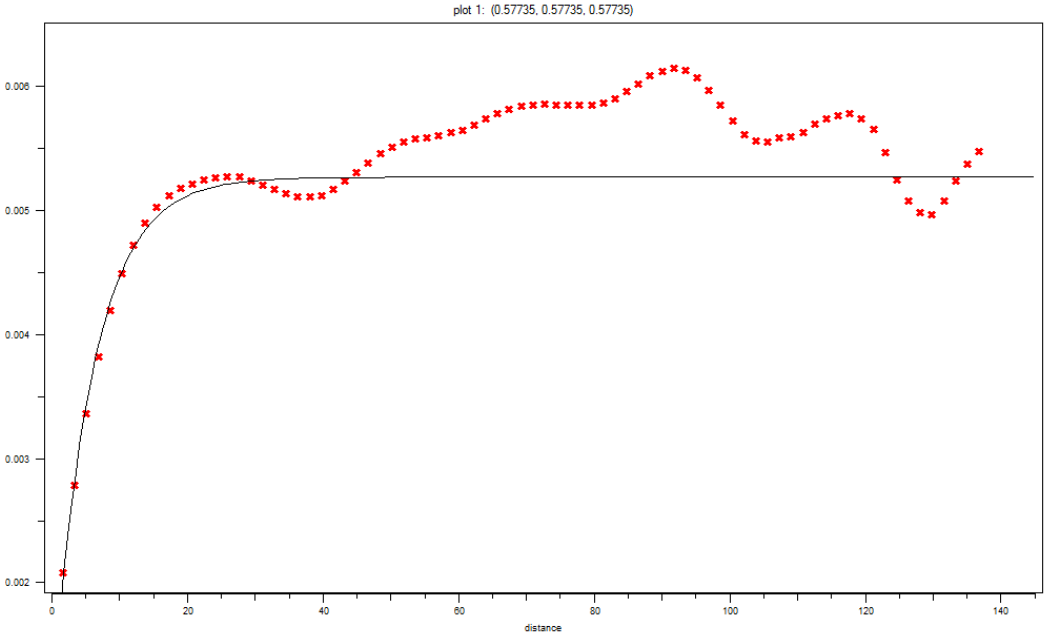

Figure 5. 41. Variogram of the first MCS realization

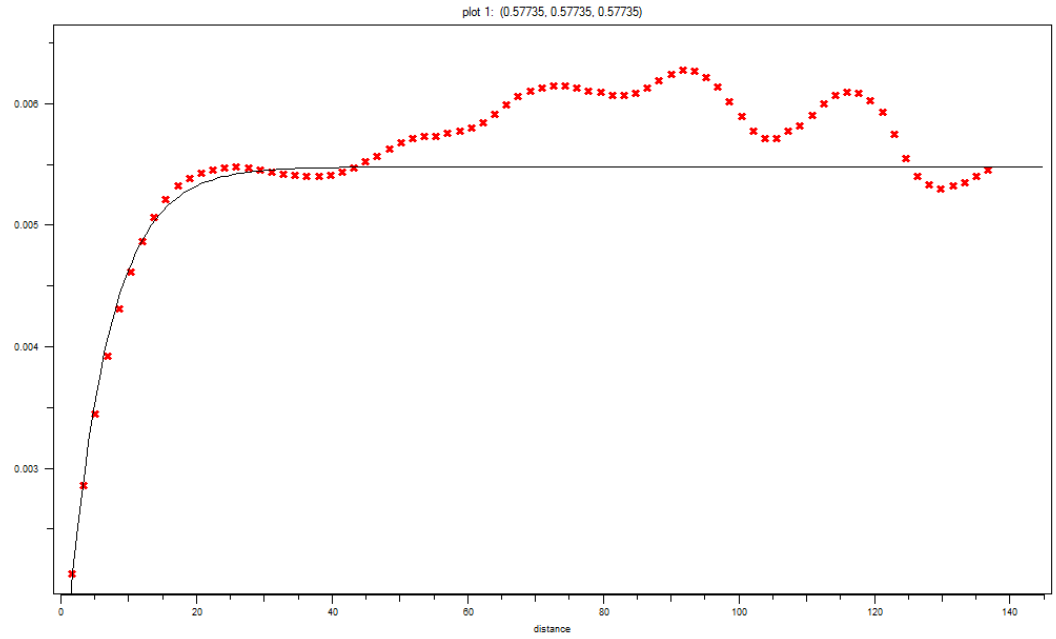

Figure 5. 42. Variogram of the eleventh MCS realization

5.4.2 Analysis of Porosity Uncertainty Impact

In order to investigate the impact of the porosity uncertainty in the developed reservoir model, the porosity realizations of the 50 Monte Carlo simulations (MCS) generated earlier are used to simulate the original reservoir 50 times as explained in Section 4.7.1. The OOIP and ROIP values of the new 50 reservoir models are compared with those of the original reservoir. The results show that the OOIP and ROIP values of all the new models underestimate the original results. As shown in Figures 5.43 and 5.44 the OOIP and ROIP values of the generated reservoirs are in the ranges (67,946 – 66,198) M STB and (51,467 – 50,143) M STB, respectively. The corresponding percentage errors of these values with respect to those of the original reservoir are both in the range (-4.586% – -7.041%) (Figures 5.43 and 5.44).

The reliability of the information acquired from only 50 MCS is checked by using the percentage error as explained in Section 5.1. As expected the percentage error is normally distributed, N (0.050157, 1.9959). The calculated probability values verify that the results obtained with only 50 MCS are reliable. In other words, more MCS will provide the same information obtained with only 50 realizations since the probability of obtaining reservoirs having OOIP and ROIP within the limits of the fitted normal distribution is 95% (Table 5.10).

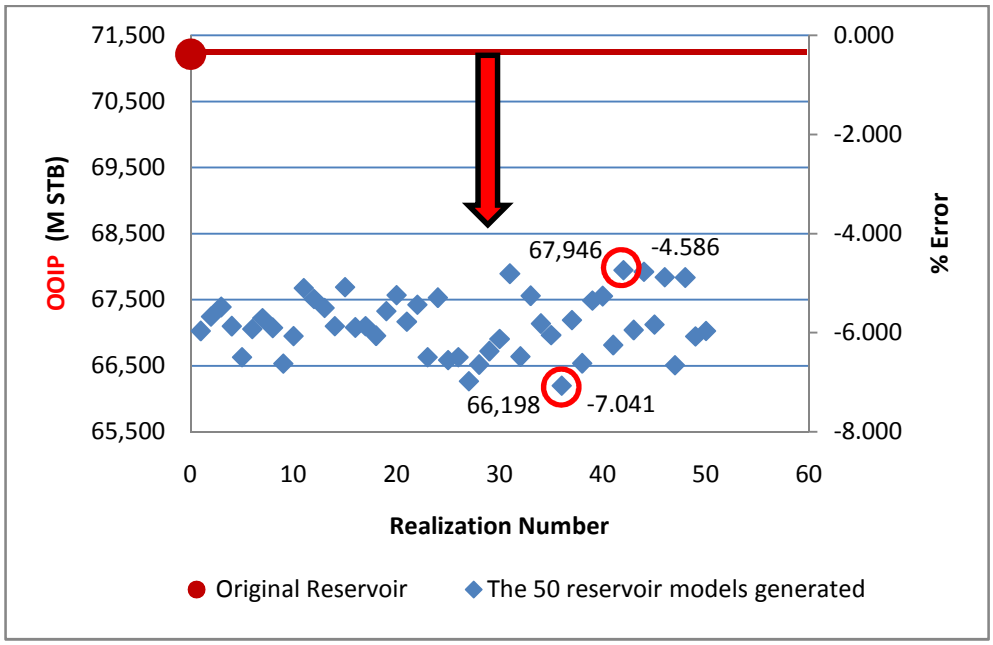

Figure 5. 43. The OOIP values of the 50 reservoir models generated using the 50 porosity MCS and their percentage errors with respect to the OOIP of the original reservoir model

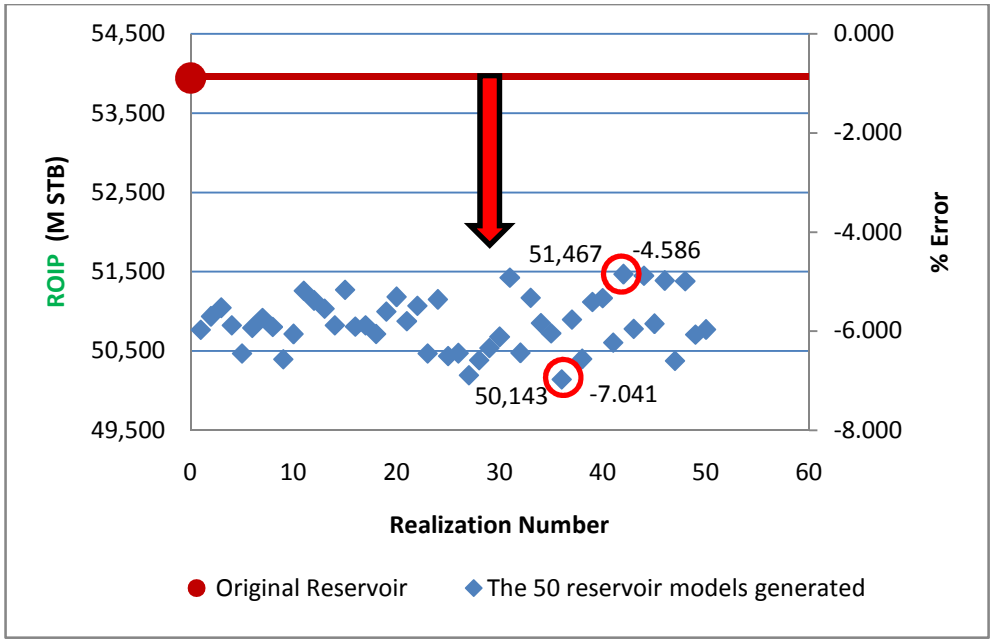

Figure 5. 44. The ROIP values of the 50 reservoir models generated using the 50 porosity MCS and their percentage errors with respect to the ROIP of the original reservoir model

Table 5. 10. Probabilities of finding an error within or beyond the limits of the calculated distribution using 50 MCS

Probability	Value
$P(x < -7.0410)$	0.0186
$P(x > -4.5865)$	0.0312
$P(-7.0410 < x < -4.5865)$	0.9503

5.4.2.1 Analyzing the Impact of Different Porosity Uncertainty values

Aiming at investigating the effect of different uncertainty values on the prediction of OOIP and ROIP values, the Ω_{total} of 0.01, 0.02, 0.05, 0.10, and 0.15 are considered and 30 MCS are performed for each case. The descriptive statistics of the considered cases are given in Table 5.11. The results show that with 0.01 and 0.02 uncertainties the OOIP and ROIP values are overestimated (Figures 5.45 and 5.46). The reason behind that is the data are forced to be around the mean when these two small uncertainty values are used. As a result, all the generated realizations fail to capture the variability of the real hard data. The highest and lowest limits of the OOIP and ROIP in each case and their corresponding percentage errors with respect to the original reservoir model are reported in Table 5.12.

As the uncertainty increases from 0.01 to 0.15 the values of OOIP and ROIP are moving from overestimation to underestimation. The reason behind that might be the synthetic origin of the hard data, which are also uncertain. Thus, high and low uncertainties in real world hard data not necessarily show the same respond. However, the aim here is to examine the impact of hard data uncertainty in the reservoir models, so, the results found show that a small uncertainty in the hard data has a great impact in the simulated reservoir outputs. Thus, more time and money should be devoted to decrease the uncertainty of collected hard data which facilitate the simulation of more accurate reservoir models.

Table 5. 11. Descriptive statistics of the porosity data generated using different coefficient of variation (c.o.v) (i.e. uncertainty) values

	mean	StDev for 1%	StDev for 2%	StDev for 5%	StDev for 10%	StDev for 15%
Shale	0.074045	0.00074	0.001481	0.003702	0.007404	0.011107
Channel	0.258696	0.002587	0.005174	0.012935	0.02587	0.038804

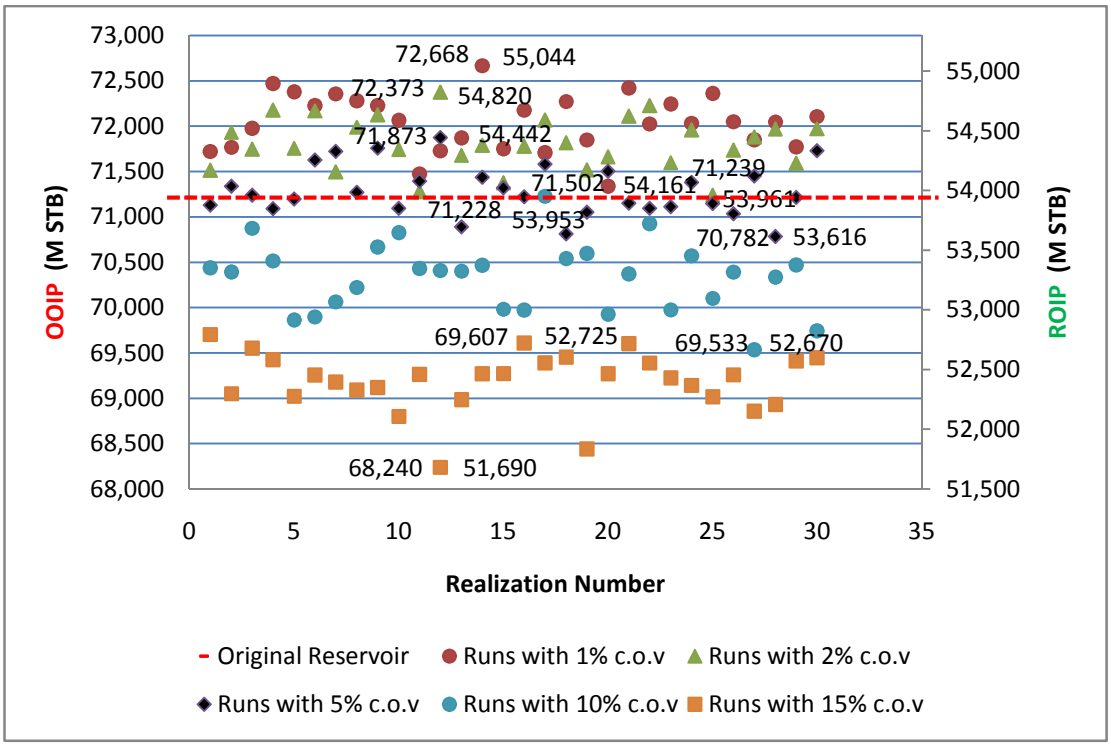

Figure 5. 45. The OOIP and ROIP values corresponding to reservoir models generated using different coefficient of variation (c.o.v) (i.e. uncertainty) values

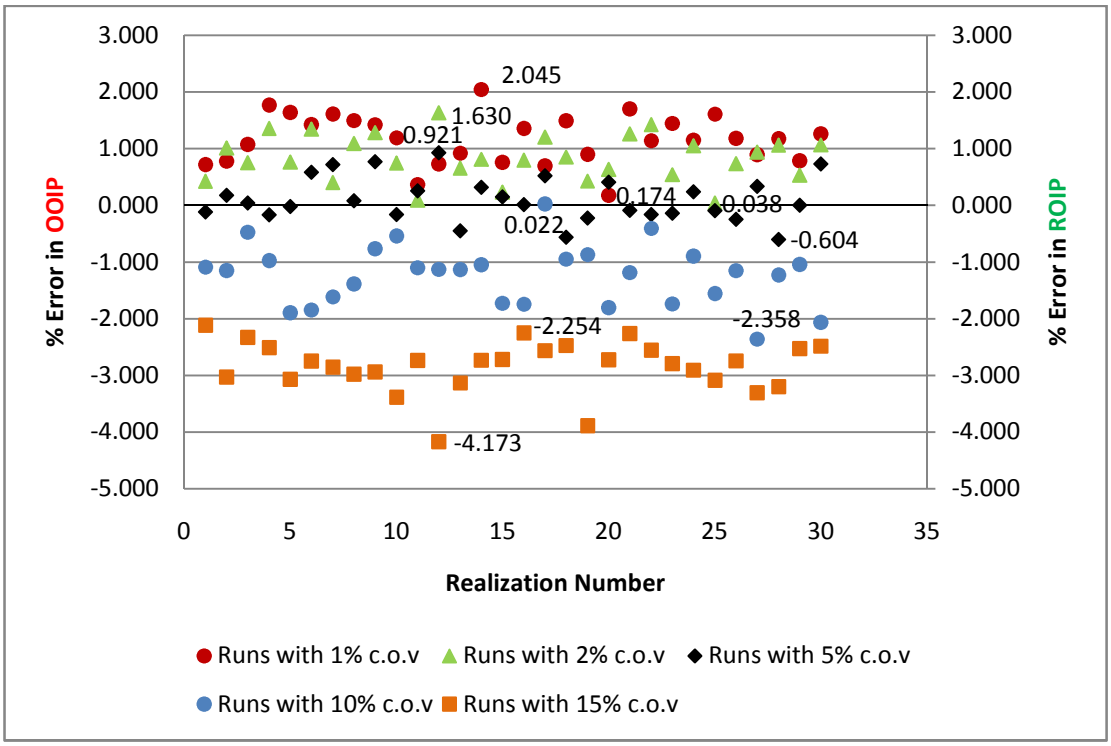

Figure 5. 46. The percentage errors in OOIP and ROIP values corresponding to reservoir models generated using different coefficient of variation (c.o.v) (i.e. uncertainty) values with respect to the original reservoir model

Table 5. 12. The highest and lowest limits for the OOIP and ROIP of the reservoir models generated using different coefficient of variation (c.o.v) (i.e. uncertainty) values, and their corresponding percentage errors with respect to the original reservoir model

Case	OOIP (M STB)		ROIP (M STB)		% Error	
	Highest limit	Lowest limit	Highest limit	Lowest limit	Highest limit	Lowest limit
1% c.o.v	72,668	71,502	55,044	54,161	2.045	0.174
2% c.o.v	72,373	71,239	54,820	53,961	1.630	0.038
5% c.o.v	71,873	70,782	54,442	53,616	0.921	-0.604
10% c.o.v	71,228	69,533	53,953	52,670	0.022	-2.358
15% c.o.v	69,607	68,240	52,725	51,690	-2.254	-4.173

5.4.2.2 Analysis of Porosity Uncertainty Impact Utilizing Different Upscaling Method

In this section the upscaling is performed using the median instead of the arithmetic mean. So, the 1000 ASCII files of porosity data exported out of SGeMS in Section 4.3.3 are upscaled by taking the median of the data in each file instead of their arithmetic mean. However, the median upscaling method outputs more underestimating results than the arithmetic upscaling method (Figures 5.47). In other words, the uncertainty of the results obtained with the median upscaling method is larger than that of the ones obtained with the arithmetic upscaling method. The maximum and minimum differences between the OOIP and ROIP values of the reservoirs generated using the two upscaling methods are shown with black arrows in Figures 5.47. The values of these differences for the OOIP are 7,618 M STB and 6,841 M STB, respectively. For the ROIP, in addition, they are 5,771 M STB and 5,182 M STB, respectively. The reason why the median upscaling method resulted in smaller values than the arithmetic upscaling method is the bimodal structure of the hard data. So, the use of median upscaling method is not appropriate for the present study.

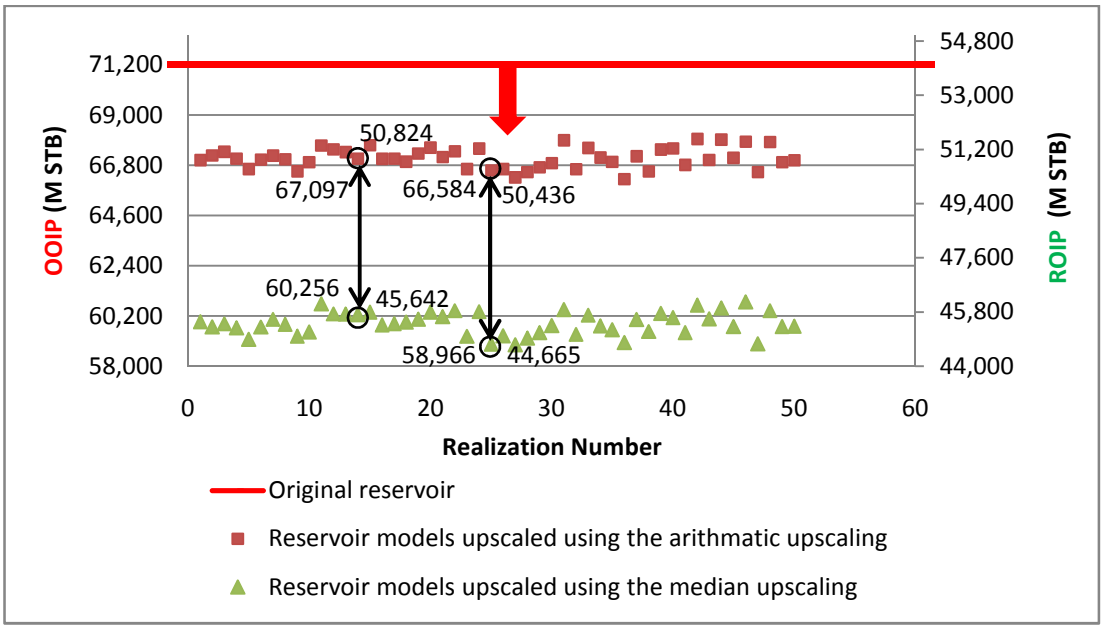

Figure 5. 47. The OOIP and ROIP values corresponding to reservoir models generated with 50 MCS using both the median and average upscaling methods. The black arrows show the maximum and minimum differences between the results of the upscaling methods

CHAPTER 6

CONCLUSIONS

In this study the uncertainties of reservoir models generated using a proposed multiple-point geostatistics based modeling methodology are analyzed and quantified. The uncertainty types analyzed are the model related and parameter related uncertainties. The former is the training image uncertainty while the latter is the hard data uncertainty. In addition, the sensitivity of the proposed multiple-point geostatistics modeling methodology is investigated. At the end of this research the following concluding remarks are obtained:

- The proposed multiple-point geostatistics modeling methodology including SNESIM algorithm allow good reproduction of the original reservoir with confidence limits ranging between 3% and -2.4%. In other words, the proposed method is producing accurate results with accuracy of about ±3%.

- The proposed modeling methodology is sensitive to the variogram model used. Thus, selection of the most representative variogram model should be given great care. So, the choice of the variogram model should be based on the interpretation of the available geological information.

- It was found that 2D training images as well as 3D training image having up to 4 Z slices are not suitable for modeling 3D reservoirs. Then, based on the investigation of other parameters' impact on the reservoir model thresholds are set. With these thresholds representative and reliable reservoir models are obtained. The thresholds defined are 5 Z direction slices, 3 channels and 2 medium or low amplitudes waves in each channel. In addition, it was found that

the training images meeting the thresholds defined produce more accurate results if their channel proportions are higher. In other words, the higher the channel proportion in a training image the more accurate the model outputs are.

- As the number of channels and waves in a training image increase the uncertainty of the simulated reservoir decreases. However, the increase in the number of Z slices from 5 to 8 and in the amplitude level have no noticeable effect on the uncertainty of the reservoir. So, it is unnecessary to generate training images with more than 5 Z slides when modeling 3D reservoirs.

- The number of channel in a training image, the amplitude level of their waves, and the number of the Z slices in the training image have no defined effect on the OOIP and ROIP. In other words, their effect is random. However, the amount of the OOIP and ROIP are directly proportional to the number of waves in the channels of the training image.

- When reservoirs are modeled using all the constructed training images the OOIP and ROIP are predicted with an uncertainty range of +1.549% – -0.345%. However, this uncertainty range (i.e. +1.549 – -0.345) decreased by eliminating the cases that are not meeting the parameters thresholds. As a result, the uncertainty range of the OOIP and ROIP prediction is reduced to 0.382% – 0.104%. This verifies that the defined thresholds provide the most representative reservoir models.

- The training images that meet the thresholds of the parameters defined output the most representative reservoir models. These models are used to establish a history matching workflow to improve the accuracy of history matching models. So, the present study assists the fields of reservoir history matching.

- The investigation of hard data uncertainty impact on reservoirs modeled using the proposed multiple-point geostatistics methodology showed that a small uncertainty in the hard data has a great impact on the simulated reservoir outputs. For example, 1% uncertainty resulted in reservoirs having OOIP percentage errors ranging between 2.045 and 0.174. Thus, more time and money should be devoted to decrease the hard data uncertainty which facilitate the simulation of more accurate reservoir models.

- In the proposed multiple-point geostatistics modeling methodology if the hard data have a bimodal structure the use of median upscaling method is inappropriate since it results in erroneous reservoir models.

CHAPTER 7

RECOMMENDATIONS

Future studies should focus on:

- Investigating more sources of uncertainty while modeling reservoirs with multiple-point geostatistics techniques. Some sources of uncertainty are variogram anisotropy, channel thickness and orientation.
- Investigating the uncertainty associated with upscaling methods.
- Developing a methodology that combines all sources of uncertainty in order to quantify the total uncertainty of reservoirs modeled using the proposed multiple-point geostatistics methodology.
- Investigating the impact of high-amplitude-wave channels on reservoir by using bigger-size training images
- Verifying the findings of the present study with real case studies. For example, the uncertainty of the synthetic porosity data in this study showed a great impact on the original and recoverable oil in place values, therefore, real porosity data could be used in future studies to verify such impact.
- Developing a multiple-point geostatistics algorithm that includes a training image generating option. This option should contain all the parameters defined in the present study, so that users have complete control on the generation of the training image.

- Representing other reservoir structures with proper mathematical functions to decrease the uncertainty associated for better multiple-point geostatistics applications. For example, lens-type reservoirs could be represented with ellipsoidal functions.

REFERENCES

Ang, A.H.S., and Tang, W.H., 1984. Probability Concepts in Engineering Planning and Design, Vol.2. Decision, risk, and reliability. John Wiley and Sons.

Arpat, G. and J. Caers, 2007, Conditional Simulation with Patterns, Mathematical Geology, vol. 39, no. 2, p. 177-203.

Arpat, G. B., 2005, Sequential simulation with patterns, Ph.D. thesis, Stanford University, United States -- California.

Arslan, I. and Stanford University Dept of Geological and, Environmental Sciences, 2005, Structural Model Selection, Stanford University.

Barrera, A. E., 2006, Improved Geological Modeling and Dynamic Data Integration Using the Probability Perturbation Approach, M.Sc. thesis, Department of Petroleum and Geosystems Engineering thesis, University of Texas at Austin.

Barrera, A. E., J. Ni, and S. Srinivasan, 2005, Multiple Point Geostatistics: Optimal Template Selection and Implementation in Multi-Threaded Computational Environments, in Leuangthong, O. and C. V. Deutsch, eds., Geostatistics Banff 2004, Springer Netherlands, vol. 14, p. 621-630.

Boisvert, J. B., O. Leuangthong, J. M. Ortiz, and C. V. Deutsch, 2008, A methodology to construct training images for vein-type deposits, Computers & Geosciences, vol. 34, no. 5, p. 491-502.

Boisvert, J., M. Pyrcz, and C. Deutsch, 2007, Multiple-Point Statistics for Training Image Selection, Natural Resources Research, vol. 16, no. 4, p. 313-321.

Boucher, A., 2009, Considering complex training images with search tree partitioning, Computers & Geosciences, vol. 35, no. 6, p. 1151-1158.

Caers, J. and A. G. Journel, 1998, Stochastic Reservoir Simulation Using Neural Networks Trained on Outcrop Data.

Caers, J., 2002, Stochastic inverse modeling under realistic prior model constraints using multiple-point geostatistics.

Caers, J. and T. Zhang, 2004, Multiple-point Geostatistics: A Quantitative Vehicle for Integrating Geologic Analogs into Multiple Reservoir Models, Memoirs-American Association of Petroleum Geologists, no. 80, p. 383-394.

Castro, S. A., 2007, A probabilistic approach to jointly integrate 3D/4D seismic, production data and geological information for building reservoir models, Ph.D. thesis, Stanford University, United States -- California.

Century Geophysical Corporation Website, http://www.century-geo.info/dnn/, (accessed June 2012)

Chugunova, T. and L. Hu, 2008, Multiple-Point Simulations Constrained by Continuous Auxiliary Data, Mathematical Geosciences, vol. 40, no. 2, p. 133-146.

Comunian, A., P. Renard, J. Straubhaar, and P. Bayer, 2011, Three-dimensional high resolution fluvio-glacial aquifer analog – Part 2: Geostatistical modeling, Journal of Hydrology, vol. 405, no. 1–2, p. 10-23.

Comunian, A., P. Renard, and J. Straubhaar, 2012, 3D multiple-point statistics simulation using 2D training images, Computers & Geosciences, vol. 40, no. 0, p. 49-65.

de Vries, L., J. Carrera, O. Falivene, O. Gratacós, and L. Slooten, 2009, Application of Multiple Point Geostatistics to Non-stationary Images, Mathematical Geosciences, vol. 41, no. 1, p. 29-42.

dell'Arciprete, D., R. Bersezio, F. Felletti, M. Giudici, A. Comunian, and P. Renard, 2012, Comparison of three geostatistical methods for hydrofacies simulation: a test on alluvial sediments, Hydrogeology Journal, vol. 20, no. 2, p. 299-311.

Deutsch, C. V. and A. G. Journel, 1997, GSLIB geostatistical software library and user's guide.

Deutsch, C. V., 1992, Annealing techniques applied to reservoir modeling and the integration of geological and engineering (well test) data, Ph.D. dissertation, Stanford University, United States -- California.

Deutsch, C. and L. Wang, 1996, Hierarchical object-based stochastic modeling of fluvial reservoirs, Mathematical Geology, vol. 28, no. 7, p. 857-880.

Du, Y., T. Zhang, W. Chen, S. Z. Li, and Y. L. Wang, 2009, 3D Porosity Simulation of Porous Media Using Continuous Multiple-point Geostatistics, 2009 Ieee International Conference on Intelligent Computing and Intelligent Systems, Proceedings, Vol 4, p. 376.

Duzgun, H. S. B., 2004, Reliability-Based Design of Rock Slopes, Ph.D. dissertation, Department of Mining Engineering, Middle East Technical University, Turkey.

Eskandari, K., 2008, Growthsim: A Complete Framework for Integrating Static and Dynamic Data into Reservoir Models, Ph.D. dissertation, Department of Petroleum and Geosystems Engineering, The University of Texas at Austin, 220 pages p.

Farmer, C. L., 1988, The generation of stochastic fields of reservoir parameters with specified geostatistical distributions, Institute of Mathematics and Its Applications Conference Series, vol. 18, p. 235-252.

Feyen, L. and J. Caers, 2006, Quantifying geological uncertainty for flow and transport modeling in multi-modal heterogeneous formations, Advances in Water Resources, vol. 29, no. 6, p. 912-929.

Guardiano, F. B., R. M. Srivastava, and A. Soares, 1993, Multivariate geostatistics - beyond bivariate moments, Geostatistics Troia 92, Vols 1 and 2, vol. 5, p. 133.

Hajizadeh, A., A. Safekordi, and F. A. Farhadpour, 2011, A multiple-point statistics algorithm for 3D pore space reconstruction from 2D images, Advances in Water Resources, vol. 34, no. 10, p. 1256-1267.

Haldorsen, H. H. and E. Damsleth, 1990, Stochastic modeling, Journal of Petroleum Technology, vol. 42, p. 404-412.

Harding, A., S. Strebelle, M. Levy, J. Thorne, D. Xie, S. Leigh, R. Preece, and R. Scamman, 2005, Reservoir Facies Modelling: New Advances in MPS, , vol. 14, p. 559-568.

Holden, L., R. Hauge, O. Skare, and A. Skorstad, 1998, Modeling of fluvial reservoirs with object models, Mathematical Geology, vol. 30, p. 473-496.

Huysmans, M. and A. Dassargues, 2010, Application of Multiple-Point Geostatistics on Modelling Groundwater Flow and Transport in a Cross-Bedded Aquifer, , vol. 16, p. 139-150.

Huysmans, M. and A. Dassargues, 2011, Direct Multiple-Point Geostatistical Simulation of Edge Properties for Modeling Thin Irregularly Shaped Surfaces, Mathematical Geosciences, vol. 43, no. 5, p. 521-536.

Huysmans, M. and A. Dassargues, 2012, Modeling the effect of clay drapes on pumping test response in a cross-bedded aquifer using multiple-point geostatistics, Journal of Hydrology, vol. 450–451, no. 0, p. 159-167.

Journel, A. G., 1974, Geostatistics for Conditional Simulation Of Ore Bodies, Economic Geology, vol. 69, p. 673.

Journel, A. G. and A. Soares, 1993, Geostatistics - Roadblocks and Challenges, Geostatistics Troia 92, Vols 1 and 2, vol. 5, p. 213-224.

Journel, A. G., 2002, Combining Knowledge from Diverse Sources: An Alternative to Traditional Data Independence Hypotheses, Mathematical Geology, vol. 34, no. 5, p. 573-596.

Journel, A. G. and T. Zhang, 2006, The Necessity of a Multiple-Point Prior Model, Mathematical Geology, vol. 38, no. 5, p. 591-610.

Journel, A. G., 2005, Beyond Covariance: The Advent of Multiple-Point Geostatistics, vol. 14, p. 225-233.

Krishnan, S. and A. Journel, 2003, Spatial Connectivity: From Variograms to Multiple-Point Measures, Mathematical Geology, vol. 35, no. 8, p. 915-925.

Krishnan, S., 2005, Combining diverse and partially redundant information in the Earth sciences, Ph.D. thesis, Stanford University, United States -- California.

Li, H. M. and J. Caers, 2011, Geological modelling and history matching of multi-scale flow barriers in channelized reservoirs: methodology and application, Petroleum Geoscience, vol. 17, p. 17-34.

Lima, H. M., 2005, Geostatistic in Reservoir Characterization: from estimation to simulation methods, Estudios geológicos., vol. 61, no. 3/6, p. 135-146.

Liu, X., S. Srinivasan, and D. Wong, 2002, Geological Characterization Of Naturally Fractured Reservoirs Using Multiple Point Geostatistics, .

Liu, Y., 2003, Downscaling seismic data into a geologically sound numerical model, Ph.D. thesis, Stanford University, United States -- California.

Liu, Y., A. Harding, R. Gilbert, and A. G. Journel, 2005, A Workflow for Multiple-point Geostatistical Simulation, , vol. 14, p. 245-254.

Liu, Y., 2006, Using the Snesim program for multiple-point statistical simulation, Computers & Geosciences, vol. 32, no. 10, p. 1544-1563.

Maharaja, A., 2005, Stochastic Modeling of the Rhine-Meuse Delta using Mutiple-point Geostatistics, , vol. 14, p. 653-659.

Maharaja, A., 2008, TiGenerator: Object-based training image generator, Computers & Geosciences, vol. 34, no. 12, p. 1753-1761.

Mariethoz, G., P. Renard, and J. Straubhaar, 2011, Extrapolating the Fractal Characteristics of an Image Using Scale-Invariant Multiple-Point Statistics, Mathematical Geosciences, vol. 43, no. 7, p. 783-797.

Okabe, H. and M. J. Blunt, 2005, Pore space reconstruction using multiple-point statistics, Journal of Petroleum Science and Engineering, vol. 46, no. 1–2, p. 121-137.

Okabe, H. and M. J. Blunt, 2004, Multiple-point Statistics to Generate Pore Space Images, vol. 14, p. 763-768.

Remy, N., A. Boucher, and J. Wu, 2009, Applied geostatistics with SGeMS: a user's guide, Cambridge; New York, Cambridge University Press, 264 p.

SpeQ Mathematics Website, http://www.speqmath.com/index.php?id=1, (accessed June 2011)

Srinivasan, S., 2000, Integration of production data into reservoir models: A forward modeling perspective, Ph.D. thesis, Stanford University, United States -- California.

Srivastava, M., 1992, Iterative methods for spatial simulation, vol. 5.

Stoyan, D., W. S. Kendall, and J. Mecke, 1987, Stochastic geometry and its applications, Chichester W. Sussex; New York, Wiley, 345 p. p.

Straubhaar, J., P. Renard, G. Mariethoz, R. Froidevaux, and O. Besson, 2011, An Improved Parallel Multiple-point Algorithm Using a List Approach, Mathematical Geosciences, vol. 43, no. 3, p. 305-328.

Strebelle, S., 2002, Conditional Simulation of Complex Geological Structures Using Multiple-Point Statistics, Mathematical Geology, vol. 34, no. 1, p. 1-21.

Strebelle, S., 2006, The Importance of Imposing Non-stationary Soft Constraints to Geostatistical Model in Sparse Well Environment, paper presented at the XIth International Congress For Mathematical Geology, Liege, Belgium.

Strebelle, S., K. Payrazyan, and J. Caers, 2002, Modeling of a Deepwater Turbidite Reservoir Conditional to Seismic Data Using Multiple-Point Geostatistics.

Strebelle, S. and N. Remy, 2005, Post-processing of Multiple-point Geostatistical Models to Improve Reproduction of Training Patterns, , vol. 14, p. 979-988.

Strebelle, S. and T. Zhang, 2005, Non-Stationary Multiple-point Geostatistical Models, , vol. 14, p. 235-244.

Strebelle, S. B. and A. G. Journel, 2001, Reservoir Modeling Using Multiple-Point Statistics.

Strebelle, S. B., 2000, Sequential simulation drawing structures from training images, Ph.D. thesis, Stanford University, United States -- California.

Tahmasebi, P., A. Hezarkhani, and M. Sahimi, 2012, Multiple-point geostatistical modeling based on the cross-correlation functions, Computational Geosciences, vol. 16, no. 3, p. 779-797.

Tran, T. T., 1994, Improving variogram reproduction on dense simulation grids, Computers & Geosciences, vol. 20, no. 7–8, p. 1161-1168.

Viseur, S., 1999, Stochastic Boolean Simulation of Fluvial Deposits : A New Approach Combining Accuracy with Efficiency. .

Webshaker Website, http://webshaker.ucsd.edu/homework/Creating_A_Sine_Wave_In_Excel.pdf , (accessed May 2011)

Wu, J., 2007, 4D seismic and mulitple-point pattern data integration using geostatistics, Ph.D. thesis, Stanford University, United States -- California.

Zhang, T., S. Pedersen, C. Knudby, and D. McCormick, Memory-Efficient Categorical Multi-point Statistics Algorithms Based on Compact Search Trees, Mathematical Geosciences, p. 1-17.

Zhang, T., S. Bombarde, S. B. Strebelle, and E. Oatney, 2005, 3D Porosity Modeling of a Carbonate Reservoir Using Continuous Multiple-Point Statistics Simulation, .

Zhang, T., 2006, Filter-based training pattern classification for spatial pattern simulation, Ph.D. thesis, Stanford University, United States -- California.

Zhang, T., 2008, Incorporating Geological Conceptual Models and Interpretations into Reservoir Modeling Using Multiple-Point Geostatistics, Earth Science Frontiers, vol. 15, no. 1, p. 26-35.

APPENDIX A

PARAMETERS DESCRIPTION OF THE USED ALGORITHMS

1. Parameters Description of SNESIM Algorithm

The description of SNESIM algorithm parameters given here after is based on the work of Remy et al. (2009). The SNESIM algorithm interface contains four pages, namely: General, Conditioning, Rotation/Affinity, and Advanced (Figure A.1). The parameters described here are the ones used in this study.

1. **Simulation Grid Name:** is the name of the grid where the simulation will take place.

2. **Property Name Prefix:** is the prefix given by the user for the simulation output. Then, a "_real#" suffix is added to the generated realization by the algorithm. "#" is a number.

3. **# of Realization:** is the number of realization the user wishes to generate.

4. **Seed:** is a large odd integer to initialize the pseudo-random number generator.

5. **Training Image (object and property):**
    - Object: the name of the grid containing the TI to be used.
    - Property: the TI property which must be a categorical variable and must have a value between "0" and "number of categories-1". This parameter is selected automatically one the user select the TI for the object parameter.

6. **# of Categories:** the number of categories contained in the TI used. If the TI contains sand and non-sand categories then the # of categories is 2.

7. **Target Marginal Distribution:** are the target categories' proportions and must be ordered by starting from the proportion of the category "0" till that of the last category, separating each two by a space. The sum of all target proportions must be 1 otherwise SGeMS fail and shut in when the algorithm is run.

8. **# of Nodes in Search Template:** is the number of nodes contained in the search template. The larger the value of this parameter, the better the simulation quality if the used TI is large, but the more RAM memory is demanded. Usually, for a fairly good realization generation 60 nodes for a 2D TI and 80 nodes for a 3D TI are used.

9. **Search Template Geometry (ranges and angels):** these two parameters are defining the size of the ellipsoid by which the neighboring conditioning data are searched. The search ellipsoids are characterized by six parameters: three range and three angels. The three ranges: max, med, and min stands for the dimensions of the major axis, medium axis, and minor axis, respectively. The three angles are the azimuth, dip, and rake. These angles account for the anisotropy of the conditional data variogram. As a rule of thumb, the ranges of the searching ellipsoid should have a value more than twice the range of the conditional data variogram.

10. **Hard Data (object):** is the grid containing the hard data which is used as conditioning data. The hard data object must be a point set. If the user whishes to carry out an unconditional simulation then this object should be left as default which is "None".

11. **Hard Data (property):** is the property containing the categorical hard conditioning data (e.g. well facies).

12. **Use Probability Data Calibrated from Soft Data:** this is selected when the user is wishing to condition the simulation to soft data (e.g. seismic) too.

13. **Soft Data (Choose Properties):** use this to select the soft data categorical properties. The order of the selected properties is very important. The property should be ordered as in the Target Marginal Distribution box. Note that, it is not possible to choose soft data properties unless they are given in the same simulation grid selected for parameter "1".

14. **Tau Values for Training Image and Soft Data:** are defined by the user to give weights to the influence of TI and soft data on the conditional probabilities calculated while generating a realization. The first tau value is for the TI (τ_1) while the second value is for the soft conditioning data (τ_2). The default values are "1 1" which indicates the conditional independence of TI and soft data (Journel, 2002). More details of the tau expression are given in Krishnan (2005) and Remy et al. (2009).

15. **Vertical Proportion:** is 1D grid with the number of cells in the X and Y directions being 1 while the number of cells in the Z direction is the same as that of the simulation grid. The default is "None" which means there is no vertical proportion of the data used.

16. **Use Azimuth Rotation:** is to manage non-stationary simulations by rotating the TI used. The default is not to use rotation.

17. **Use Scaling:** is to manage non-stationary simulations utilizing the affinity concept. The default is not to use scaling. If scaling is required, then selecting the "Use Global Affinity" box is an indication to scale the TI used with user-defined constant factors (or affinity values).
18. **Global Affinity Change:** when the "Use Global Affinity" box is selected, three Affinity values are input here for the X, Y, and Z directions, respectively. The

Affinity factor (f) changes the width of the simulated categories in a given direction. If the affinity in a given direction is f, then the category width in that direction becomes f times the original width (the width of that category in the TI). So, the width of the simulated category increases with the increase of f.

19. **Min # of Replicates:** is the minimum number of training replicates of a certain conditioning data event to be found in the search tree before retrieving its conditional probability. The default is 1.

20. **Servosystem Factor:** is a parameter that controls the servosystem correction. It takes a value between 0 and 1. The higher this parameter is, the closer the proportions reproduced to the target marginal distribution proportions but, at a cost of losing the structural information of facies (Liu, 2006). The default value is 0.5.

21. **Re-simulation Threshold:** The threshold value needed for re-simulation. When a data event is not repeated enough in The TI, SNESIM algorithm drops one datum from that event, and then repeats the search. The datum dropped is the one with the largest distance from the center. The simulated nodes having a number of dropped conditional nodes larger than the input threshold value are re-simulated (Arpat, 2005).The default value is (-1) which means no re-simulation is performed.

22. **Re-simulation Iteration #:** is the number of iteration to repeat the re-simulation procedure. The default value is 1. To ignore this parameter the value should be set to -1.

23. **# of Multigrids:** SNESIM algorithm discards any conditioning data that does not fall within a given search template centered at a certain node. This spoils the reproduction of long range correlation if the search template is small (Tran,

1994). Thus, the multi-grid approach of Tran (1994) is implemented in SNESIM to compensate for the dropping of the furthest data values. The default value is 3.

24. **Debug Level:** this parameter controls the outputs in the simulation grid. It can take three values (0, 1, and 2). When 0, which is the default value, is used only the realization of the simulation is output. In the case of a 1 debug level, the simulation generates two outputs, the realization and a map showing the number of nodes dropped during the simulation. When this parameter is set to 2 the simulation generates intermediate simulation results as well as the previous two outputs.

25. **Use Sub-grids:** if selected, it divides the simulation nodes on the current multi-grid into three groups that are simulated in sequence. For 3D simulations it is strongly recommended to use this option.

26. **Previously Simulated Nodes:** is the number of nodes in a sub-grid to be used for conditioning data. The default value is 4.

27. **Use Regions:** this option is used to perform simulation with the region concept. If not selected, the simulation is carried over the entire grid.

28. **Template Expansion (isotropic expansion):** by selecting this option, the isotropic expansion method is used to generate the series of cascaded search templates and multiple grids.

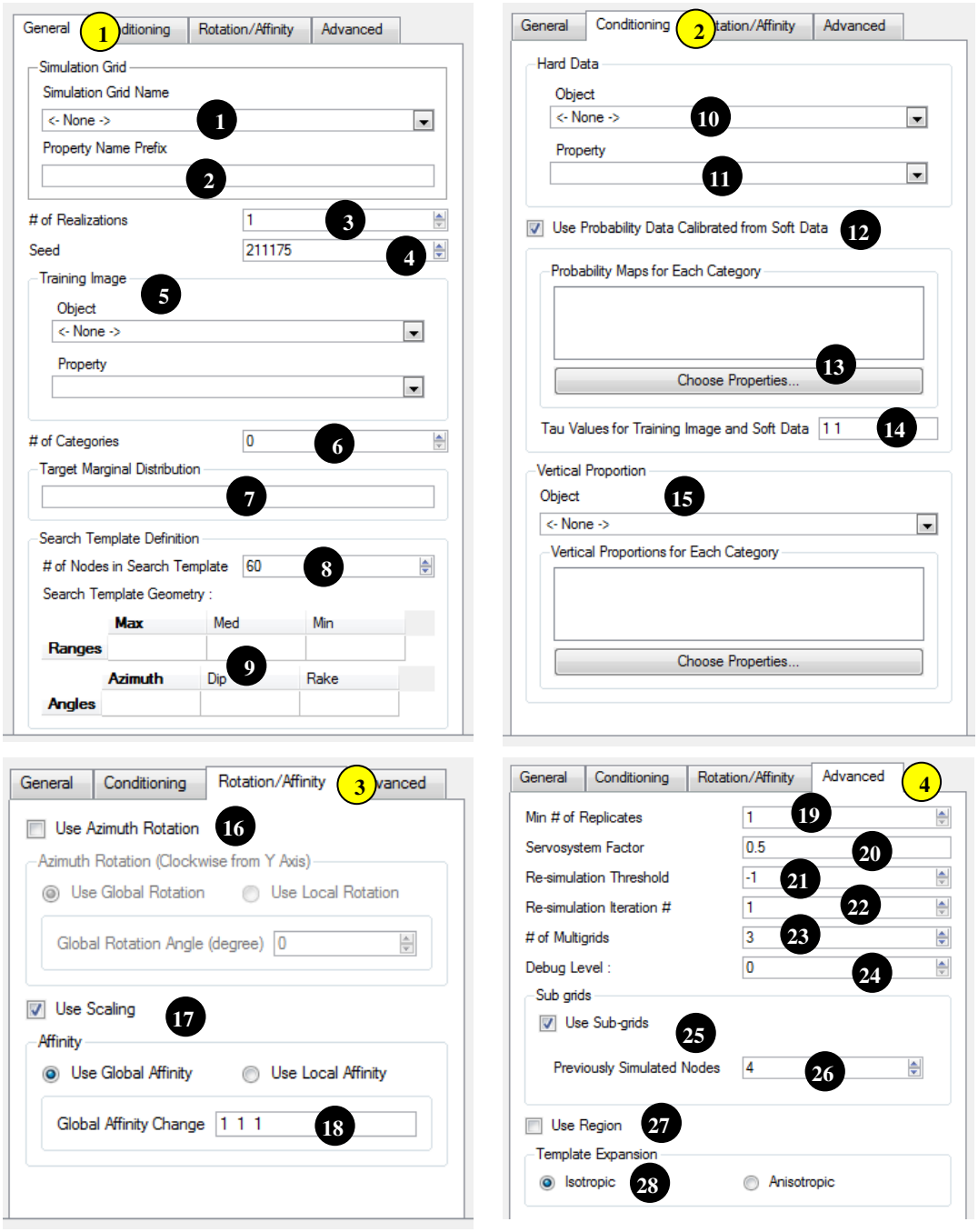

Figure A. 1. SNESIM algorithm interface

2. Parameters Description of SGSIM Algorithm

The description of SGSIM algorithm parameters given here after is based on the work of Remy et al. (2009). The SGSIM algorithm interface contains three pages, namely: General, Data, and Variogram (Figure A.2). The parameters described here are the ones used in this study.

1. **Simulation Grid Name:** is the name of the grid where the simulation will take place.

2. **Property Name Prefix:** is the prefix given by the user for the simulation output. Then, a "_real#" suffix is added to the generated realization by the algorithm. "#" is a number.

3. **Nb of Realization:** is the number of realization the user wishes to generate.

4. **Seed:** is a large odd integer to initialize the pseudo-random number generator.

5. **Kriging Type:** there are four different options namely, Simple Kriging, Ordinary Kriging, Kriging with Trends, and Kriging with Locally Varying Mean.

6. **Hard Data:**
    - **Object:** the name of the grid containing the conditioning data.
    - **Property:** the property containing the data that the user would like to condition to.

7. **Assign Hard Data to Simulation Grid:** to relocate the hard data onto the simulation grid. If the relocation fails, the algorithm does not proceed. The advantage of this parameter is increasing the execution speed of the algorithm significantly.

8. **Max Conditioning Data:** the maximum number of data to be retain in the search template.

9. **Search Ellipsoid Geometry (ranges and angels):** the same as in Section 1 of this appendix.

10. **Use Target Histogram:** if selected it increases the speed of the algorithm execution because the data are normal score transformed before the simulation, then, the simulated field is retransformed to the original space.

11. **Reference Distribution from:** the location from where to select the reference distribution.

12. **Property with reference distribution (object and property):** the object and its property of which the reference distribution is used.

13. **Variogram:** either variogram model parameters are in put manually or loaded from an existing variogram model using the available loading option.

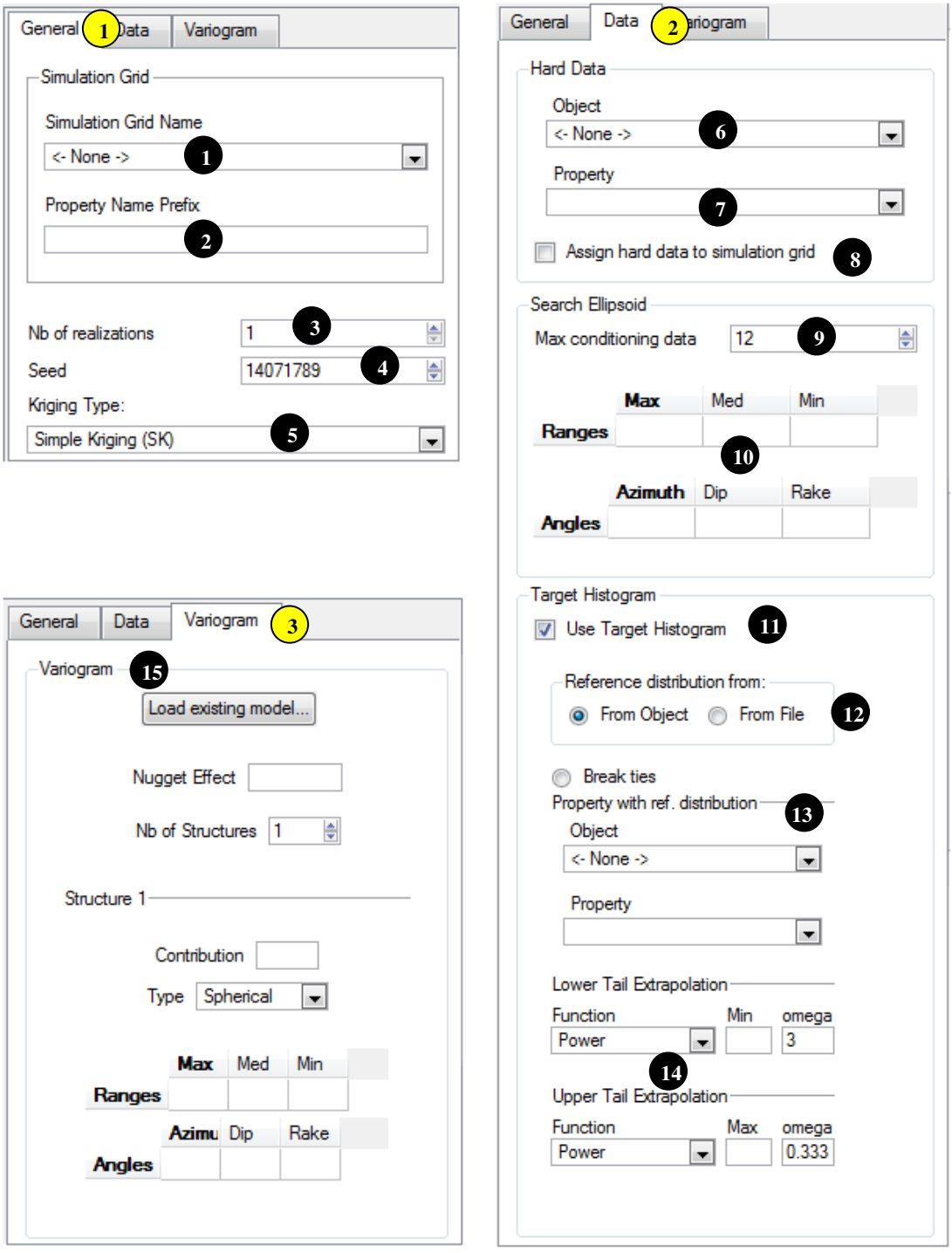

Figure A. 2. SGSIM algorithm interface

APPENDIX B

VARIOGRAM COMPUTATION

In SGeMS the variogram computation method depends on the grid type. The grid type is either point-set or Cartesian grid. Thus, there are two variogram computing methods in SGeMS. The hard data (facies) grid is a point-set grid while the simulated realizations have Cartesian grids. Each of these grid types requires different parameters to compute the experimental variogram. Descriptions of these parameters are given in Remy et al. (2009).

1. Hard Data (Facies) Variogram

The following table list the parameters used to calculate the experimental variogram of the point-set grid having the hard data.

Table B. 1. The parameters used to calculate the variogram of the point-set grid having the hard data

Grid name	Well_simple
Head and tail properties	facies
Number of lag (see Section 1.1 below)	85
Lag separation	0.5
Lag tolerance	0.25
Number of directions	1
Azimuth/ dip/ tolerance/ bandwidth	0/0/91/100

1.1 Lag Number Selection

A common rule of thumb is to restrict the Variography to half the diagonal of the data extent. In a case of a 3D field there are four diagonals the smallest diagonal should be used to checked whether the range is produced with it or not. If not then the second smallest diagonal is checked. This is done until the range is seen in the experimental variogram. The diagonal that is enough to produce the range is the one that should be use. The diagonals of the reservoir grid used in this study are shown in Figure B.1.

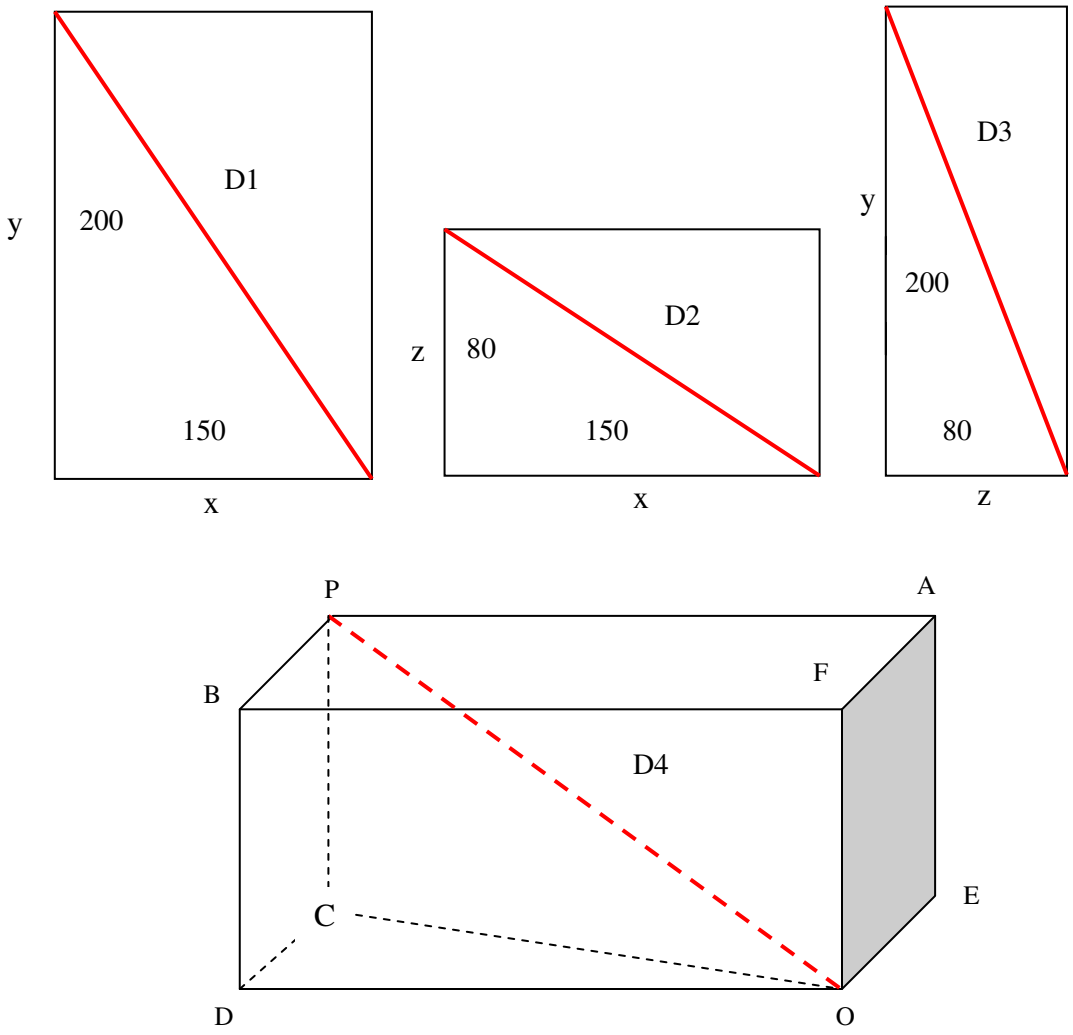

Figure B. 1. The Diagonals of the reservoir grid utilized in the present study

$$D_1 = \frac{\sqrt{150^2 + 200^2}}{2} = 125$$

$$D_2 = \frac{\sqrt{150^2 + 80^2}}{2} = 85$$

$$D_2 = \frac{\sqrt{200^2 + 80^2}}{2} = 107.7$$

$$D_2 = |OP| = \sqrt{|OC|^2 + |PC|^2}$$

But, $$|OC| = \sqrt{|OD|^2 + |DC|^2}$$

So, $$|OP| = \sqrt{|OD|^2 + |DC|^2 + |PC|^2}$$

$$D_2 = \frac{\sqrt{150^2 + 200^2 + 80^2}}{2} = 131$$

2. Simulated Realizations Variogram

The following table list the parameters used to calculate the experimental variogram of the Cartesian grid having the simulated realization of facies.

Table B. 2. The parameters used to calculate the variogram of the Cartesian grid having the simulated realization of facies

Grid name	Well_simple
Head and tail properties	The realization simulated by SNESIM
Number of lag	85
Number of directions	1
x / y / z (see Section 2.1 below)	1/1/1 (to compute the Omni-directional variogram in 3D)

2.1 Computation of the Omni-directional Variogram in 3D

$$|OP| = \sqrt{|DC|^2 + |OD|^2 + |PC|^2}$$

$$|OP| = \sqrt{\mathrm{x}^2 + \mathrm{y}^2 + \mathrm{z}^2}$$

$$\cos\alpha = \frac{|OE|}{|OP|} = \frac{x}{\sqrt{\mathrm{x}^2 + \mathrm{y}^2 + \mathrm{z}^2}}$$

$$\cos\beta = \frac{|OD|}{|OP|} = \frac{y}{\sqrt{\mathrm{x}^2 + \mathrm{y}^2 + \mathrm{z}^2}}$$

$$\cos\theta = \frac{|OF|}{|OP|} = \frac{z}{\sqrt{\mathrm{x}^2 + \mathrm{y}^2 + \mathrm{z}^2}}$$

So, if $\mathrm{x} = \mathrm{y} = \mathrm{z} = 1$

Then, $\cos\alpha = \cos\beta = \cos\theta = \frac{1}{\sqrt{3}} = 0.57735$

And, $\alpha = \beta = \theta = arccos\ \frac{1}{\sqrt{3}} = 54.736°$

So, if an Omni-directional variogram is to be used for a 3D grid, the x, y, and z are selected as 1, 1, and 1, respectively. Then, the angles that the variogram vector makes with all the direction is the same and it is 54.736º.

APPENDIX C

PARAMETER FILES OF THE SIMULATION ALGORITHMS

1. SNESIM Algorithm Parameter File

```
<parameters>  <algorithm name="snesim_std" />
  <GridSelector_Sim  value="grid"  />
  <Property_Name_Sim  value="Hypothetical Original__with seed of 519175" />
  <Nb_Realizations  value="1" />
  <Seed  value="519175" />
  <PropertySelector_Training  grid="training_image"   property="data"  />
  <Nb_Facies  value="2" />
  <Marginal_Cdf  value="0.546 0.454" />
  <Max_Cond  value="80" />
  <Search_Ellipsoid  value="21 21 21  0 0 0" />
  <Hard_Data  grid="well_simple"   property="facies"  />
  <Use_ProbField  value="1"  />
  <ProbField_properties count="2"   value="P(mud|seis);P(sand|seis)"  />
```

<TauModelObject value="1 1" />

<VerticalPropObject value="" />

<VerticalProperties count="0" value="" />

<Use_Global_Affinity value="1" />

<Global_Affinity value="2 1 0.5" />

<Affinity_property value="Hypothetical Original__with seed of 519175" />

<Affinity_categories value="2 2 2 1 1 1 0.5 0.5 0.5 " />

<Use_Local_Affinity value="0" />

<Use_Affinity value="1" />

<Use_Rotation value="0" />

<Cmin value="1" />

<Constraint_Marginal_ADVANCED value="0.5" />

<resimulation_criterion value="-1" />

<resimulation_iteration_nb value="1" />

<Nb_Multigrids_ADVANCED value="1" />

<Debug_Level value="0" />

<Subgrid_choice value="1" />

<Previously_simulated value="4" />

```
  <expand_isotropic  value="1"  />
  <expand_anisotropic  value="0"  />
  <aniso_factor  value="" />
  <Region_Indicator_Prop  value="P(mud|seis)"  />
  <Active_Region_Code  value="" />
  <Use_Previous_Simulation  value="0"  />
  <Use_Region  value="0"  />
</parameters>
```

2. SGSIM Algorithm Parameter File

```
<parameters>  <algorithm name="sgsim" />
  <Grid_Name  value="Estimated_Porosity"  />
  <Property_Name  value="est_por_original reservoir" />
  <Nb_Realizations  value="1" />
  <Seed  value="14071789" />
  <Kriging_Type  value="Simple Kriging (SK)"  />
  <Assign_Hard_Data  value="1"  />
  <Hard_Data  grid="well_simple"   property="porosity"  />
  <Max_Conditioning_Data  value="25" />
  <Search_Ellipsoid  value="80 80 80  0 0 0" />
  <Use_Target_Histogram  value="1"  />
  <nonParamCdf  ref_on_file ="0"  ref_on_grid ="1"
break_ties ="0" filename =""   grid ="well_simple"  property ="porosity">
<LTI_type  function ="No extrapolation"  extreme ="0"  omega ="3" />
<UTI_type  function ="No extrapolation"  extreme ="0"  omega ="0.333" />
</nonParamCdf>
```

```
 <Variogram  nugget="0.04" structures_count="1"  >
 <structure_1  contribution="0.1895"  type="Exponential"   >
  <ranges max="22"  medium="21"  min="8.1"   />
  <angles x="0"  y="0"  z="0"   />
 </structure_1>
</Variogram>
</parameters>
```

APPENDIX D

DEVELOPED CODES

1. Python Code for Porosity Exporting

```
import sgems,nt
a=0
b=0
c=0
while c<10:
 print a
 print b
 print c
 a=a+1
 lower_limit = (((a-1)%10)*15)
 upper_limit = ((a%10)*15)
 if upper_limit == 0:
   upper_limit=150
 def sgems2cmg(grid_name, prop_name, file_name, cmg_keyword, nx, ny, nz):
     prop = sgems.get_property(grid_name, prop_name)
     fid = open(file_name,'w')
     index=0
       for k in range((((c+1)*8)-1),(((c)*8)-1),-1):
            for j in range((((b+1)*20)-1),((b*20)-1),-1):
                 for i in range(lower_limit,upper_limit):
                              index = i+j*nx+k*nx*ny
```

```
                    fid.write(str(prop[index])+';')
                    index = index+1
    fid.close()
 sgems2cmg('Estimated_Porosity', 'est_por_original reservoir__real0', 'C:\porosity values\cube_'+str((c*100)+a)+'.txt', 'POR', 150,200,80)
 if a%10 == 0:
  b=b+1
 if a == 100:
  c=c+1
  a=0
  b=0
```

2. Visual Basic Code for Arithmetic Upscaling of Porosity Data

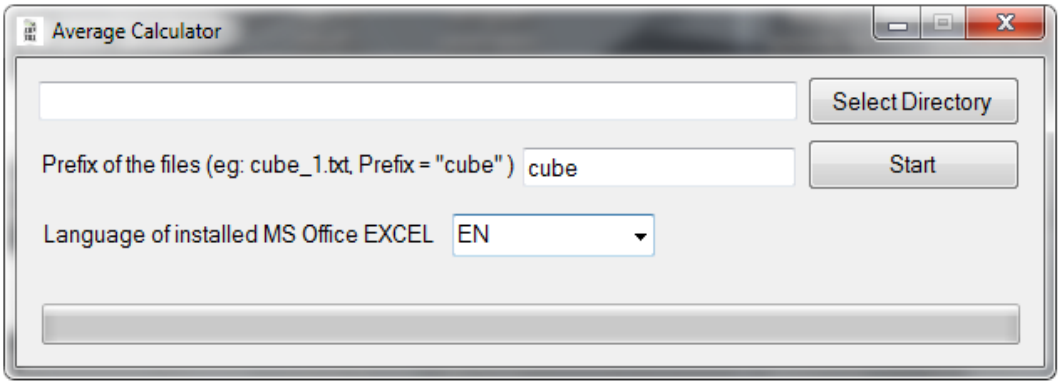

Figure D. 1. Interface of the developed Visual Basic code for the arithmetic upscaling of porosity data

The Code:

```
Imports Excel = Microsoft.Office.Interop.Excel
Public Class Form1

    Public Sub Button1_Click(ByVal sender As System.Object, ByVal e As System.EventArgs) Handles Button1.Click
        Dim FolderBrowserDialog1 As New FolderBrowserDialog

        ' Then use the following code to create the Dialog window
        ' Change the .SelectedPath property to the default location
        With FolderBrowserDialog1
            ' Desktop is the root folder in the dialog.
            .RootFolder = Environment.SpecialFolder.Desktop
            ' Select the C:\Windows directory on entry.
            .SelectedPath = "C:\"
            ' Prompt the user with a custom message.
            .Description = "Select the source directory"
```

```
        If .ShowDialog = DialogResult.OK Then
            TextBox2.Text = .SelectedPath
            ' Display the selected folder if the user clicked on the OK button.
        End If
    End With
End Sub

Private Sub Button2_Click(ByVal sender As System.Object, ByVal e As System.EventArgs) Handles Button2.Click

    Dim xlApp As Excel.Application
    Dim xlWorkBook As Excel.Workbook
    Dim xlWorkSheet As Excel.Worksheet
    Dim misValue As Object = System.Reflection.Missing.Value

    xlApp = New Excel.Application
    xlWorkBook = xlApp.Workbooks.Add(misValue)

    If ComboBox1.Text = "TR" Then
        xlWorkSheet = xlWorkBook.Sheets("Sayfa1")
    ElseIf ComboBox1.Text = "EN" Then
        xlWorkSheet = xlWorkBook.Sheets("Sheet1")
    End If
    Dim fileReader As String
    Dim list, second
    Dim sum
    Dim i As Integer
    Dim x_axis As Integer
    Dim file As Double
    x_axis = 2
```

```
        For file = 1 To 1000
            sum = 0
            If file Mod 20 = 1 Then
                x_axis = x_axis + 1
            End If
            fileReader = My.Computer.FileSystem.ReadAllText(TextBox2.Text + "\" +
TextBox1.Text + "_" & file & ".txt")
            list = Split(fileReader, ";")
            For i = 0 To UBound(list)
                second = Replace(list(i), ".", ".")
                sum += second * 1
                PB.Value = file / 10
            Next
            xlWorkSheet.Cells(x_axis, ((file - 1) Mod 20) + 1) = Replace(sum /
UBound(list), ",", ".")
        Next
        xlWorkSheet.SaveAs(TextBox2.Text + "\averages.xlsx")

        xlWorkBook.Close()
        xlApp.Quit()

        releaseObject(xlApp)
        releaseObject(xlWorkBook)
        releaseObject(xlWorkSheet)
        MsgBox("Excel file created in " + TextBox2.Text + "\ as ""averages.xlsx""")
        Process.Start("explorer.exe", TextBox2.Text)
    End Sub

    Private Sub releaseObject(ByVal obj As Object)
        Try
```

```
            System.Runtime.InteropServices.Marshal.ReleaseComObject(obj)
            obj = Nothing
        Catch ex As Exception
            obj = Nothing
        Finally
            GC.Collect()
        End Try
    End Sub

End Class
```

3. Visual Basic Code to Convert Training Images into Binary Files Having GSLIB Format

```
Imports System.IO
Public Class Form1

  Public Function PureBW(ByVal image As System.Drawing.Bitmap, Optional ByVal Mode As BWMode = BWMode.By_Lightness, Optional ByVal tolerance As Single = 0) As System.Drawing.Bitmap
      Dim x As Integer
      Dim y As Integer
      PictureBox2.Image = image
      image = PictureBox2.Image
      If tolerance > 1 Or tolerance < -1 Then
         Throw New ArgumentOutOfRangeException
         Exit Function
      End If
      Dim height1 As Integer
      If 2 Mod image.Height = 1 Then
         height1 = (image.Height - 1) / 2

      Else
         height1 = image.Height / 2

      End If

      For y = image.Height - 1 To 0 Step -1
         For x = 0 To image.Width - 1 Step 1
```

```
            Dim clr As Color = image.GetPixel(x, y)
            If Mode = BWMode.By_RGB_Value Then
                If (CInt(clr.R) + CInt(clr.G) + CInt(clr.B)) > 383 - (tolerance * 383)
Then
                    image.SetPixel(x, y, Color.White)

                Else
                    image.SetPixel(x, y, Color.Black)

                End If
            Else
                If clr.GetBrightness > 0.5 - (tolerance / 2) Then
                    image.SetPixel(x, y, Color.White)

                Else
                    image.SetPixel(x, y, Color.Black)

                End If
            End If
        Next
        ProgressBar1.Value = (1 - (y / (image.Height - 1))) * 100

    Next
    Button3.Enabled = True
    Return image

End Function
```

```
Public Function PureBW_text(ByVal image As System.Drawing.Bitmap, Optional
ByVal Mode As BWMode = BWMode.By_Lightness, Optional ByVal tolerance As
Single = 0) As System.Drawing.Bitmap
    Dim oWrite As System.IO.StreamWriter
    Dim Path = TextBox1.Text
    Dim search_Format As Array = Split(TextBox1.Text, ".")
    Dim file_format As String
    file_format = search_Format(UBound(search_Format))
    Path = Replace(Path, file_format, "txt")
    oWrite = File.CreateText(Path)
    oWrite.WriteLine("GSLIB output file" & vbCrLf & "1" & vbCrLf & "data")



    Dim x As Integer
    Dim y As Integer
    image = PictureBox2.Image
    If tolerance > 1 Or tolerance < -1 Then
      Throw New ArgumentOutOfRangeException
      Exit Function
    End If

    Dim a As Integer = 0
    For y = image.Height - 1 To 0 Step -1
      For x = 0 To image.Width - 1 Step 1
        a = a + 1
        Dim clr As Color = image.GetPixel(x, y)
        If Mode = BWMode.By_RGB_Value Then
          If (CInt(clr.R) + CInt(clr.G) + CInt(clr.B)) > 383 - (tolerance * 383)
Then
            oWrite.WriteLine("0.0")
```

```
                Else
                    oWrite.WriteLine("1.0")
                End If
            Else
                If clr.GetBrightness > 0.5 - (tolerance / 2) Then

                    oWrite.WriteLine("0.0")
                Else

                    oWrite.WriteLine("1.0")
                End If
            End If

        Next
        ProgressBar1.Value = (1 - (y / (image.Height - 1))) * 100

    Next
    oWrite.Close()
    Return image

End Function
Enum BWMode
    By_Lightness
    By_RGB_Value
End Enum

Public Sub Button1_Click(ByVal sender As System.Object, ByVal e As
System.EventArgs) Handles Button1.Click
    Dim OpenFileDialog1 As New OpenFileDialog
```

```
        ' Then use the following code to create the Dialog window
        ' Change the .SelectedPath property to the default location

        With (OpenFileDialog1)

            .Title = "Select the image file"
            If .ShowDialog = DialogResult.OK Then
                TextBox1.Text = .FileName
                Dim filename = .SafeFileName
                Dim initial_image = TextBox1.Text
                Try
                    Dim img As System.Drawing.Image =
System.Drawing.Image.FromFile(initial_image)
                Catch generatedExceptionName As OutOfMemoryException
                    ' Image.FromFile throws an OutOfMemoryException
                    ' if the file does not have a valid image format or
                    ' GDI+ does not support the pixel format of the file.
                    '
                    MsgBox("An error occured while loading your file: Please be sure file is
an image file.", MsgBoxStyle.Critical, "Error!")
                    Exit Sub
                End Try
                ' Display the selected folder if the user clicked on the OK button.
                PictureBox1.Image = New System.Drawing.Bitmap(TextBox1.Text)
                Button3.Enabled = False
            Else

            End If
        End With
    End Sub
```

```
    Private Sub Button2_Click(ByVal sender As System.Object, ByVal e As
System.EventArgs) Handles Button2.Click
        Dim conv_meth As String
        Dim initial_image = TextBox1.Text
        conv_meth = ComboBox1.Text
        If conv_meth = "By_RGB_Value" Then
            Me.PictureBox2.Image = PureBW(Me.PictureBox1.Image,
BWMode.By_RGB_Value, (TextBox2.Text / 100))
        ElseIf conv_meth = "By_Lightness" Then
            Me.PictureBox2.Image = PureBW(Me.PictureBox1.Image,
BWMode.By_Lightness, (TextBox2.Text / 100))
        End If
        Me.PictureBox1.Image = New System.Drawing.Bitmap(TextBox1.Text)
    End Sub
    Private Sub Button3_Click(ByVal sender As System.Object, ByVal e As
System.EventArgs) Handles Button3.Click
        Dim conv_meth As String
        Dim initial_image = TextBox1.Text
        conv_meth = ComboBox1.Text
        If conv_meth = "By_RGB_Value" Then
            Me.PictureBox2.Image = PureBW_text(Me.PictureBox1.Image,
BWMode.By_RGB_Value, (TextBox2.Text / 100))
        ElseIf conv_meth = "By_Lightness" Then
            Me.PictureBox2.Image = PureBW_text(Me.PictureBox1.Image,
BWMode.By_Lightness, (TextBox2.Text / 100))
        End If

    End Sub
End Class
```

4. Visual Basic Code to Perform MCS for the Clustered Porosity Hard Data

Sub SheetFunctions() ' This code generates 50 MCS for each datum of the available 4320 porosity data having a bimodal distribution. The mean and standard deviation of the shale (non-reservoir) group of data are in cells C2 and C3, respectively. Similarly, the mean and standard deviation of the channel (reservoir) group of data are in cells C5 and C6, respectively.

```
 For i = 0 To 4319

    For j = 0 To 49

    If (Cells(i + 2, "A").Value() <= 0.147) Then Cells(i + 6, j + 7) = WorksheetFunction.NormInv(Rnd(), Cells("4", "D").Value(), Cells("4", "E")) Else Cells(i + 6, j + 7) = WorksheetFunction.NormInv(Rnd(), Cells("5", "D").Value(), Cells("5", "E"))

‘Where 0.147 is the largest data in shale group of data

     If Cells(i + 6, j + 7) < 0 Then Cells(i + 6, j + 7) = 0 'this line is because porosity can not take negative values

    Next

 Next

End Sub
```

5. Visual Basic Code to Extract the MCS Realizations From Excel into Text Files of the GSLIB Format

The extraction of data must be in a new sheet where the first three columns are set as follows:

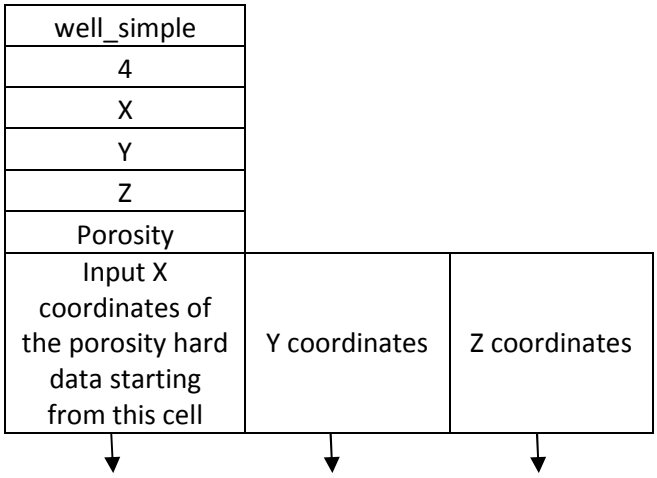

In addition, the simulated 50 realizations must be copied and pasted starting from cell L7

The code:

```
Sub columbfix()   'This code is developed to extract the MCS realizations from Excel into text files.
realization_number = 1          'This number should be change manually for each realization

realization_number = realization_number - 1
For i = 0 To realization_number
```

```
Sheet1.Range(Cells(7, i + 12), Cells(4326, i + 12)).Copy                    'Note that the number of the sheet here and in the following line must be correct for the code to work
Sheet1.Range(Cells(7, "D"), Cells(4326, "D")).PasteSpecial Transpose:=False

Next

    Dim fs As Object, a As Object, s As String
    Set fs = CreateObject("Scripting.FileSystemObject")
    Set a = fs.CreateTextFile("C:\realization-" & realization_number + 1 & ".txt", True)  'Add the exporting location after "C:" and note that the text after the last "\" is given as the file name before the number (in this case "realization")
    i = 1
    While Not IsEmpty(Cells(i, 1))
        s = s & Cells(i, 1) & " " & Cells(i, 2) & " " & Cells(i, 3) & " " & Cells(i, 4) & vbCrLf

        i = i + 1
    Wend
    a.WriteLine s
    a.Close
End Sub
```

6. Visual Basic Code for Arithmetic And Median Upscaling of Porosity Data

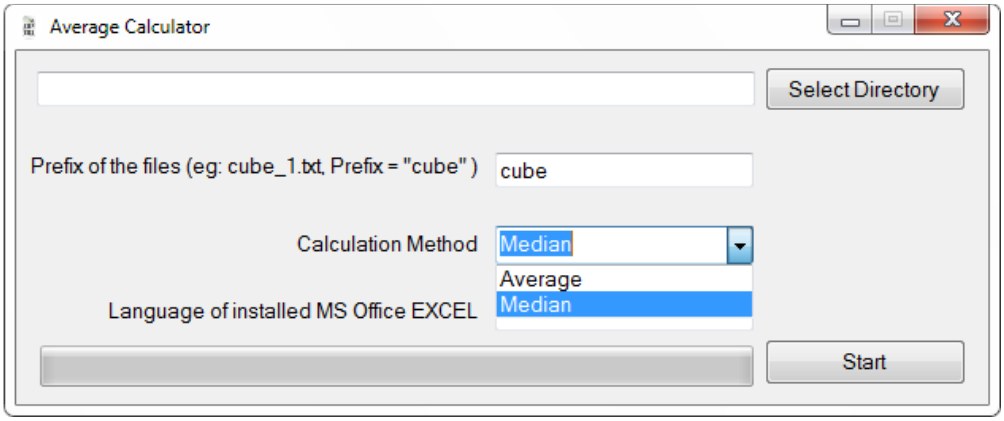

Figure D. 2. Interface of the upscaling Visual Basic code using the average or median porosity

The code:

```
Imports Excel = Microsoft.Office.Interop.Excel
Public Class Form1

    Public Sub Button1_Click(ByVal sender As System.Object, ByVal e As
System.EventArgs) Handles Button1.Click
        Dim FolderBrowserDialog1 As New FolderBrowserDialog

        ' Then use the following code to create the Dialog window
        ' Change the .SelectedPath property to the default location
        With FolderBrowserDialog1
            ' Desktop is the root folder in the dialog.
            .RootFolder = Environment.SpecialFolder.Desktop
            ' Select the C:\Windows directory on entry.
            .SelectedPath = "C:\"
```

```
            ' Prompt the user with a custom message.
            .Description = "Select the source directory"
            If .ShowDialog = DialogResult.OK Then
                TextBox2.Text = .SelectedPath
                ' Display the selected folder if the user clicked on the OK button.


            End If
        End With
    End Sub

    Private Sub Button2_Click(ByVal sender As System.Object, ByVal e As
System.EventArgs) Handles Button2.Click

        Dim xlApp As Excel.Application
        Dim xlWorkBook As Excel.Workbook
        Dim xlWorkSheet As Excel.Worksheet
        Dim misValue As Object = System.Reflection.Missing.Value

        xlApp = New Excel.Application
        xlWorkBook = xlApp.Workbooks.Add(misValue)

        If ComboBox1.Text = "TR" Then
            xlWorkSheet = xlWorkBook.Sheets("Sayfa1")
        ElseIf ComboBox1.Text = "EN" Then
            xlWorkSheet = xlWorkBook.Sheets("Sheet1")
        End If

        Dim fileReader As String
        Dim list, first, second
        Dim sum, median
```

```
        Dim i As Integer
        Dim x_axis As Integer
        Dim file As Double
        Dim sorting As New ArrayList()
        x_axis = 2
        For file = 1 To 1000
            sum = 0
            median = 0

            If file Mod 20 = 1 Then
                x_axis = x_axis + 1
            End If
            fileReader = My.Computer.FileSystem.ReadAllText(TextBox2.Text + "\" +
TextBox1.Text + "_" & file & ".txt")
            list = Split(fileReader, ";")
            If ComboBox2.Text = "Average" Then
                For i = 0 To UBound(list)
                    second = Replace(list(i), ".", ".")
                    sum += second * 1
                    PB.Value = file / 10
                Next
                xlWorkSheet.Cells(x_axis, ((file - 1) Mod 20) + 1) = Replace(sum /
UBound(list), ",", ".")
            Else

                For i = 0 To 2399
                    second = Replace(list(i), ".", ".")
                    sorting.Add(second * 1)

                    PB.Value = file / 10
```

```
            Next
            sorting.Sort()

            'it calculates 1199 and 1200 because array starts from 0, not 1
            median = (sorting(1199) + sorting(1200)) / 2
            xlWorkSheet.Cells(x_axis, ((file - 1) Mod 20) + 1) = Replace(median, ",",
"."
            sorting.RemoveRange(0, 2399)
        End If

    Next

    If ComboBox2.Text = "Average" Then
        xlWorkSheet.SaveAs(TextBox2.Text + "\!averages.xlsx")
        xlWorkBook.Close()
        xlApp.Quit()

        releaseObject(xlApp)
        releaseObject(xlWorkBook)
        releaseObject(xlWorkSheet)

        MsgBox("Excel file created in " + TextBox2.Text + "\ as ""!averages.xlsx""")
        Process.Start("explorer.exe", TextBox2.Text)
    Else
        xlWorkSheet.SaveAs(TextBox2.Text + "\!median.xlsx")
        xlWorkBook.Close()
        xlApp.Quit()

        releaseObject(xlApp)
        releaseObject(xlWorkBook)
```

```
            releaseObject(xlWorkSheet)

            MsgBox("Excel file created in " + TextBox2.Text + "\ as ""!median.xlsx""")
            Process.Start("explorer.exe", TextBox2.Text)
        End If

    End Sub

    Private Sub releaseObject(ByVal obj As Object)
        Try
            System.Runtime.InteropServices.Marshal.ReleaseComObject(obj)
            obj = Nothing
        Catch ex As Exception
            obj = Nothing
        Finally
            GC.Collect()
        End Try
    End Sub

End Class
```

APPENDIX E

CMG DATA OF THE ORIGINAL RESERVOIR

1. PVT and Relative Permeability Data

Table E. 1. PVT data

Pressure (p) (psi)	Solution gas-oil ratio (rs) (SCF/STB)	Formation volume factor (bo) (rbb/STB)	Gas expansion factor (eg) (SCF/rbb)	Oil viscosity (viso) (cp)	Gas viscosity (visg) (cp)
14.7	1.0	1.0620	0.1667	6.0	1.0400
264.7	90.5	1.1500	0.0121	82.7	0.9750
514.7	180.0	1.2070	0.0063	159.0	0.9100
1014.7	371.0	1.2950	0.0032	313.0	0.8300
2014.7	636.0	1.4350	0.0016	620.0	0.6950
2514	775.0	1.5000	0.0013	773.0	0.6410
3014.7	930.0	1.5650	0.0011	926.0	0.5940
4014.7	1270.0	1.6950	0.0008	1233.0	0.5100
5014.7	1600.0	1.8270	0.0007	1541.0	0.4490
9014.7	2984.0	2.3570	0.0004	2591.0	0.2030

Table E. 2. Water - oil relative permeability

Sw	Krw	Krow
0.13	0	1
0.191	0.0051	0.999
0.25	0.0102	0.769
0.294	0.0168	0.7241
0.357	0.0275	0.6206
0.414	0.0424	0.504
0.49	0.0665	0.3714
0.577	0.097	0.3029
0.63	0.1148	0.1555
0.673	0.1259	0.0956

Table E. 3. Liquid - gas relative permeability

Sl	Krg	Krog
0.2	0.17	0
0.395	0.112	0.0294
0.433	0.1022	0.0461
0.515	0.0855	0.0883
0.569	0.0761	0.1172
0.614	0.0654	0.1433
0.663	0.05	0.1764
0.719	0.0372	0.217
0.75	0.0285	0.2255
0.805	0.0195	0.2919

2. CMG Data File

```
**************************************************************************
**                                                                      **
**                  Hypothetical Model by Mohamed Fadlelmula            **
**                                                                      **
**                                  2012                                **
**                                                                      **
**                  Middle East Technical University,                   **
**              Department of Petroleum and Natural gas Engineering,    **
**                              Ankara, Turkey                          **
**                                                                      **
**************************************************************************

** ==============  INPUT/OUTPUT CONTROL  ==================
** 2012-03-01, 6:17:58 PM, M
RESULTS SIMULATOR IMEX 200600
*TITLE1  'Original Reservoir Model'
*INUNIT     *FIELD          ** All the data values are in field units
*OUTUNIT    *FIELD
*INTERRUPT  *STOP
*MAXERROR    20             ** Maximum error number, this is the default value
*WRST       *TIME
*WPRN       *GRID    *TIME
*OUTPRN     *GRID    *All     ** OUTPRN is to print the data on the screen while
the simulation is going on
                    **(for each time step, if it is written after defining time step)
*OUTSRF     *GRID    *All     ** OUTSRF is to print the data in output file
** ==============  GRID AND RESERVOIR DEFINITION  =============
*GRID  *CART 10 10 10         ** CART indicates a rectangular Cartesian grid, with
uniform depth/uniform thickness layers
*KDIR  *DOWN                 ** First layer at the top of the reservoir
*DI    *CON 500               ** Dimension of I direction blocks is constant for each
block as 500 ft so in total it is
                    ** approximately 5000 ft = 1500 m = 1.5 km
*DJ    *CON 1640              ** Dimension of J direction blocks is constant for each
block as 1640 ft so in total it is
                    ** approximately 16400 ft = 5000 m = 5 km
*DK    *CON 8                 ** Dimension of K direction blocks is constant for each
block as 8 ft so in total it is
                    ** 80 ft (16 of it water, so 64 ft is oil)
*DTOP 100*5000  ** Top of the grids in (ft) is 5000
```

** 100 is the number of grids in the upper layer (i.e. 10i x 10j)

**$ Property: NULL Blocks Max: 1 Min: 1
**$ 0 = null block, 1 = active block
NULL CON 1
*NOLIST ** NOLIST keyword is inserted in the data file, the data file is not listed from the
  ** point of the *NOLIST keyword until a *LIST keyword or the end of data file is reached

*POR *All
Here the simulated and upscaled 1000 porosity data are placed
****
*PERMI *All
Here the 1000 permeability data corresponding to the above 1000 porosity data are placed
PERMJ EQUALSI
PERMK EQUALSI

**$ Property: Pinchout Array Max: 1 Min: 1
**$ 0 = pinched block, 1 = active block
PINCHOUTARRAY CON 1
*LIST
** ========== OTHER RESERVOIR PROPERTIES ==========
**THTYPE *con 1 ** Unless you have multiple rock types, you do not need *ROCKTYPE or * THTYPE
*CPOR 3.0E-6 ** Rock (or formation) compressibility 1/Psi
*PRPOR 14.7 ** Reference pressure, this pressure is the fluid (pore) pressure at which the values input using *POR are
  ** to hold, in(psi)
** ========== FLUID DEFINITIONS ==========
*MODEL *BLACKOIL ** A black-oil model, modeling flow of oil, water, and gas.
 *PVT
  ** p rs bo eg viso visg
   14.7000 1.00000 1.06200 6.00000 1.04000 0.0080000
   264.700 90.50000 1.15000 82.70000 0.9750000 0.0096000
   514.700 180.000 1.20700 159.000 0.9100000 0.0112000
   1014.700 371.000 1.29500 313.000 0.8300000 0.0140000
   2014.700 636.000 1.43500 620.000 0.6950000 0.0189000
   2514.000 775.000 1.50000 773.000 0.6410000 0.0208000
   3014.700 930.000 1.56500 926.000 0.5940000 0.0228000
   4014.700 1270.000 1.69500 1233.000 0.5100000 0.0268000
   5014.700 1600.000 1.82700 1541.000 0.4490000 0.0309000
   9014.700 2984.000 2.35700 2591.000 0.2030000 0.0470000

```
  *DENSITY *OIL    46.244    ** in  lbm/ft3
  *DENSITY *GAS     0.0647   ** in  lbm/ft3
  *DENSITY *WATER  62.238    ** in  lbm/ft3
  *CO     9.1512E-6            ** Oil Compressibility at the corresponding pressure in
1/Psi
  *CVO    4.6000E-5            ** Pressure dependence of the viscosity curve for oil
above the bubble point pressure in cp/psi
  *BWI   1.0410                ** The water formation volume factor (for PVT region) in
RB/STB
  *CW    3.0E-6               ** Water compressibility (for a PVT region) in 1/Psi
  *REFPW 14.7                  ** Reference pressure (for a PVT region) in Psi
  *VWI   0.96                  ** Viscosity of water phase at the reference pressure pw in
cp
  *CVW    0.0                  ** Pressure dependence of water viscosity (viscosity
units/pressure units) in cp/psi
**$ Property: PVT Type  Max: 1  Min: 1
PTYPE CON           1
**  ==============  ROCK-FLUID PROPERTIES  ==================
*ROCKFLUID
*RPT 1        ** Indicates that this set of relative permeability curves will be defined
by table entries
 *SWT        ** Indicates the start of the water-oil relative permeability table
**   Sw          Krw         Krow
**  -----       ------      ------
   0.130        0.0         1.0
   0.191        0.0051      0.999
   0.250        0.0102      0.769
   0.294        0.0168      0.7241
   0.357        0.0275      0.6206
   0.414        0.0424      0.504
   0.490           0.0665      0.3714
   0.577           0.097       0.3029
   0.630           0.1148      0.1555
   0.673           0.1259      0.0956
   0.719           0.1381      0.0576
   0.789           0.1636      0.0
   1.0          1.0         0.0
*SLT        ** Indicates the start of a liquid-gas relative permeability table dependent
on liquid saturation
          ** SL is the total liquid saturation (fraction)
```

```
**   Sl       Krg       Krog
**  -----     ------    ------
    0.200     0.17      0.0
    0.395     0.112     0.0294
    0.433     0.1022    0.0461
    0.515     0.0855    0.0883
    0.569     0.0761    0.1172
    0.614     0.0654    0.1433
    0.663     0.05      0.1764
    0.719     0.0372    0.217
    0.750     0.0285    0.2255
    0.805     0.0195    0.2919
    0.850     0.0121    0.3373
    0.899     0.0026    0.5169
    1.0       0.0       1.0
** ==============  INITIAL CONDITIONS  ======================
*INITIAL
*VERTICAL    *BLOCK_CENTER          *WATER_OIL_GAS      ** Use vertical equilibrium calculation.


   *PB *CON    4014.7         ** Bubble point pressure
   *REFDEPTH   5000           ** A reference depth
   *REFPRES    4800           ** Associated pressure.
   *DWOC       5064           ** Depth to water-oil contact
   *DGOC        4000            ** Depth to gas-oil contact (the gas is kept out of the calculation for simplicity)
** ==============  NUMERICAL CONTROL  ======================
*NUMERICAL
** All these can be defaulted because the defaults used in the numerical solution techniques provide a good and efficient solution
  ** to most simulation problems.(Here the default values are used)
**DTMAX     121.0             ** A real number to specify the maximum time-step size allowed,  if it is not present in the input-data-file,
                        ** then the maximum time step size is 365 days
*ITERMAX 60                  **ITERMAX is used to specify the maximum number of iterations allowed in the Jacobian matrix solution routine

**MAXSTEPS      100          ** Maximum number of time steps
**NORM *PRESS  1000.0        ** Normal maximum changes per time step
**NORM *SATUR     0.20
**AIM  *THRESH    0.25 .25   ** Use threshhold switching criteria
**NCUTS       6     ** Controls the number of time-step size cuts allowed in a single time step, If it does not appear in the data set, then the default is 4 cuts
*RUN
```

```
** ==============  RECURRENT DATA  ======================
DATE 1992 1 1                         ** Simulation starting date
**$
WELL  'Well-1'
PRODUCER 'Well-1'                       ** Define the type of well.
*OPERATE  *MAX  *STO  1478   *CONT              ** Initially, operate on a rate
constraint.
*OPERATE  *MIN  *BHP  50.0  *CONT  *REPEAT   ** If the BHP falls below 50
psi, switch to bottomhole pressure constraint.
                                ** The (REPEAT) subkeyword specifies that if the
constraint is violated, the timestep
                                 ** should be repeated after switching to operating on
the violated constraint.
**$         rad  geofac  wfrac  skin
GEOMETRY  K  0.375  0.249  1.  0.
PERF  GEO  'Well-1'
**$ UBA    ff  Status  Connection
   3 3 1  1.  OPEN    FLOW-TO  'SURFACE'  REFLAYER
   3 3 2  1.  OPEN    FLOW-TO  1
   3 3 3  1.  OPEN    FLOW-TO  2
   3 3 4  1.  OPEN    FLOW-TO  3
   3 3 5  1.  OPEN    FLOW-TO  4
   3 3 6  1.  OPEN    FLOW-TO  5
   3 3 7  1.  OPEN    FLOW-TO  6
   3 3 8  1.  OPEN    FLOW-TO  7
LAYERXYZ  'Well-1'
**$ perf geometric data: UBA, block entry(x,y,z) block exit(x,y,z), length
   3  3  1    1250.000000   4100.000000   5000.008000   1250.000000   4100.000000
5007.992000  8.000000
   3  3  2    1250.000000   4100.000000   5008.008000   1250.000000   4100.000000
5015.992000  8.000000
   3  3  3    1250.000000   4100.000000   5016.008000   1250.000000   4100.000000
5023.992000  8.000000
   3  3  4    1250.000000   4100.000000   5024.008000   1250.000000   4100.000000
5031.992000  8.000000
   3  3  5    1250.000000   4100.000000   5032.008000   1250.000000   4100.000000
5039.992000  8.000000
   3  3  6    1250.000000   4100.000000   5040.008000   1250.000000   4100.000000
5047.992000  8.000000
   3  3  7    1250.000000   4100.000000   5048.008000   1250.000000   4100.000000
5055.992000  8.000000
   3  3  8    1250.000000   4100.000000   5056.008000   1250.000000   4100.000000
5063.992000  8.000000
**$
WELL  'Well-2'
```

```
PRODUCER 'Well-2'
*OPERATE *MAX *STO 2217 *CONT ** Initially, operate on a rate constraint.
*OPERATE *MIN *BHP 50.0 *CONT *REPEAT
**$ rad geofac wfrac skin
GEOMETRY K 0.375 0.249 1. 0.
PERF GEO 'Well-2'
**$ UBA ff Status Connection
  6 6 1 1. OPEN FLOW-TO 'SURFACE' REFLAYER
  6 6 2 1. OPEN FLOW-TO 1
  6 6 3 1. OPEN FLOW-TO 2
  6 6 4 1. OPEN FLOW-TO 3
  6 6 5 1. OPEN FLOW-TO 4
  6 6 6 1. OPEN FLOW-TO 5
  6 6 7 1. OPEN FLOW-TO 6
  6 6 8 1. OPEN FLOW-TO 7
LAYERXYZ 'Well-2'
**$ perf geometric data: UBA, block entry(x,y,z) block exit(x,y,z), length
  6 6 1 2750.000000 9020.000000 5000.008000 2750.000000 9020.000000 5007.992000 8.000000
  6 6 2 2750.000000 9020.000000 5008.008000 2750.000000 9020.000000 5015.992000 8.000000
  6 6 3 2750.000000 9020.000000 5016.008000 2750.000000 9020.000000 5023.992000 8.000000
  6 6 4 2750.000000 9020.000000 5024.008000 2750.000000 9020.000000 5031.992000 8.000000
  6 6 5 2750.000000 9020.000000 5032.008000 2750.000000 9020.000000 5039.992000 8.000000
  6 6 6 2750.000000 9020.000000 5040.008000 2750.000000 9020.000000 5047.992000 8.000000
  6 6 7 2750.000000 9020.000000 5048.008000 2750.000000 9020.000000 5055.992000 8.000000
  6 6 8 2750.000000 9020.000000 5056.008000 2750.000000 9020.000000 5063.992000 8.000000
**$
WELL 'Well-3'
PRODUCER 'Well-3'
*OPERATE *MAX *STO 3694 *CONT ** Initially, operate on a rate constraint.
*OPERATE *MIN *BHP 50.0 *CONT *REPEAT
**$ rad geofac wfrac skin
GEOMETRY K 0.375 0.249 1. 0.
PERF GEO 'Well-3'
**$ UBA ff Status Connection
  9 9 1 1. OPEN FLOW-TO 'SURFACE' REFLAYER
```

```
   9 9 2  1.  OPEN    FLOW-TO  1
   9 9 3  1.  OPEN    FLOW-TO  2
   9 9 4  1.  OPEN    FLOW-TO  3
   9 9 5  1.  OPEN    FLOW-TO  4
   9 9 6  1.  OPEN    FLOW-TO  5
   9 9 7  1.  OPEN    FLOW-TO  6
   9 9 8  1.  OPEN    FLOW-TO  7
LAYERXYZ  'Well-3'
**$ perf geometric data: UBA, block entry(x,y,z) block exit(x,y,z), length
   9 9 1   4250.000000   13940.000000   5000.008000   4250.000000   13940.000000
5007.992000  8.000000
   9 9 2   4250.000000   13940.000000   5008.008000   4250.000000   13940.000000
5015.992000  8.000000
   9 9 3   4250.000000   13940.000000   5016.008000   4250.000000   13940.000000
5023.992000  8.000000
   9 9 4   4250.000000   13940.000000   5024.008000   4250.000000   13940.000000
5031.992000  8.000000
   9 9 5   4250.000000   13940.000000   5032.008000   4250.000000   13940.000000
5039.992000  8.000000
   9 9 6   4250.000000   13940.000000   5040.008000   4250.000000   13940.000000
5047.992000  8.000000
   9 9 7   4250.000000   13940.000000   5048.008000   4250.000000   13940.000000
5055.992000  8.000000
   9 9 8   4250.000000   13940.000000   5056.008000   4250.000000   13940.000000
5063.992000  8.000000
WSRF GRID TNEXT
*DATE 1993 01 01
WSRF GRID TNEXT
*DATE 1994 01 01
WSRF GRID TNEXT
*DATE 1995 01 01
WSRF GRID TNEXT
*DATE 1996 01 01
WSRF GRID TNEXT
*DATE 1997 01 01
WSRF GRID TNEXT
*DATE 1998 01 01
WSRF GRID TNEXT
*DATE 1999 01 01
WSRF GRID TNEXT
*DATE 2000 01 01
WSRF GRID TNEXT
*DATE 2001 01 01
WSRF GRID TNEXT
*DATE 2002 01 01
```

```
WSRF GRID TNEXT
*DATE 2003 01 01
WSRF GRID TNEXT
*DATE 2004 01 01
WSRF GRID TNEXT
*DATE 2005 01 01
WSRF GRID TNEXT
*DATE 2006 01 01
WSRF GRID TNEXT
*DATE 2007 01 01
WSRF GRID TNEXT
*DATE 2008 01 01
WSRF GRID TNEXT
*DATE 2009 01 01
WSRF GRID TNEXT
*DATE 2010 01 01
WSRF GRID TNEXT
*DATE 2011 01 01
WSRF GRID TIME
*DATE 2012 01 01

*STOP            **History run ends here
```

CURRICULUM VITA

Personal Information

Name: Mohamed M. Fadlelmula F.

Nationality: Sudanese

Date and place of birth: 22/04/1979 Riyadh, Saudi Arabia

Email: mfmining@yahoo.com

Education:

B.Sc.

2000-2005	Middle East Technical University (METU), Ankara Department: Mining Engineering Cumulative GPA: 2.77/4.00, Ranked the 8th among 65 graduates

M.Sc.

2005-2007	Middle East Technical University (METU), Ankara Department: Mining Engineering Study Area: Rock Mechanics Cumulative GPA: 3.64/4.00

Ph.D.

2008-2012	Middle East Technical University (METU), Ankara Department: Petroleum and Natural Gas Engineering Study Area: Reservoir Engineering Cumulative GPA: 3.64/4.00

Work experience:

10/2008-07/2012	Graduate teaching assistant Department of Petroleum and Natural Gas Engineering, Middle East Technical University
06/2004-07/2004	Intern at Park Technique Lignite Coal Mine, Cayirhan, Turkey
06/2003-07/2003	Intern at General Directorate of Mineral Research and Exploration (MTA), Ankara, Turkey

Languages:

Arabic (Native)
English (Fluent spoken and written)
Turkish (Fluent spoken and written)

Computer Skills:

Reservoir simulation: CMG, SGeMS, Petrel (basic)
Pressure transient analysis: Kappa software (Saphir)
Programming: C, Visual Basic, Python
Miscellaneous: Microsoft Office (Word, PowerPoint, Excel), Vulcan, FLAC, Phase2

Publications:

Conference Papers

1. Fadlelmula, F.M.M., Akin, S., 2011. The impact of Training Image modification on reservoir modeling using Multiple-Point Geostatistics, SPE Student Technical Conference, Wietze, 13-14 October.

2. Fadlelmula, F.M.M., Akin, S., and Duzgun, H.S.B., 2011. Quantification and Analysis of Uncertainties in Reservoir Modeling Using Multiple-Point Geostatistics, Proc. of the18th International Petroleum and Natural Gas Congress and Exhibition of Turkey, IPETGAS 2011, 11-13 May, Ankara, pp 44-45.

3. Fadlelmula, F.M.M., Duzgun, H.S.B., and Karpuz, C., 2008. Reliability-Based Modeling of Wedge Failures, Proc. of Asian Pacific Symposium on Structural Reliability and Its Applications, APPSRA'08, 18-20 June, Hong Kong, pp 341-348.

Book

1. Fadlelmula, F.M.M., 2009. Probabilistic Modeling of Failure in Rock Slopes. VDM Publishing House Ltd., Mauritius. (ISBN 978-3-639-19929-1)

Paper in preparation

1. Fadlelmula, F.M.M., Akin, S., Duzgun, H.S.B. The Impact of Training Image Uncertainty in Reservoir Modeling Using Multiple-Point Geostatistics.

Hobbies:

Traveling, camping, weight-lifting, swimming, playing Frisbee, American football and volleyball